

Cell mapping methods : modifications and extensions

Citation for published version (APA):

Spek, van der, J. A. W. (1994). *Cell mapping methods : modifications and extensions*. [Phd Thesis 1 (Research TU/e / Graduation TU/e), Mechanical Engineering]. Technische Universiteit Eindhoven.
<https://doi.org/10.6100/IR411481>

DOI:

[10.6100/IR411481](https://doi.org/10.6100/IR411481)

Document status and date:

Published: 01/01/1994

Document Version:

Publisher's PDF, also known as Version of Record (includes final page, issue and volume numbers)

Please check the document version of this publication:

- A submitted manuscript is the version of the article upon submission and before peer-review. There can be important differences between the submitted version and the official published version of record. People interested in the research are advised to contact the author for the final version of the publication, or visit the DOI to the publisher's website.
- The final author version and the galley proof are versions of the publication after peer review.
- The final published version features the final layout of the paper including the volume, issue and page numbers.

[Link to publication](#)

General rights

Copyright and moral rights for the publications made accessible in the public portal are retained by the authors and/or other copyright owners and it is a condition of accessing publications that users recognise and abide by the legal requirements associated with these rights.

- Users may download and print one copy of any publication from the public portal for the purpose of private study or research.
- You may not further distribute the material or use it for any profit-making activity or commercial gain
- You may freely distribute the URL identifying the publication in the public portal.

If the publication is distributed under the terms of Article 25fa of the Dutch Copyright Act, indicated by the "Taverne" license above, please follow below link for the End User Agreement:

www.tue.nl/taverne

Take down policy

If you believe that this document breaches copyright please contact us at:

openaccess@tue.nl

providing details and we will investigate your claim.

Cell Mapping Methods: Modifications and Extensions

Proefschrift

ter verkrijging van de graad van doctor
aan de Technische Universiteit Eindhoven
op gezag van de Rector Magnificus, prof.dr. J.H. van Lint,
voor een commissie aangewezen door het College van Dekanen
in het openbaar te verdedigen
op woensdag 16 februari 1994 om 16.00 uur

door

Josephus Antonius Wilhelmus van der Spek

geboren op 7 mei 1966 te Asten

Dit proefschrift is goedgekeurd door de promotoren:

prof.dr.ir. D.H. van Campen

prof.dr.ir. E.A. Muijderman

en de copromotor:

dr.ir. A. de Kraker

Cell Mapping Methods: Modifications and Extensions

CTP-DATA KONINKLIJKE BIBLIOTHEEK, DEN HAAG

Spek, Josephus Antonius Wilhelmus van der

Cell mapping methods: modifications and extensions /
Josephus Antonius Wilhelmus van der Spek. - Eindhoven :
Eindhoven University of Technology
Thesis Eindhoven. - With ref. - With summary in Dutch.
ISBN 90-386-0183-2
Subject headings: non-linear dynamics / cell mapping /
chaos.

Druk: CopyPrint 2000, Enschede

Voor Petra

Contents

Summary	x
Abbreviations	xii
1 Introduction	1
2 Cell Mapping Methods	9
2.1 Simple cell mapping	9
2.1.1 Introduction	9
2.1.2 Cell state space	10
2.1.3 System evolution	10
2.1.4 Center point method	12
2.1.5 Example	13
2.1.6 Remarks	15
2.2 Generalized cell mapping	16
2.2.1 Introduction	16
2.2.2 Classification of cells	17
2.2.3 Limiting probability	18
2.2.4 Sampling method	18
2.2.5 Example	19
2.2.6 Remarks	20
2.3 Interpolated cell mapping	21
2.3.1 Introduction	21
2.3.2 Trajectory approximation	22
2.3.3 ICM criteria	24
2.3.4 Example	25
2.3.5 Remarks	26
2.4 Multiple mapping	28

2.4.1	Introduction	28
2.4.2	State space distortion	28
2.4.3	Multiple mapping concept	29
2.4.4	Example	30
2.4.5	Remarks	31
2.5	Recapitulation	32
3	Modifications of Cell Mapping Methods	33
3.1	Overview of modifications	33
3.2	CPU-time reduction for autonomous systems	34
3.2.1	Introduction	34
3.2.2	Van der Pol equation	35
3.2.3	Alternative approach	36
3.2.4	Aeroelastic nonlinear oscillator	38
3.2.5	Remarks	40
3.3	Modifications for discontinuous systems	41
3.3.1	Introduction	41
3.3.2	A forced zero-stiffness impact oscillator	42
3.3.3	Simple cell mapping	43
3.3.4	Interpolated cell mapping	45
3.3.5	Conclusion	47
3.4	Modified ICM procedure	48
3.4.1	Introduction	48
3.4.2	The modification	48
3.4.3	Examples	49
3.4.4	Conclusion	51
3.5	Mixed cell mapping	52
3.5.1	Introduction	52
3.5.2	Method explanation	52
3.5.3	Example: modified Duffing equation	53
3.5.4	Conclusion	54
3.6	Integration interval extension	55
3.6.1	Beam with nonlinear support	55
3.6.2	Simple cell mapping	56
3.6.3	Conclusion	58

4	Extensions of Cell Mapping Methods	59
4.1	Parameter variation methods for cell mapping	59
4.1.1	Introduction	59
4.1.2	PVSCM Method	60
4.1.3	PVICM method	67
4.1.4	Conclusions	70
4.2	Cell mapping for multi-DOF systems	71
4.2.1	Introduction	71
4.2.2	MDCM concept	72
4.2.3	MDCM method	73
4.2.4	MDCM algorithm	74
4.2.5	Application: 4-DOF beam with nonlinear support	79
4.2.6	Concluding remarks	80
5	Applications	83
5.1	Rotor with rubbing	83
5.1.1	Introduction	83
5.1.2	The rotor model	84
5.1.3	Investigation by means of ASCM	87
5.1.4	Discussion	92
5.1.5	Concluding remarks	92
5.2	Portable CD player under jogging condition	93
5.2.1	Introduction	93
5.2.2	The CD model	93
5.2.3	MDCM application	95
5.2.4	Concluding remarks	100
6	Conclusions and Guidelines	101
6.1	Conclusions	101
6.2	Guidelines	102
A	SCM algorithm	105
B	Interpolation Indices and Functions	107
C	Derivation of Equation (5.10)	109
	References	111
	Samenvatting	115

Summary

In this thesis, modifications and extensions of cell mapping (CM) methods are presented. CM methods are tools for the global investigation of the long term behaviour of nonlinear dynamic systems. By means of CM, periodic as well as chaotic solutions of the equations of motion can be determined. Additionally, application of CM enables the determination of the basins of attraction of the stable solutions.

First, an overview is given of existing CM methods. The *simple* cell mapping (SCM) method is based on a discretization of the state space in cells, followed by a determination—by means of numerical integration—of corresponding image cells. Groups of periodic cells represent the system's long term behaviour. The *generalized* cell mapping (GCM) method is a generalization of SCM. Because of the probabilistic approach involved, GCM is particularly suited for the description of chaotic behaviour. Under *interpolated* cell mapping (ICM), approximations of state space trajectories are created by means of interpolation. Finally, *multiple* mapping (MM) is a modification to ICM, yielding more accurate results in case of high state space distortions.

Next, some modifications are presented which increase the accuracy and efficiency of the existing CM methods. For autonomous systems, a dimension reduction method is given. Subsequently, modifications are given which are necessary to make cell mapping methods applicable to discontinuous systems. For ICM, a modification is introduced which speeds up the interpolation process. Further, a combination of ICM and MM is discussed, termed *mixed* cell mapping (MCM). Finally, the advantages are shown of using an extended integration interval under SCM.

In addition to these modifications, two substantial extensions of the existing CM methods are presented. The first extension contains a parameter variation technique, suited for the sensitivity-analysis of CM results with respect to system parameters. With this technique, the evolution of the basin boundaries due to a parameter variation can be obtained in relatively little

CPU-time. In this way, global bifurcations can easily be predicted. The introduced concept has been elaborated for both SCM and ICM.

The second extension is a new CM method, termed *multi-DOF* cell mapping (MDCM), which can be applied to systems of many degrees of freedom. Since the number of cells—and hence the CPU-time and storage requirements—grows exponentially with the state space dimension, application of conventional CM methods to these systems is very impractical. Under MDCM, the CPU-time grows only linearly with the system dimension while the order of the storage requirements remains constant.

For illustration purposes, application of CM methods is performed to two practical nonlinear dynamic systems. First, the global behaviour of a rotor with rubbing is investigated. Here, emphasis is put on the basins of attraction of a coexisting quasi-periodic and chaotic attractor, which correspond to a motion of roll and slip, respectively. Second, the 'joggability' of a portable CD player is studied. By means of MDCM, the response of the player to a periodic excitation is determined for a set of relevant initial conditions.

It is concluded that the presented modifications and extensions have merit. Further, the additional value of CM methods is emphasized with respect to more established methods of investigation, such as periodic solvers and regular numerical integration. Finally, general guidelines are given for the investigation of nonlinear dynamic systems as well as for the application of CM methods.

Abbreviations

ASCM	Alternative SCM
CD	Compact Disc
CM	Cell Mapping
CPU	Central Processing Unit
DOF	Degrees Of Freedom
GCM	Generalized Cell Mapping
ICM	Interpolated Cell Mapping
LP	Limiting Probability
MCM	Mixed Cell Mapping
MD	Multiple-Domicile
MDCM	Multi-DOF Cell Mapping
MICM	Modified ICM
MM	Multiple Mapping
MMM	Modified MM
MV	Mean Value
ODE	Ordinary Differential Equation
PG	Persistent Group
PVICM	Parameter Variation for ICM
PVSCM	Parameter Variation for SCM
SCM	Simple Cell Mapping
SD	Single-Domicile
TPICM	Tensor Product ICM

Chapter 1

Introduction

In engineering practice, there is a great need for efficient, powerful, and accurate methods to predict the long term dynamic behaviour of nonlinear mechanical structures. As important examples, one can think of rotordynamic systems, such as pumps and generators, or systems with nonlinear supports. In this thesis, a promising dynamic system investigation method is discussed in detail.

A theoretical approach in the prediction of dynamic behaviour is given by the procedure of mathematical modelling of the mechanical structure one is investigating. In this thesis, mechanical systems are considered which are discretized with respect to space. This approach results in a set of second order ordinary differential equations (ODE's):

$$\ddot{\mathbf{q}} = \mathbf{F}(\mathbf{q}, \dot{\mathbf{q}}, t, \boldsymbol{\mu}). \quad (1.1)$$

Here, $\mathbf{q} = [q_1(t) \dots q_l(t)]^T$ is the column containing the system's generalized coordinates, with l the number of degrees of freedom (DOF) of the system. Further, $\dot{\mathbf{q}}$ and $\ddot{\mathbf{q}}$ are the columns containing the velocities \dot{q}_i and the accelerations \ddot{q}_i , respectively ($i = 1, \dots, l$). The column $\boldsymbol{\mu} = [\mu_1 \dots \mu_k]^T$ contains the system parameters, such as the system frequency, the system damping, and so on. Finally, (\cdot) stands for differentiation with respect to time t . Defining the state of the system as $\mathbf{x} = [q_1 \dots q_l \ \dot{q}_1 \dots \dot{q}_l]^T$, (1.1) can be written as a set of N first order ODE's:

$$\dot{\mathbf{x}} = \bar{\mathbf{F}}(\mathbf{x}, t, \boldsymbol{\mu}). \quad (1.2)$$

Here, $N = 2l$ is the dimension of the state space. Both (1.1) and (1.2) are used in this thesis for the mathematical description of dynamic systems.

In most cases, the dynamic response of a mechanical structure results from excitation through an external force. In (1.1), this force is represented by means of the explicit dependence of the right-hand side F on time t . The study of the long term behaviour of a mechanical system is in particular relevant when the external force has a deterministic character, especially when it is periodic. For this reason, only periodic external forces are considered in this thesis. Hence, F satisfies

$$\mathbf{F}(\mathbf{q}, \dot{\mathbf{q}}, t + T, \boldsymbol{\mu}) = \mathbf{F}(\mathbf{q}, \dot{\mathbf{q}}, t, \boldsymbol{\mu}), \quad \forall t \geq 0, \quad (1.3)$$

where T is the period time of the external force. When the external force—and hence F —is time-independent, the system is called *autonomous*.

Having modelled the mechanical system by a set of ODE's, the next step is the determination of its long term behaviour, represented by the stable solutions. Finding the stable solutions of (1.1), also called *attractors*, has now become the first task for the investigator. Besides stable solutions, also unstable solutions of (1.1) may exist. These solutions represent *saddle solutions* and *repellers* of the mechanical system (see e.g. Thompson and Stewart [29]). Localization of these solutions may provide important additional information for the system behaviour and can be viewed as a second task for the investigator.

When a model is created for the relevant phenomena of the dynamic behaviour of a real mechanical system, two main features should be included in general. First, the model should be *dissipative*. In every real mechanical system, energy is being dissipated in a certain way, e.g. by damping, friction, or nonelastic collisions. This aspect should also be represented by the model. Second, the model should be *nonlinear*. Although linear models may be suited to obtain a first impression of the behaviour of a mechanical system, they will not necessarily be able to predict real characteristics of the behaviour. Hence, an accurate mathematical model of a mechanical system will mostly contain one or more nonlinear ODE's. This has some important consequences for the solution strategy of (1.1).

Whether a dissipative system is linear or nonlinear has great influence on the determination of its long term behaviour. In a dissipative linear system, only one steady-state long term solution for the generalized coordinates exists. This solution has the same frequency as the external force, while its amplitude is proportional to the amplitude of the external force. Each initial state of the system leads to this solution. The behaviour of the system before settling on the steady-state solution is called *transient* behaviour.

In contrast to linear systems which are relatively simple, a nonlinear system may reveal a broad spectrum of strange phenomena. In this, it is useful to note two important characteristics of a nonlinear system:

- Coexistence of attractors. Even when the system is dissipative, more than one attractor may exist for the same set of system parameters. To which one the system is attracted depends on its initial state.
- Occurrence of *chaotic* behaviour. Although being excited in a periodic way, the system may respond in a chaotic, i.e. nonperiodic way. When this chaotic behaviour is stable, one speaks of a chaotic attractor. In spite of the deterministic equations that describe the behaviour of the system, a chaotic motion is so extremely sensitive to changes in the initial state that it can be called *unpredictable*.

Additionally, many types of *bifurcations* may occur in nonlinear systems. Bifurcations are sudden changes of the solutions in multiplicity, form, type, magnitude, or stability, caused by a variation of a system parameter. For more information about nonlinear systems, chaos, and corresponding phenomena, the reader is referred to Thompson and Stewart [29].

To illustrate the two main features of a nonlinear system, the modified Duffing equation [29, page 101] is considered:

$$\ddot{q} + d\dot{q} - q + q^3 = a \cos(\omega t). \quad (1.4)$$

This equation models a vertical Euler support column, loaded beyond its buckling point, additionally harmonically excited with amplitude a and period $2\pi/\omega$ (see Fig. 1.1a). In the unforced case, this system has two stable equilibrium points at $q = 1$ and $q = -1$ (buckled states) and an unstable equilibrium point at $q = 0$. A small external harmonic force converts the stable equilibrium states to periodic attractors. For larger driving amplitudes, competing periodic and chaotic attractors may come into existence [29].

For $d = 0.15$, $a = 0.3$, $\omega = 1.0$, a periodic and a chaotic attractor coexist (Kreuzer [20]). This can be shown by means of numerical methods. Taking $q(0) = \dot{q}(0) = 1.0$, numerical integration yields a trajectory that converges to a periodic motion. On the other hand, an initial state of $q(0) = \dot{q}(0) = 0.0$ produces a trajectory that settles on a chaotic attractor. In Fig. 1.1, a time-history and a state space plot are shown for the periodic and the chaotic motion for $t = 0..100$.

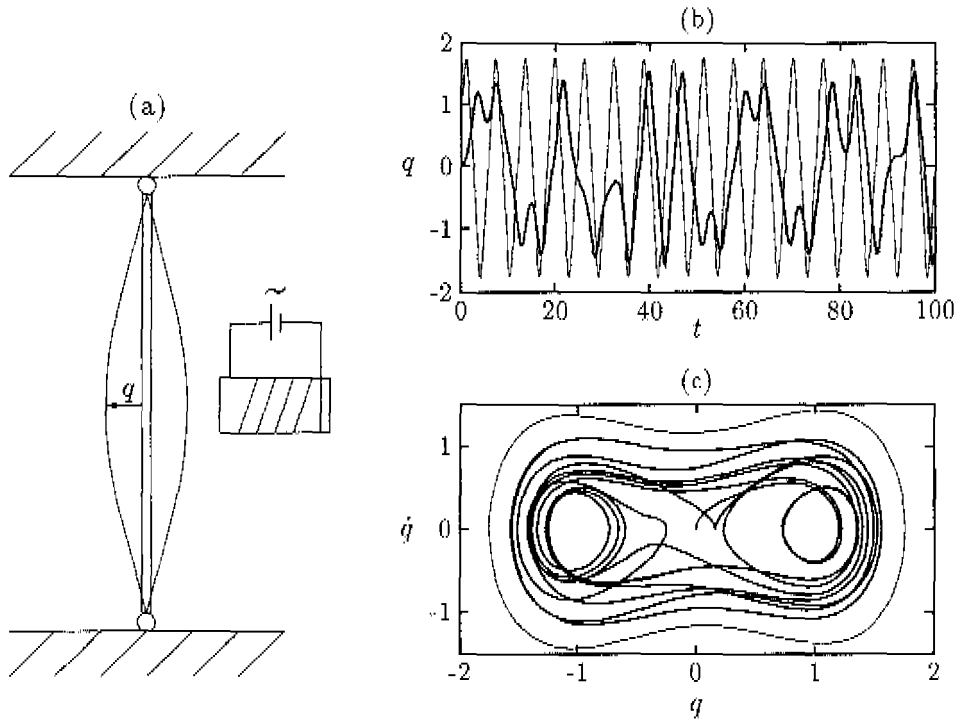


Figure 1.1: Attractors of the modified Duffing equation (1.4) for $d = 0.15$, $a = 0.3$, $\omega = 1.0$: periodic attractor (thin line) and chaotic attractor (thick line). (a) Corresponding system: Euler support column. (b) Time-history plot. (c) State space plot.

To get a better insight in the chaotic motion of the considered system, it is useful to inspect the state (q, \dot{q}) of the system at discrete equidistant times $t = t_0 + nT$, $n = 0, 1, \dots$, where $T = 2\pi/\omega$ is the system's forcing period and $t_0 \in [0, T)$. The collection of states obtained in this way is called a *Poincaré section*. Fig. 1.2 shows a Poincaré section of the periodic and chaotic attractor for $t_0 = 0$ and $n = 0, 1, \dots, 5000$.

With this example in mind, the question arises how to investigate a nonlinear system. For this purpose, one can make use of several kinds of methods and tools. Numerical integration can be applied, in the form of various schemes, as was done in the example mentioned above. However, different initial states may lead to different attractors. Hence, the equations of motion may have to be integrated for numerous initial states to locate all attractors.

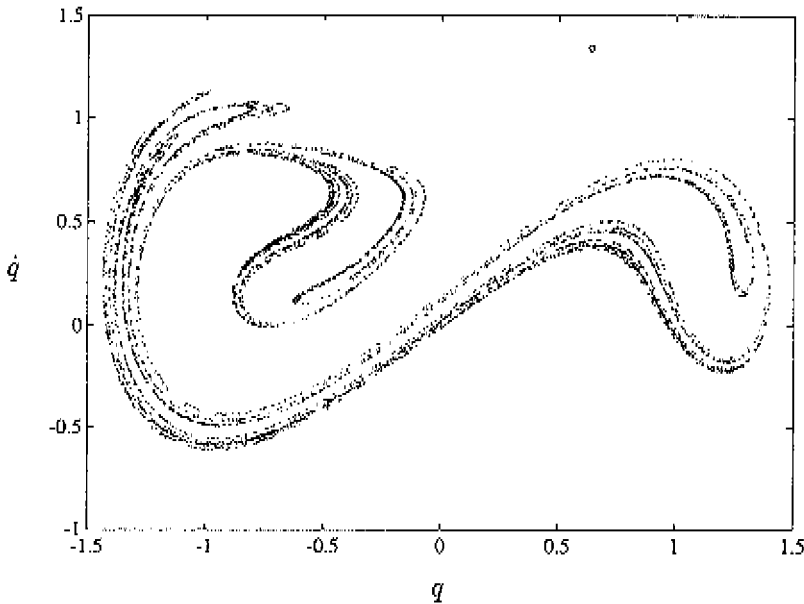


Figure 1.2: Poincaré section of coexisting periodic (\circ) and chaotic (\cdot) attractors of the modified Duffing equation (1.4) for $d = 0.15$, $\alpha = 0.3$, $\omega = 1.0$.

For the determination of periodic behaviour in nonlinear dynamic systems, several methods exist, of which the *time discretization* method and the *shooting* method are most known (Van de Varst [37], Crooijmans [3], Fey [8], Meijaard [24]). For a certain initial approximation, these methods provide a periodic solution (if there exists one) in most cases. By means of a *path-following* method, the evolution of this periodic solution can be followed when a particular system parameter is varied, including the passage of bifurcation points. However, no information can be obtained about possible chaotic attractors or other, coexisting, periodic attractors.

The feature of coexistence of attractors gives rise to an extra task in the investigation of nonlinear systems. Besides locating a specific attractor and studying the influence of system parameters (bifurcation research) on this attractor, an additional subject of investigation is found in the determination of a global overview of attractors and *basins of attraction*. A basin of attraction is the set of all initial states leading to a particular attractor. In Fig. 1.3, the basins of attraction are shown for the two attractors of the mod-

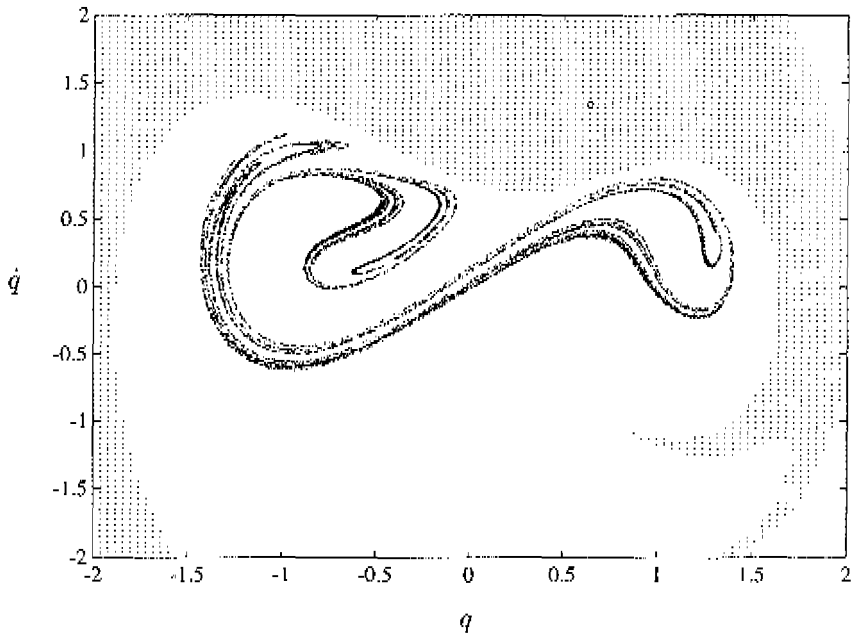


Figure 1.3: Attractors and basins of attraction of the modified Duffing equation (1.4) for $d = 0.15$, $a = 0.3$, $\omega = 1.0$: Periodic attractor (\circ) and basin of attraction ($::$); chaotic attractor (\cdot) and basin of attraction (left blank).

ified Duffing equation (1.4) in the region $-2 \leq q, \dot{q} \leq 2$. This picture was obtained by numerical integration of (1.4) with $(q(0), \dot{q}(0)) = (ih, jh)$, $h = 0.04$, $i, j = -50, \dots, 50$. Trajectories that showed no convergence to the periodic attractor in less than 40 excitation periods were considered to settle on the chaotic attractor. This way of determining the basins of attraction is very time-consuming.

Knowledge about the basins of attraction can be important from an engineering point of view. These basins give an idea of the robustness of the existing solutions with respect to changes in the initial conditions. When a specific solution is desired, it can be investigated for which system parameter values the corresponding basin of attraction is optimal in the sense that it covers all the relevant initial states of the mechanical system. Determination of the basins of attraction can therefore be of great use in the design of mechanical structures.

A new approach in the dynamic behaviour investigation of a nonlinear system was introduced with the *cell mapping* method (Hsu [12, 14]). The cell mapping method is based on a discretization of the state space in so-called *cells*. This special approach makes it possible to find all attractors—periodic and chaotic—of the system, as well as their corresponding basins of attraction, in a bounded subset of the state space.

Three main types of cell mapping (CM) can be distinguished: *simple* cell mapping (SCM), *generalized* cell mapping (GCM), and *interpolated* cell mapping (ICM). The SCM method is a robust and efficient tool for the detection of attractors and the determination of basins of attraction. The GCM method is more suited when dealing with chaotic behaviour or with basins of attraction with fractal basin boundaries. The ICM method is a sophisticated deduction of SCM, in which the original concept of cells is combined with interpolation methods, yielding more accurate results (Tongue [30, 31]).

The CM method is the subject of research presented in this thesis. In Chapter 2, the existing cell mapping methods are presented. This includes SCM, GCM, as well as ICM. Further, a variation on ICM termed *multiple mapping* (MM) (Tongue [32]) is discussed. The above-mentioned modified Duffing equation is used as example of application for all methods.

Modifications to the existing CM methods in order to get more accurate results or a more efficient algorithm are presented in Chapter 3. Especially, a strategy is shown for applying CM methods to discontinuous dynamic systems, which are frequently met in engineering practice [24].

In Chapter 4, two main extensions of the existing methodology are presented and discussed. The first extension contains a parameter variation technique for CM. This technique enables the determination of the basins of attraction, initially obtained by SCM or ICM, for a varied system parameter value in relatively little CPU-time. The second extension deals with the tackling of systems of many DOF's. Since the number of cells grows exponentially with the system dimension, regular application of CM methods will cause computational problems for systems with state space dimension $N > 4$.

Part of the methods, modifications, and extensions discussed in Chapters 2, 3, and 4 are applied to two practical dynamic systems in Chapter 5. The global behaviour of a rotor with rubbing as well as the motion of a portable CD player during jogging are investigated. Both applications are modelled by 2-DOF models.

This thesis is finished with conclusions and guidelines in Chapter 6.

All numerical results in this thesis were produced on a Silicon Graphics IRIS R4000 32 Mb workstation, unless stated otherwise. Numerical integration was carried out by means of a fourth-order six-stage Runge-Kutta scheme (England [6]) with variable time step. The applied scheme is especially suited for the integration of sets of nonlinear ODE's (England [7], Lambert [21, page 133]). In practice, the choice of the integration scheme should be adjusted to the characteristics of the considered ODE's.

Chapter 2

Cell Mapping Methods

In this chapter, an overview is given of existing cell mapping methods. In Section 2.1, an outline is given of the simple cell mapping (SCM) method. The generalized cell mapping (GCM) method, is discussed in Section 2.2. In Section 2.3, the interpolated cell mapping (ICM) method is treated. Additionally, a variation on ICM, termed multiple mapping (MM), is presented in Section 2.4. The modified Duffing equation, discussed in Chapter 1, is used as example of application. Chapter 2 is closed with a discussion on the existing cell mapping methods.

2.1 Simple cell mapping

2.1.1 Introduction

When using numerical techniques to solve (dynamic) problems, roundoff errors are introduced due to the computer's limited precision. Moreover, in experimental methods a limited measurement accuracy exists. This means that in both numerical and experimental methods physical quantities cannot be obtained exactly. A state variable, describing part of the state of a dynamic system, should therefore not be regarded as a continuous variable, which can assume every possible value $x \in \mathbb{R}$, but as a discrete quantity.

This motivation was used by Hsu to defend the concept of the SCM method [12]. Under SCM, the state space \mathbb{R}^N or part of it is divided into a discrete collection of N -dimensional *cells*, where N is the state space dimension. Restricting the state of the system to this set of cells enables the efficient determination of all attractors and basins of attraction. The discretized state space is called *cell state space*.

2.1.2 Cell state space

A dynamic system with Euclidian state space \mathbb{R}^N is considered ($N \geq 2$). Generally, the state of a dynamic system is restricted to a bounded subset of the state space. For convenience, this subset, denoted by Ω , is taken to be rectangular. Let $\mathbf{x} = [x_1 \dots x_N]^T$ be the state vector, then for each state variable x_i a lower and upper boundary $x_i^{(l)}$ and $x_i^{(u)}$ exist:

$$x_i^{(l)} \leq x_i \leq x_i^{(u)}, \quad i = 1, \dots, N.$$

To create a cell state space, Ω is divided into cells. In principle, the cells can be of arbitrary form, as long as they fill up Ω . Practically, the choice of rectangular cells is preferable. The division of Ω in rectangular cells can be realized by dividing each interval $[x_i^{(l)}, x_i^{(u)}]$ into M_i intervals of equal length h_i . Hence,

$$h_i = \frac{x_i^{(u)} - x_i^{(l)}}{M_i}, \quad i = 1, \dots, N. \quad (2.1)$$

In this way, Ω is divided into M rectangular cells, with

$$M = \prod_{i=1}^N M_i. \quad (2.2)$$

Each cell is denoted by an index $j \in \{1, \dots, M\}$. The region $\mathbb{R}^N \setminus \Omega$ is called the *sink cell* and is denoted by index 0. The cells in Ω are called *regular cells*. In Fig. 2.1, a cell state space is shown for $N = 2$.

The fundamental step in the SCM theory is the following: The state of the system at time t is no longer described by the state vector $\mathbf{x}(t)$, but by the index $\xi(t) \in \{0, \dots, M\}$ of the cell containing the state vector. Hence,

$$\xi(t) = j \iff \mathbf{x}(t) \in \text{cell } j.$$

All possible states within one cell are denoted by the same index and are therefore treated as one and the same state. Hence, a cell can be regarded as an indivisible entity of the state of the system.

2.1.3 System evolution

Next, the description of the system evolution in time in terms of cells is considered. By inspecting the state of the system at discrete equidistant times, the evolution of the system is given by a sequence of positive integers

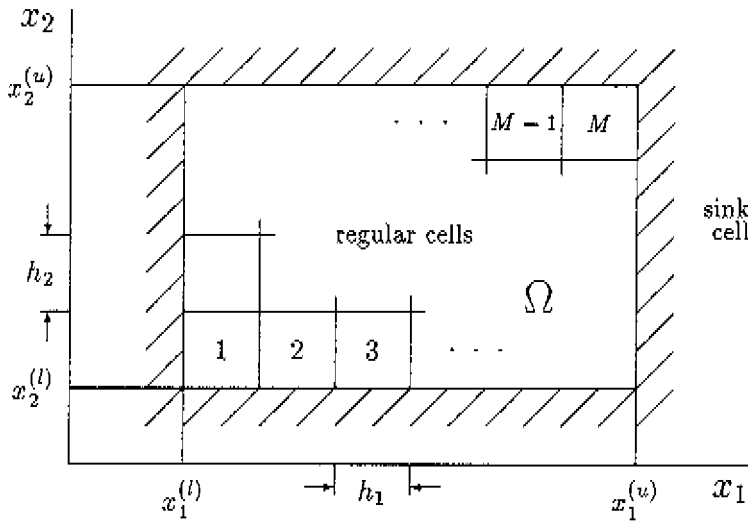


Figure 2.1: Discretization of a two-dimensional state space.

$\xi(0), \xi(1), \xi(2), \dots$. Here, $\xi(n)$ corresponds to the cell containing the state of the system at $t = n\Delta t$, ($n = 0, 1, 2, \dots$), with Δt the time between two state inspections.

In this thesis, only evolutions are considered which satisfy

$$\xi(n + 1) = C(\xi(n)). \tag{2.3}$$

The mapping $C : \mathbb{N} \rightarrow \mathbb{N}$ is called a SCM. By (2.3), it is implied that the next state of the system is completely determined by its current state and is explicitly independent of the mapping step n . In the next subsection, it is shown how to create such a mapping C for a system governed by a set of ODE's.

When the system enters the sink cell, its evolution is no longer followed. By definition, the system stays there forever. Hence

$$C(0) = 0.$$

Under SCM, two kinds of regular cells are distinguished: *periodic* and *transient* cells. A cell ξ satisfying

$$\xi = C^m(\xi)$$

for some $m \in \mathbb{N}$, is called a periodic cell with *period* m , or simply, a $P - m$ cell. Here, C^m denotes the cell mapping C applied m times. If a cell ξ is a $P - m$ cell, then the cells $C(\xi), \dots, C^{m-1}(\xi)$ are also $P - m$ cells. Such a group of periodic cells is called a *periodic group* of m cells, or $P - m$ group. By definition, the sink cell is a $P - 1$ cell. Periodic groups represent the long term behaviour of the investigated system.

A cell ξ which is not periodic is called a *transient* cell. Since the number of regular cells is finite, only two possibilities exist for a transient cell: it is mapped onto a regular periodic cell in a finite number of steps, or it is mapped into the sink cell in a finite number of steps. Transient cells of the former kind represent the basins of attraction of the periodic groups.

From the above possibilities it is evident that in the context of simple cell mapping only periodic motions occur. Due to the finite number of cells, the system sooner or later will enter the sink cell or a previously entered cell. Yet, the cell mapping approach is applicable to systems which exhibit chaotic behaviour when taking the following assumptions for granted (Kreuzer [20]):

- Chaotic motions are represented by periodic groups of relatively long period.
- A chaotic attractor is represented by a set of cells covering part of the attractor in state space.

Concerning the *stability* of a periodic group, the following conventions are made: A periodic group is stable when it is surrounded by transient cells leading to this group. When a periodic group has no corresponding transient cells, it is a repeller. In all other cases, the group is a saddle solution.

When for all cells in the region of interest the image cell has been found, it can be determined to which periodic group each cell belongs, as a periodic or as a transient cell. In the context of SCM, the dynamic behaviour in the region of interest has completely been determined then. In Hsu [14], an algorithm is given for the determination of periodic groups and corresponding transient cells. In Appendix A, this algorithm is briefly discussed.

2.1.4 Center point method

For a system governed by a set of ODE's, a SCM can be created by means of the *center point method* ([14, page 153]). According to this method, the image cell $C(\xi)$ of a regular cell ξ is determined as follows:

- Calculate the center point of cell ξ .

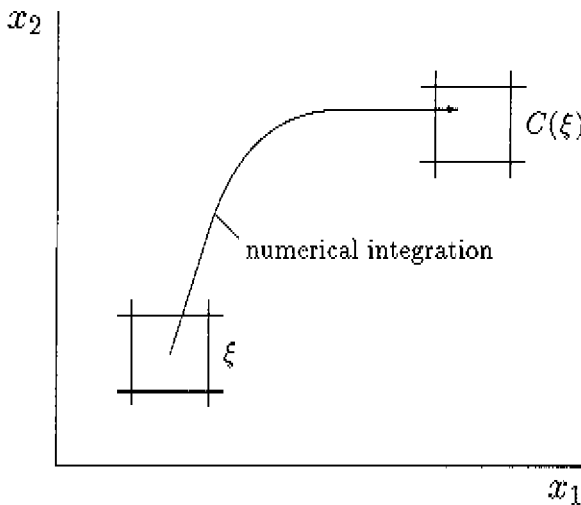


Figure 2.2: Center point method in a two-dimensional state space.

- Integrate the set of ODE's over a period Δt using the center point as initial state. Here, Δt is the time between two state inspections.
- Determine the image cell $C(\xi)$ which contains the end point of the calculated trajectory.

Hence, the center point is used as a reference point for each cell. In Fig. 2.2, the center point method is illustrated for a system with two-dimensional state space.

When the system is explicitly dependent on time in a periodic way, the interval Δt between the state inspections should be chosen equal to the corresponding period T . In doing so, a SCM is obtained that is independent of the mapping step n . For autonomous systems, Δt can be chosen arbitrarily, provided that it is not too small (Section 3.2, Hsu[14, page 154]).

2.1.5 Example

As an example, the modified Duffing equation (1.4) is considered. Defining $x_1 = q$, $x_2 = \dot{q}$, (1.4) is transformed into

$$\begin{aligned} \dot{x}_1 &= x_2, \\ \dot{x}_2 &= -dx_2 + x_1 - x_1^3 + a \cos(\omega t). \end{aligned} \tag{2.4}$$

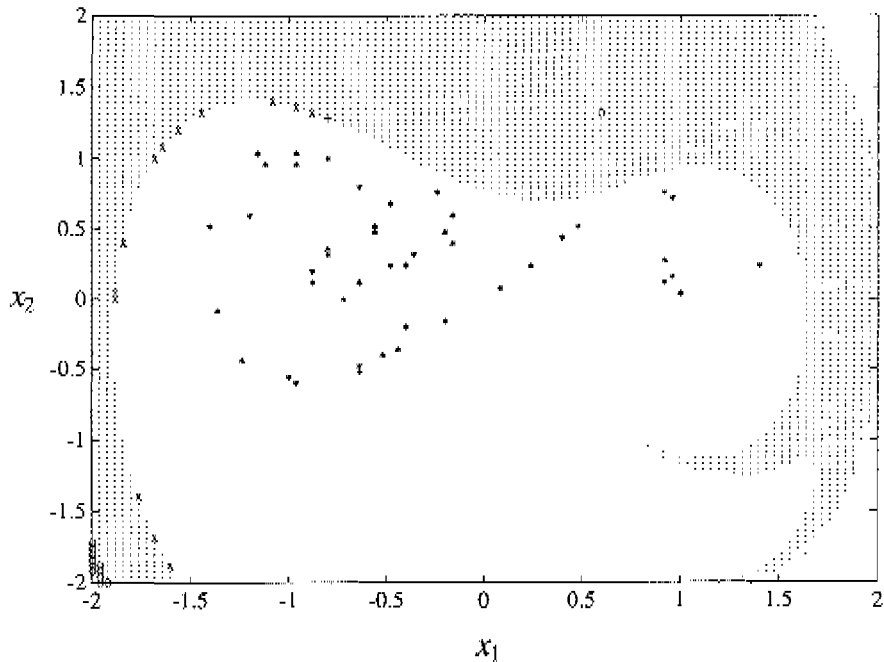


Figure 2.3: SCM results for the modified Duffing equation (2.4) for $d = 0.15$, $a = 0.3$, $\omega = 1.0$: Stable $P - 1$ group (\circ) and transient cells (\cdot); stable periodic groups ($*$) and transient cells (left blank); $P - 1$ group ($+$) and transient cells (\times); cells mapped into the sink cell (\circ , lower left corner).

The region of interest Ω is defined as $-2.02 \leq x_1, x_2 \leq 2.02$. Taking $h_1 = h_2 = 0.04$, which implies $M_1 = M_2 = 101$, the total number of regular cells is given by $M = 10201$. By means of the center point method, the image cell of each regular cell is determined. The integration interval is chosen equal to the excitation period: $\Delta t = 2\pi/\omega$.

In Fig. 2.3, the results are shown for $d = 0.15$, $a = 0.3$, $\omega = 1.0$:

- A $P - 1$ cell (\circ) (center point $(0.6, 1.32)$) with a large basin of attraction (\cdot). The cell represents the stable periodic solution with period Δt .
- A $P - 19$, a $P - 16$, and a $P - 10$ group ($*$), together representing the chaotic attractor. The corresponding basins of attraction are left blank.

- A $P - 1$ cell (+) (center point $(-0.8, 1.28)$) with a basin of attraction consisting of 13 cells (x), positioned at the boundary separating the basins of attraction of the periodic and the chaotic attractor. Hence, this cell represents a saddle solution.
- 11 Cells (o) which are mapped into to the sink cell.

Comparing these results with the results obtained by numerical integration in Chapter 1, it can be concluded that the periodic attractor as well as its basin of attraction are determined quite accurately. The chaotic attractor is represented by three periodic groups of relatively long period. The basins of attraction of these groups give a good approximation of the chaotic attractor's actual basin of attraction as determined in Chapter 1. Additionally, the saddle solution, whose stable manifolds separate the two basins of attraction, is found under SCM. The position of the saddle solution with respect to the attractors plays an important role in bifurcation research. Finally, it should be noted that the CPU-time needed for SCM is only 1.5% of the required CPU-time for numerical integration (see Table 2.1 at the end of this chapter).

2.1.6 Remarks

The SCM method is a robust tool for obtaining a global impression of the dynamic behaviour of a nonlinear system. Attractors and basins of attraction can be determined quite accurately. Periodic groups of relatively long period indicate the possible existence of chaotic behaviour. The capability of determining repellers and saddle solutions depends on the cell size and the position of the actual solution with respect to the cell boundary.

For more detailed information about a determined periodic group, a regular numerical integration may be performed, taking the center point of one of the periodic cells as initial state. In this way, the type and position of the attractor are easily obtained. This was done for the periodic groups in the considered example, thus obtaining the relation between the $P - 19$, $P - 16$, and $P - 10$ group. To determine the type of a solution, also the *Liapunov exponents* can be calculated (see e.g. [29]).

When the basin boundaries are fractal, the SCM method does not determine them very precisely. In particular, this holds when the fractal boundary layers are small with respect to the applied cell size. For those cases, the GCM method will produce more accurate results. This method is treated in the next section.

2.2 Generalized cell mapping

2.2.1 Introduction

Under SCM, each regular cell is mapped onto a *single* image cell. In reality, the image of a cell will be given by some bounded region, covering more than one cell, as shown in Fig. 2.4. This means that for each regular cell the number of image cells should not be restricted to one. This is the idea behind the concept of GCM (Hsu [13], Hsu et al. [15]).

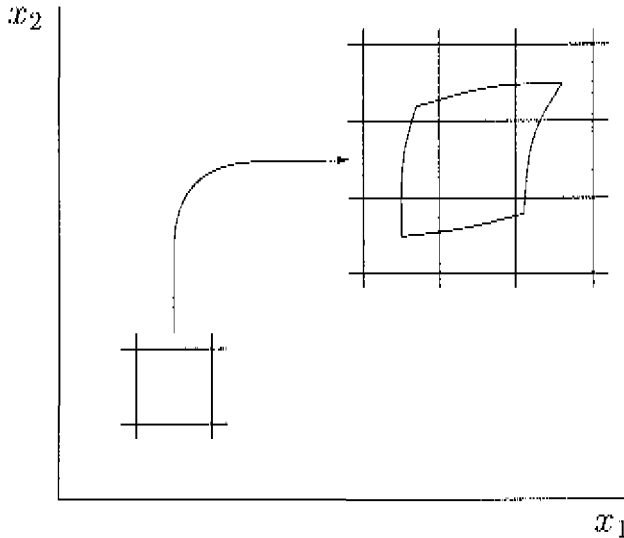


Figure 2.4: Real image of a cell, covering several cells.

Under GCM, a regular cell can have several image cells, each with a fraction of the total probability. The state of the system at $t = n\Delta t$, with Δt the time between two state inspections, is denoted by the cell probability vector $\mathbf{p}(n) = [p_1(n) \dots p_M(n)]^T$. Here, M is the total number of regular cells and

$$p_i(n) = \text{Prob}\{\xi(n) = i\}, \quad n \in \mathbb{N}, \quad i = 1, \dots, M. \quad (2.5)$$

In words, $p_i(n)$ denotes the probability of the state of the system being in cell i at $t = n\Delta t$.

To describe the system evolution, the *transition probability matrix*, or

simply *transition matrix*, $\mathbf{P}(n) = (p_{ij}(n))$ is introduced, with

$$p_{ij}(n) = \text{Prob}[\xi(n+1) = i \mid \xi(n) = j], \quad n \in \mathbb{N} \quad i, j = 1, \dots, M. \quad (2.6)$$

Here, $p_{ij}(n)$ is the *transition probability* from cell j at $t = n\Delta t$ to cell i at $t = (n+1)\Delta t$. For a periodically excited system, the time step Δt between two state inspections can be chosen equal to the system period, in which case p_{ij} , and hence P , are independent of the mapping step n . For the sink cell (index 0), the following holds by definition:

$$p_{i0} = \begin{cases} 1 & i = 0 \\ 0 & \text{otherwise.} \end{cases} \quad (2.7)$$

By means of the introduced definitions, the evolution of the system can be put in the following form:

$$\mathbf{p}(n+1) = \mathbf{P}\mathbf{p}(n). \quad (2.8)$$

By (2.8), a finite, discrete, stationary Markov chain is defined (see e.g., Isaacson and Madsen [16]).

The transition matrix \mathbf{P} fully determines the dynamic behaviour of the system. The attractors and basins of attraction may be found by examining the properties of \mathbf{P} by means of the theory of Markov chains. First, some definitions of this theory are introduced.

2.2.2 Classification of cells

According to the theory of Markov chains, two types of cells can be distinguished under GCM: *persistent* and *transient cells*. A persistent cell i has the property that when the system is in i at a certain moment, it will return to i at some time in the future. Following the Markov theory, persistent cells can be formed into *persistent groups* (PG's), which are closed. When the system enters a persistent cell, it will stay in the PG to which this cell belongs. The PG's of a Markov chain, deduced from a dynamic system, correspond to the attractors of that system. By definition, the sink cell is a persistent group by itself.

When a cell is not persistent, it is transient by definition. For finite Markov chains, the system will leave the transient cells with probability one and will settle on a PG. Transient cells can be divided in *single-domicile* (SD) and *multiple-domicile* (MD) cells, according to the number of domiciles (one or more than one, respectively). Starting in a SD cell, the system will lead

to a particular PG with probability one. Hence, the collection of SD cells of a PG represents the corresponding basin of attraction. Starting in a MD cell, the system can lead to several PG's with corresponding probabilities, the sum of which of course equals one. The MD cells represent the basin boundaries, also called *separatrices*.

2.2.3 Limiting probability

For each cell i of a PG one can determine the *limiting probability* (LP) p_i^* , which is the probability of the system being in i at $t = \infty$ under condition that it ever entered the PG to which i belongs. In Hsu [14], algorithms are given for the determination of the LP distribution of a persistent group.

Especially for PG's consisting of many cells, the LP distribution can give some useful information. Such PG's usually represent chaotic attractors. The LP distribution then gives an idea of which parts of the attractor are 'visited' very frequently by the system and which parts very rarely. Thus, a better picture is obtained of the chaotic attractor as a whole.

2.2.4 Sampling method

The main part of constructing a GCM is the determination of the cell transition probabilities. When applying the GCM method to a system governed by a set of ODE's, the transition probabilities can be determined by means of the *sampling method* [14, page 268]:

- Choose for a regular cell j L points, in some way distributed over j .
- Integrate the set of ODE's over a period Δt , using these points as initial states. Again, Δt is the time between two state inspections.
- Determine the cells which contain the end points of the calculated trajectories. These cells are taken to be the image cells of cell j .

Let l be the number of image cells, with index i_1, \dots, i_l , containing L_{i_1}, \dots, L_{i_l} end points, respectively. The cell transition probabilities p_{ij} , $i = 0, \dots, M$, are now defined as follows:

$$p_{ij} = \begin{cases} L_i/L & i \in \{i_1, \dots, i_l\}, \\ 0 & \text{otherwise.} \end{cases} \quad (2.9)$$

Doing this for each regular cell j yields the transition matrix P .

2.2.5 Example

The GCM method is applied to the modified Duffing equation (2.4) with $d = 0.15$, $a = 0.3$, $\omega = 1.0$. The same region of interest Ω is used as under SCM ($|x_i| \leq 2.02$, $i = 1, 2$). Again, Ω is divided into 101×101 cells. The transition probabilities are calculated with the sampling method, using 9 integration points for each cell. Algorithms given by Hsu [14] are used to determine the PG's, the SD and MD cells, and the LP distribution. In Fig. 2.5, the results of this simulation are shown:

- A PG consisting of 10 cells (x) corresponding to the periodic attractor. The basin of attraction of this PG is given by its SD cells (·).
- A PG consisting of 966 cells (o) corresponding to the chaotic attractor. The basin of attraction (the SD cells) is given by the white area in Fig. 2.5.
- 6 Cells (+) which are mapped into the sink cell.
- A large number of MD cells (*).

Fig. 2.6 shows the LP distribution for both PG's. For each persistent cell, the LP is expressed in the mean value (MV) which equals $1/10$ for the PG representing the periodic attractor and $1/966$ for the PG representing the chaotic attractor. Cells denoted by 'x', have a LP value of $f \cdot MV$, with $f \geq 1.5$. For cells denoted by '+' and '.', we have $f \in [0.5, 1.5)$ and $f \in [0.0, 0.5)$, respectively.

Finally, to obtain a better picture of the basins of attraction, the MD cells have been divided in two groups: cells leading to the periodic solution with probability $p > 0.5$ (o), and cells leading to the chaotic attractor with probability $p > 0.5$ (*) (Fig. 2.6). This information has been obtained by determining the *group absorption* probabilities for the MD cells (see e.g. [14]). For this purpose, use has been made of an algorithmic approach given by Bestle and Kreuzer [1].

Compared to SCM, the chaotic attractor has been determined more accurately under GCM (several periodic groups versus one PG). The periodic attractor is represented by a small PG, which is not as accurate as the $P - 1$ cell found with SCM. The domains of attraction have been determined just as accurate as under SCM. The saddle solution has not been found under GCM.

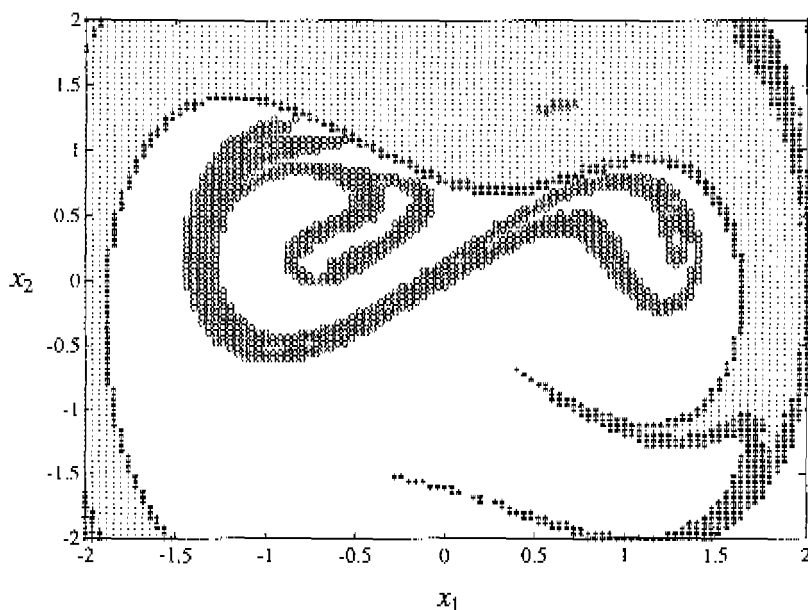


Figure 2.5: GCM results for the modified Duffing equation (2.4): PG (\cdot), representing the periodic attractor, and transient cells (\cdot); PG (\circ), representing the chaotic attractor, and transient cells (left blank); MD cells ($*$); cells mapped into the sink cell ($+$).

2.2.6 Remarks

The GCM method is very suited for the description of chaotic behaviour. The PG that represents a chaotic attractor gives a good picture of this attractor in general. Further, additional properties of chaotic attractors can be determined, such as the LP distribution or the largest Liapunov exponent (Kim and Hsu [18]). Under GCM, the basins of attraction of all stable solutions are determined more accurately than under SCM in general. When two basins of attraction are separated by a thick layer of MD cells, additional research has to be done to obtain an accurate separatrix.

On the other hand, periodic solutions are not found as accurate as with SCM. Repellers and saddle solutions are generally not found at all. Therefore, the GCM method may be considered as a very useful addition to SCM, especially if one is interested in chaotic attractors and their properties.

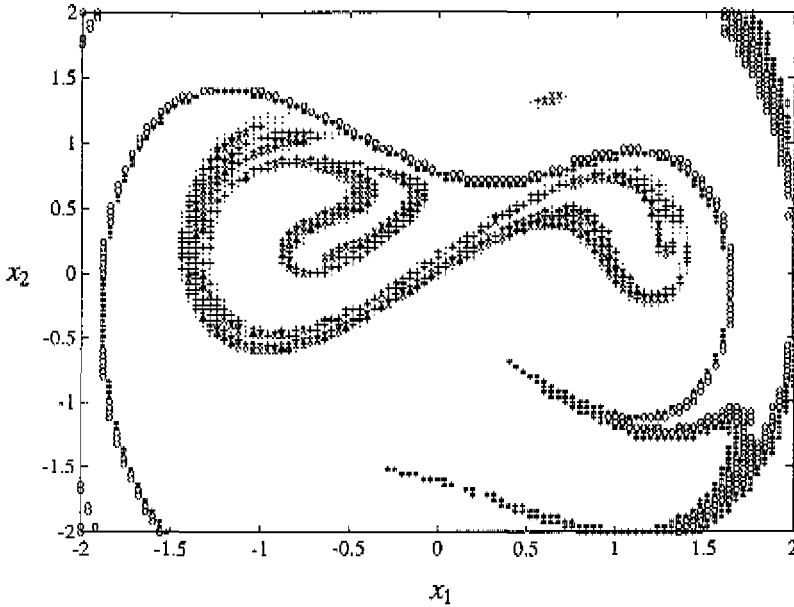


Figure 2.6: Probabilistic properties of the PG's and the MD cells.

2.3 Interpolated cell mapping

2.3.1 Introduction

In spite of the satisfying results found with the cell mapping methods discussed so far, two important drawbacks of these methods need to be stressed. First, because of the finite number of cells, a restriction is placed on the period length of a solution. Hence, chaotic behaviour is always represented by a finite number of cells. Second, due to the discretization of the state space, errors have to be taken into account when determining the system's dynamic behaviour. Especially for systems with fractal basins of attraction, the SCM and GCM methods may produce spurious results.

These drawbacks motivated Tongue to introduce the ICM method [30, 31]. The concept of ICM is actually very different from SCM and GCM. Under the latter ones, cells are being mapped onto image cells. By repeated mapping application, structures of cells are found which show some kind of recurrent character. Additional research is required to obtain the actual

type of behaviour (periodic, quasi-periodic, or chaotic).

Compared with SCM and GCM, ICM is a more straightforward technique which approximates numerical integration. For an arbitrary initial state, an approximate trajectory can be created. After transient behaviour has vanished, this trajectory will settle on an attractor. The initial state can then be added to the corresponding basin of attraction. Doing this for a huge number of initial states in a region of interest Ω , the attractors and basins of attraction in Ω can be obtained.

2.3.2 Trajectory approximation

In the N -dimensional state space, the region of interest Ω is uniformly covered with M grid points¹, denoted by \mathbf{x}^i , $i = 1, \dots, M$. Here, M is given by (2.2) with M_i the number of grid points in x_i -direction ($i = 1, \dots, N$). The corresponding distance h_i between two neighbouring grid points satisfies

$$h_i = \frac{x_i^{(u)} - x_i^{(l)}}{M_i - 1}, \quad i = 1, \dots, N, \quad (2.10)$$

where $x_i^{(u)}$ and $x_i^{(l)}$ denote the upper and lower boundary, respectively, of x_i . In Fig. 2.7, an ICM grid is shown for a two-dimensional state space.

For each grid point \mathbf{x}^i , a sequence of image points $\phi^{i,1}, \phi^{i,2}, \dots$ is constructed. Here, $\phi^{i,n}$ represents the approximate state of the system at $t = n\Delta t$, $n = 1, 2, \dots$ corresponding to an initial state \mathbf{x}^i . Hence,

$$\phi^{i,0} = \mathbf{x}^i, \quad i = 1, \dots, M.$$

Again, Δt equals the excitation period of the system. For autonomous systems, Δt is arbitrary but fixed. For each grid point \mathbf{x}^i , the first image point $\phi^{i,1}$ is obtained by numerical integration and denoted by \mathbf{y}^i . Hence,

$$\phi^{i,1} = \mathbf{y}^i, \quad i = 1, \dots, M.$$

The second image point $\phi^{i,2}$ is determined by means of interpolation. To this end, the 2^N grid points which surround $\phi^{i,1}$ are used as interpolation points. Let l_1, \dots, l_{2^N} be the indices of the interpolation points, then

$$\phi^{i,2} = \sum_{j=1}^{2^N} P_j(\mathbf{y}^i) \mathbf{y}^{l_j}, \quad i = 1, \dots, M. \quad (2.11)$$

¹In the original ICM concept, Ω is divided into cells of which the center points serve as initial states for approximate trajectories. Since cells do not play an actual role in ICM, they are not mentioned here.

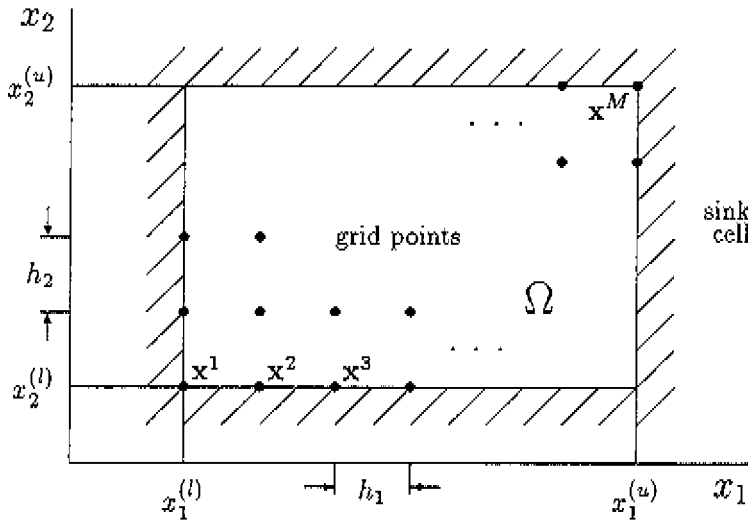


Figure 2.7: ICM grid for a two-dimensional state space.

Here, $P_j : \mathbb{R}^N \rightarrow [0, 1]$ is an interpolation function satisfying

$$P_j(\mathbf{x}^{i'}) = \delta_{ij}, \quad i, j \in \{1, \dots, 2^N\},$$

where δ_{ij} is the Kronecker delta. In Appendix B, general expressions are given for the interpolation point indices and the interpolation functions. For $N = 2$, the following holds:

$$\begin{aligned} \phi^{i,2} &= (1 - \xi_1)(1 - \xi_2)\mathbf{y}^{i_1} + \xi_1(1 - \xi_2)\mathbf{y}^{i_2} \\ &+ (1 - \xi_1)\xi_2\mathbf{y}^{i_3} + \xi_1\xi_2\mathbf{y}^{i_4}, \quad i = 1, \dots, M, \end{aligned} \tag{2.12}$$

with,

$$\xi_k = \frac{y_k^i - x_k^{i_1}}{h_k}, \quad k = 1, 2,$$

and h_k given by (2.10). In Fig. 2.8, the integration and first interpolation step are illustrated for a two-dimensional state space.

The trajectory points $\phi^{i,n}$, $n = 3, 4, \dots$, are obtained by application of the interpolation formula (2.11) replacing \mathbf{y}^i by $\phi^{i,n-1}$, for $i = 1, \dots, M$. By repeated application of (2.11), an approximate trajectory of desired length is obtained.

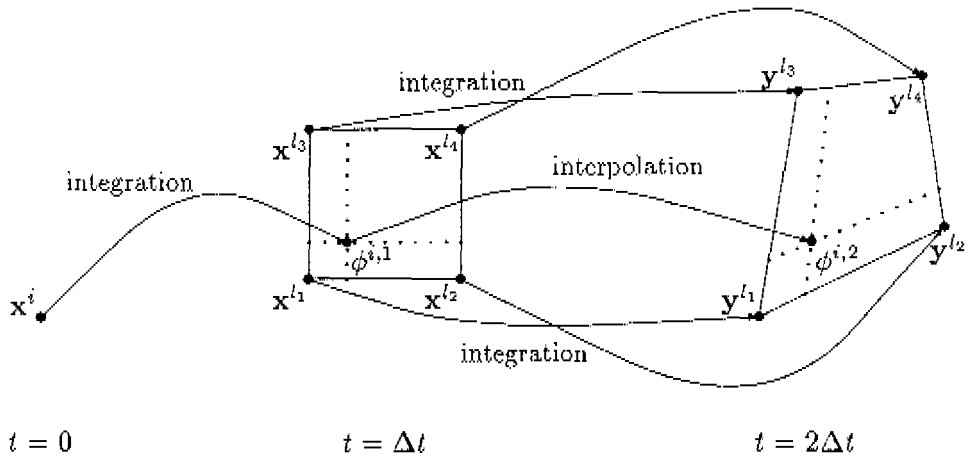


Figure 2.8: ICM procedure for a two-dimensional state space: Integration step and first interpolation step.

2.3.3 ICM criteria

For the classification of an approximate trajectory, two criteria are introduced. A sequence $\phi^{i,n}$, $n = 0, 1, 2, \dots$, is considered periodic at step l if

$$|\phi^{i,l} - \phi^{i,j}| < \text{EPS} \quad (2.13)$$

for some $j \in \{0, 1, \dots, l-1\}$ and a beforehand chosen accuracy EPS. The inequality (2.13) is called the *periodicity* criterion. A sequence which satisfies (2.13) corresponds to a periodic attractor with period $(l-j)\Delta t$. Whenever a new point in the sequence has been determined, the most efficient way of checking the periodicity criterion is downwards from $j = l-1$ to 0, since low order subharmonic behaviour is more likely to occur than high order in practice. To save CPU-time, it deserves recommendation to stop checking (2.13) when e.g. $j < l-10$.

To limit the—maybe never ending—search for periodic behaviour, the number of iteration steps in the ICM procedure by definition is bounded by the integer IMAX. When no periodic behaviour has been found within IMAX iterations, the sequence is considered to be chaotic. This is called the *chaos* criterion. It is not very obvious how to choose IMAX. If IMAX is too small, a spurious chaotic attractor may be found; if IMAX is too large, the CPU-time may become unnecessary large. The optimal choice for IMAX

depends on the required accuracy EPS and the amount of damping in the system.

A third criterion, not discussed by Tongue, is especially important in the programming context. When two initial states both lead to the same periodic attractor, the corresponding trajectory end points will still differ. To obtain correct basins of attraction, it is important to know that both trajectories lead to one and the same attractor. Therefore, when a trajectory satisfies the periodicity criterion, it should be checked whether the latest determined image point is not too close to an already existing periodic attractor. This also holds for regular numerical integration as was applied in Chapter 1.

2.3.4 Example

As an example, again the modified Duffing equation (2.4) is considered, with $d = 0.15$, $a = 0.3$, $\omega = 1.0$. The region of interest Ω is defined as $-2 \leq x_1, x_2 \leq 2$. Grid points are given by (ih_1, jh_2) , with $i, j = -50, \dots, 50$, $h_1 = h_2 = 0.04$ (notice that these points correspond to the cell center points of the examples in Sections 2.1 and 2.2). Application of ICM with $\text{EPS} = 10^{-3}$ and $\text{IMAX} = 20$ yields the following results (see Fig. 2.9):

- A periodic attractor (*) at (0.638, 1.341) with a large basin of attraction (::).
- A chaotic attractor (·), formed by the end points of trajectories that did not show any periodicity within 20 interpolation steps. The white area contains the corresponding initial conditions.
- Some periodic groups (not shown in Fig. 2.9), lying on the chaotic attractor with only a few transient points. These groups are artifacts of the ICM method, caused by the periodicity criterion. Since a chaotic attractor is 'dense', some chaotic trajectories can be regarded as being periodic, due to this criterion.
- 17 Points (o) which are mapped into the sink cell.

Comparing these results with those obtained by SCM and GCM, the following may be concluded: The periodic attractor has been localized more precisely now. The chaotic attractor looks more like the real attractor, shown in Chapter 1, than the one produced by GCM. However, part of the dots forming the chaotic attractor are not lying on the real attractor (compare Fig. 1.3); in fact, some of them are lying close to the $P - 1$ solution. These

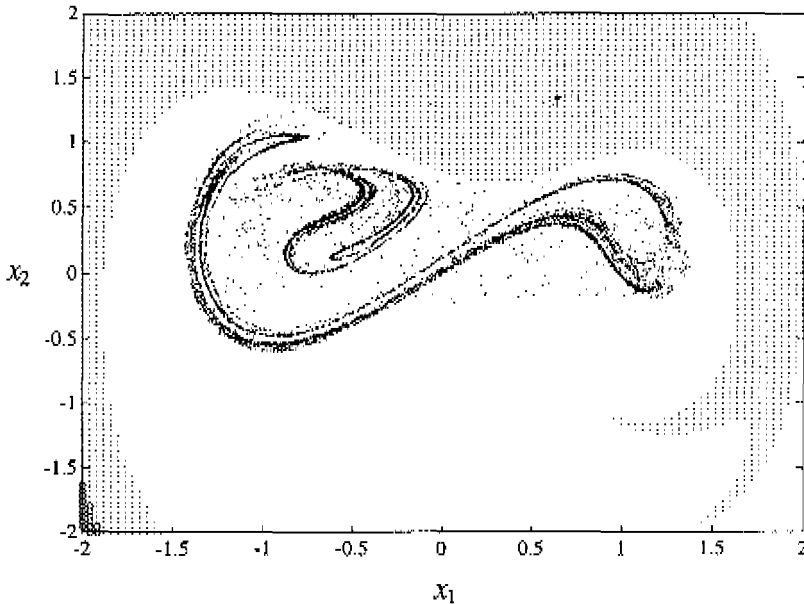


Figure 2.9: ICM results for the modified Duffing equation (2.4): Periodic attractor (*) and basin of attraction (::); chaotic attractor (·) and basin of attraction (left blank); cells mapped into the sink cell (◦).

so-called *transient dots* represent end points of trajectories that have not settled on one of the attractors yet. A larger value for IMAX will reduce the number of transient dots. Further, it should be noted that the saddle solution has not been found under ICM.

2.3.5 Remarks

The ICM method is an attractive tool for investigating nonlinear dynamic systems. With respect to SCM and GCM, the main advantages are listed below.

- The discretization error is replaced by a smaller interpolation error.
- No restriction is placed on the period length of a periodic motion.
- Chaotic motion is represented by nonperiodic motion (as it should be).

- The interpolation grid can be chosen finer than the integration grid: For instance, when tackling a problem with 101×101 integration points, afterwards a 1001×1001 interpolation resolution may be used to obtain the basins of attraction. This is an interesting aspect of ICM, keeping in mind that the interpolation part requires much less CPU-time than the integration part. Here, it should be noted that the accuracy of the results is defined by the integration grid. Use of an extended interpolation grid only produces a higher resolution plot of the basins of attraction.

However, the following critical remarks have to be made as well:

- Repellers and saddle solutions will not be found in general.
- When a trajectory is found not to repeat itself within the maximum number of interpolation steps, it is regarded as being chaotic. The initial values of all chaotic trajectories are now assumed to form the basin of attraction of a chaotic attractor. This however, may not always be true, for instance when more than one chaotic attractor exist. Plotting the end points of all chaotic trajectories gives an idea of the form of the chaotic attractor, and also (the only) information with respect to its uniqueness.
- When the maximum number of interpolation steps is chosen too small, a spurious chaotic attractor will be found. In general, the choice of the criteria may be of great influence on the results. It is not very obvious which criteria are the optimal ones; this may depend on the system characteristics.
- Application of ICM is not very suited for systems with large state space dimension N . For one interpolation step, 2^N interpolation points have to be determined and 2^N interpolation functions have to be evaluated. For large N , the CPU-profit with respect to regular numerical integration will vanish.

Concluding, the ICM method may be considered as an efficient addition to SCM, taking only a small amount of additional CPU-time. The method's drawbacks require some improvisation and ad-hoc thinking of the user.

2.4 Multiple mapping

2.4.1 Introduction

In recent years, a number of modifications on ICM have been presented. In [33], a higher order method of ICM is shown termed *tensor product interpolated cell mapping* (TPICM). Under TPICM, the bi-linear mapping is replaced by a more sophisticated mapping which preserves all the qualitative dynamic properties of the system. Although the results are more accurate than under regular ICM, the costs are so high that the TPICM method is not very recommendable. In this thesis, no attention is paid to the TPICM method.

A second modification on ICM, called *multiple mapping* (MM), is of more practical importance [32]. With respect to ICM, MM is said to produce more accurate results for slightly more CPU-time. Under MM, the regular map over one period is replaced by two maps, each covering half a period. This is done to diminish the state space distortion.

2.4.2 State space distortion

The state space of a nonlinear dynamic system is being distorted during time. As a result, trajectories starting from close initial states may be separated after only a short while. For chaotic systems, the state space distortion may be very high. According to Tongue, the state space distortion can be represented by means of the divergence of neighbouring trajectories. For a two-dimensional system, the following definition is given for the state space distortion d in $\mathbf{x} = (x_1, x_2)$ after τ seconds [32]:

$$d(\mathbf{x}, \tau) = \frac{1}{2} \left(\frac{d_1(\mathbf{x}, \tau)}{\Delta x_1} + \frac{d_2(\mathbf{x}, \tau)}{\Delta x_2} \right). \quad (2.14)$$

Here, Δx_i is the initial distance between the trajectory starting from \mathbf{x} and the neighbouring trajectory in the positive x_i -direction ($i = 1, 2$); d_i denotes the distance between the trajectories after a fixed time τ (see Fig. 2.10).

To illustrate the concept of state space distortion, the modified Duffing equation (2.4) is considered. For this system, the state space distortion d after one period $T = 2\pi/\omega$ is determined. Grid points used for ICM in the previous section are chosen as initial states. Further, $\Delta x_i = h_i = 0.04$ ($i = 1, 2$) is taken, which implies that neighbouring grid points are used to represent the initial points of neighbouring trajectories.

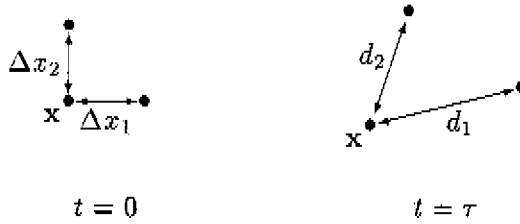


Figure 2.10: Definitions of Δx_i and d_i , ($i = 1, 2$).

In Fig. 2.11, regions of high ($d > 5$) and low ($0 < d < 1$) distortion are shown. As expected, high distortion is found on the chaotic attractor and its corresponding domain of attraction. Since a chaotic attractor undergoes *stretching* as well as *folding* during time, also regions of low distortion are found on the chaotic attractor.

2.4.3 Multiple mapping concept

In the previous subsection, the occurrence of high state space distortions is shown to be very well possible. When applying ICM to a state space with these types of distortions, large interpolation errors are introduced. After all, when at $t = T$ the integrated trajectories have already diverged very severely, the mapping image determined by interpolation cannot be very accurate.

Since the divergence of neighbouring trajectories increases with time, it is preferable to use two interpolation mappings instead of one, each covering half of the total integration time T (Tongue [32]). For this purpose, two integrations have to be carried out for each grid point \mathbf{x}^i , $i = 1, \dots, M$: one for $0 \leq t \leq T/2$, and one for $T/2 \leq t \leq T$. Both interpolation mappings should be repeatedly applied one after the other to obtain an approximate trajectory of desired length. The region of interest Ω for the second integration may differ from the one for the first integration.

The total costs for the MM method are slightly higher than for ICM. The numerical integration costs are equal in both methods (an integration over T seconds for an equal number of initial states). Under MM however, twice as many interpolation steps need to be made as under ICM to obtain the same number of mapping points. Since the numerical costs for interpolation are much smaller than for integration, the total difference in CPU-time between both methods is very small.

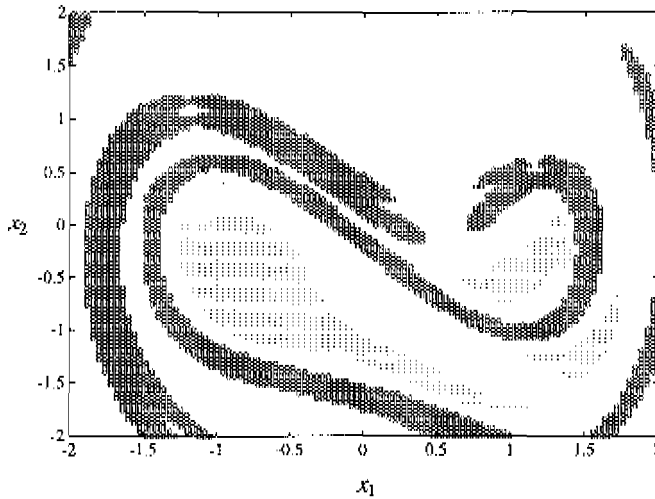


Figure 2.11: Regions of high (\cdot) and low (\circ) distortion for the modified Duffing equation (2.4).

2.4.4 Example

In Fig. 2.12, the results are shown obtained by MM application to the modified Duffing equation (2.4). The same criteria and parameters are used as under ICM. The following results are found:

- A periodic attractor ($*$) at (0.638, 1.341).
- A chaotic attractor (\cdot).
- Some periodic groups (not tagged in Fig. 2.12), lying on the chaotic attractor with only a few transient points (artifacts of the MM method).
- 138 Points (\circ) which are mapped into the sink cell.

Compared to the ICM results, the chaotic attractor is determined much more accurate under MM. Basins of attraction and the position of the periodic solution are determined just as accurate as under ICM. Since two interpolation maps are used instead of one, more grid points are mapped into the sink cell. Still, of almost 99 % of the grid points in Ω the attractor has been determined. In Table 2.1, the CPU-times are given for all CM applications performed in this chapter.

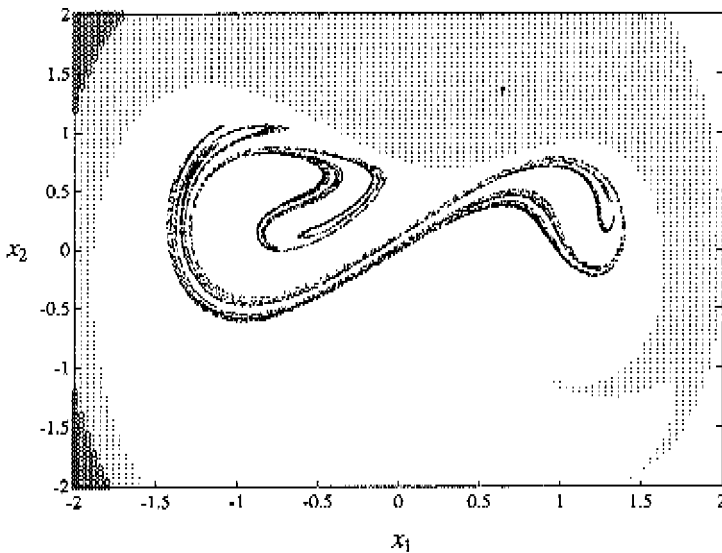


Figure 2.12: MM results for the modified Duffing equation (2.4): Periodic attractor (*) and basin of attraction (::); chaotic attractor (-) and basin of attraction (left blank); cells leading to the sink cell (o).

2.4.5 Remarks

The most obvious difference between the ICM and the MM results is the form of the chaotic attractor. Though the maximum number of interpolation steps $IMAX$ equals 20 for both methods, no transient dots are found under MM. Hence, the large number of transient dots found under ICM cannot be explained by the small value of $IMAX$. Apparently, the mapping time T is too large to obtain accurate results in the region occupied by the chaotic attractor. The use of two maps of mapping time $T/2$ (as under MM) produces a 'clean' chaotic attractor without transient dots.

In [32], the MM method was applied to a different modified Duffing equation. For the considered case, two periodic attractors coexisted. The MM method was used to determine the basin boundaries and their dimension. Because of the fractal structure of the basin boundaries, the state space distortion was locally very high. The use of MM yielded a much better approximation of the boundaries than ICM. So, whenever high state space distortions occur, MM is to be preferred to ICM.

Table 2.1: CPU-times for the modified Duffing equation (2.4).

Method	CPU-time (s)
SCM	21.3
GCM	222.1
ICM	31.9
MM	38.3
Num. int.	1432.2

2.5 Recapitulation

This chapter concludes with a short recapitulation of the considered cell mapping methods.

The SCM method gives a global overview of the dynamic behaviour in a nonlinear system. Periodic attractors are found, chaotic attractors are represented by periodic groups of relatively long period. Basins of attraction can be determined quite accurately, provided that they have no fractal boundaries. The capability of finding repellors and saddle solutions depends on the actual position of these solutions with respect to the cell boundaries.

The GCM method is particularly suited for the determination of chaotic attractors and their properties. When dealing with fractal basin boundaries, the basins of attraction are determined more accurately compared to SCM. The required CPU-time for GCM is much larger than for SCM.

The ICM method yields a precise location of periodic attractors. Chaotic attractors can be determined very accurately, under condition that the maximum number of interpolation steps is large enough. Whenever large state space distortions occur, the MM method is to be preferred to the ICM method. The CPU-time required for both methods is almost equal, but larger than for SCM.

The considered CM methods should not be seen as competitors. Depending on the system characteristics and the user's interests, a certain method should be chosen. A combination of methods is also possible, taking advantage of each method's specific strong points. Starting with SCM, the main part of ICM (the integration part) has already been carried out, as well as part of the work for GCM and MM. With the SCM results in hand, one can decide whether to do an additional GCM, ICM, or MM.

Chapter 3

Modifications of Cell Mapping Methods

In the previous chapter, an overview of the existing CM methods has been given. In this chapter, a number of modifications of these methods is presented. First, modifications dealing with special types of dynamic systems are introduced. Second, two improvements on ICM are shown. Finally, SCM is applied to a beam system with nonlinear support to show the effect of an extended integration interval.

3.1 Overview of modifications

In Section 3.2, an alternative approach for autonomous systems is presented, termed ASCM. This approach enables a substantial reduction of the necessary CPU-time. Application of the ASCM method to a Van der Pol equation and to a nonlinear aeroelastic oscillator is performed.

When investigating a discontinuous dynamic system by means of CM, the original methods have to be modified in some way. This is shown in Section 3.3. As an example, a forced zero-stiffness impact oscillator is considered.

In Section 3.4, a new criterion in the ICM procedure is proposed. As a result, a trajectory can be classified at an earlier stage than under regular ICM. This modified ICM method (MICM) yields equal results in less CPU-time. MICM is applied to a modified Duffing equation and to an impact oscillator.

A combination of ICM and MM, termed *mixed* cell mapping (MCM), is

presented in Section 3.5. Application of MCM to a modified Duffing equation is performed. It is shown that MCM is more accurate than ICM and MM but also more time-consuming.

This chapter is concluded with the application of SCM to a beam with nonlinear support in Section 3.6. It is shown that system characteristics urge the user to extend the integration interval for determining the image cells. As a result, the number of cells leading to the sink cell as well as the number of spurious periodic groups are reduced.

3.2 CPU-time reduction for autonomous systems

3.2.1 Introduction

An autonomous system is a system of which the equations of motion have the following form:

$$\dot{\mathbf{x}} = f(\mathbf{x}). \quad (3.1)$$

Here, $\mathbf{x} = [x_1(t) \dots x_N(t)]^T$ is the state of the system. In (3.1), time does not explicitly occur. Hence, at each possible state $\mathbf{x} \in \mathbb{R}^N$ the system's acceleration has a specific time-independent value. Periodic solutions of (3.1) are called *limit cycles*.

When applying CM methods to autonomous systems, initially the same procedure may be followed as for non-autonomous systems. However, after choosing a region of interest Ω and dividing it into cells, the question arises how to determine a cell's image cell. For a non-autonomous system which is periodically forced, the interval Δt , over which the equations of motion are integrated to obtain the image cell, has to be equal to (a multiple of) the forcing period to obtain a CM which does not explicitly depend on time. Since by definition time does not explicitly occur in autonomous equations, any possible value for Δt is allowed.

Although for an autonomous system any value of the integration interval Δt produces a CM which is independent of time, the choice for Δt is far from trivial. When Δt is chosen too small, spurious results may be found. In that case, many cells may be mapped onto itself, since Δt is too small to reach a state outside the cell when starting in the center point. A large value of Δt is also not very satisfying, since this would imply an unnecessary large computation time.

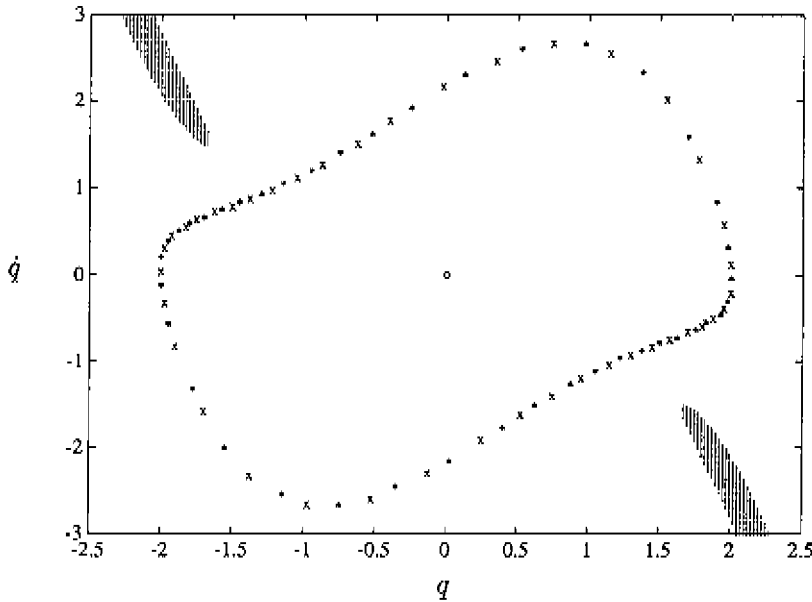


Figure 3.1: SCM results for the Van der Pol equation (3.2) for $\mu = 1.0$: Two $P - 41$ groups (*, x) representing the stable limit cycle; $P - 1$ group (o) representing the unstable equilibrium point; cells leading to the sink cell (·).

3.2.2 Van der Pol equation

One of the best known autonomous equations is probably the Van der Pol equation:

$$\ddot{q} + \mu(1 - q^2)\dot{q} + q = 0. \quad (3.2)$$

For $\mu < 0$, the stable equilibrium point $(q, \dot{q}) = (0, 0)$ is the only attractor. For $\mu > 0$, this equilibrium point loses its stability while a stable limit cycle comes into existence (see e.g. Crooijmans [3, page 1.4]).

SCM is applied to (3.2) for $\mu = 1.0$. For discretization, 201×201 cells are used of size 0.025×0.03 , covering $|q| \leq 2.5125$, $|\dot{q}| \leq 3.015$. For Δt , a value of 1.3 is chosen.¹ The results are shown in Fig. 3.1. The stable limit cycle is represented by two periodic groups of 41 cells each. The unstable

¹In [14], the same system is investigated with $\Delta t = 1.3$ using 101×101 cells.

equilibrium point is represented by one periodic cell. Further, 834 cells are mapped into the sink cell. The remaining cells in Ω are mapped onto one of the $P - 41$ groups and hence represent the basin of attraction of the limit cycle.

The results obtained in this example contain an approximation of the complete limit cycle in state space. When a non-autonomous system is investigated by means of CM, only Poincaré sections of solutions are obtained. Hence, for autonomous systems more information is obtained under SCM than for non-autonomous systems, in the same order of computation time. This implies that the same amount of information—intersection of attractors and basins of attraction with a Poincaré section—may be obtained in less computation time.

3.2.3 Alternative approach

By introducing a Poincaré section Σ in the autonomous state space, an alternative SCM approach (ASCM) may be applied. On Σ , a region of interest Ω' is chosen, e.g. the intersection of Ω with Σ . Next, Ω' is discretized into cells and a cell mapping $C : \Sigma \rightarrow \Sigma$ is created. The image cell of each cell $\xi \in \Omega'$ is determined by the center point method. The integration interval Δt is chosen such that the terminate point of the integrated trajectory lies in Σ . Hence, for each cell a different value of Δt is used, which is allowed for autonomous systems. Since the dimension of the investigated region is reduced with one, an obvious gain in computation time is achieved with respect to SCM. In Fig. 3.2, the ASCM procedure is shown for a two-dimensional autonomous state space.

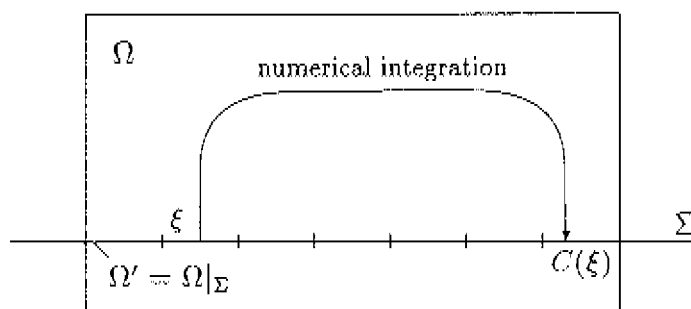


Figure 3.2: Alternative SCM (ASCM) approach for autonomous systems.

The choice of a Poincaré section in an autonomous state space is not trivial. Starting from a point in Σ , it is necessary to return to Σ within a finite time interval. This is achieved by choosing $\Sigma : \dot{q} = 0$ for a system of one DOF q , since every generalized velocity of every attractor equals zero infinitely many times (or is constantly zero for an equilibrium point).² For a general autonomous system of l DOF's, $\dot{q}_j = 0$ is a correct choice for Σ , for any $j \in \{1, \dots, l\}$.

The ASCM method is applied to the Van der Pol equation (3.2), taking $\Sigma : \dot{q} = 0$; $\Omega' : |q| \leq 2.5125$. Ω' is divided into 201 cells of length 0.025. For each cell in Ω' , integration is performed until Σ is intersected again. The cell which contains the end point is the image cell by definition. The exact intersection of a trajectory with Σ is obtained by means of the Hénon method, which is explained in Section 3.3. In Fig. 3.3, the results are shown: The limit cycle is represented by two cells with center points $q = 2.025$ and $q = -2.025$ respectively ($\dot{q} = 0$). The unstable equilibrium point is represented by a $P - 1$ cell with center point $q = 0$. All other cells are mapped onto the $P - 2$ group.

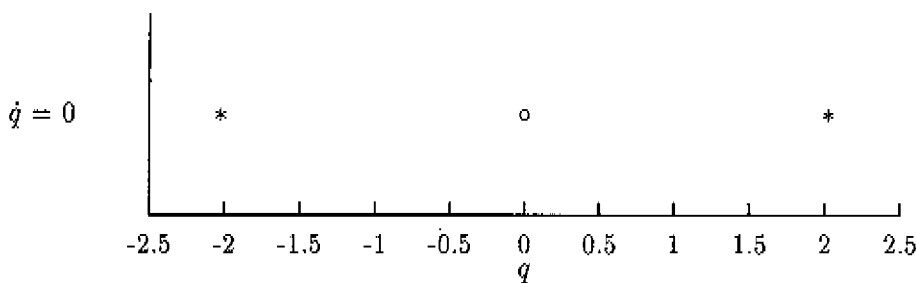


Figure 3.3: ASCM results for the Van der Pol equation (3.2) for $\mu = 1.0$: $P - 2$ group (*) representing the stable limit cycle; $P - 1$ group (o) representing the unstable equilibrium point.

The SCM and ASCM applications to the Van der Pol equation required a CPU-time of 16.1 s and 0.1 s, respectively. The extra information given by SCM—the form of the limit cycle—can be obtained by numerical integration over a very short interval taking the center point of one of the $P - 2$ cells

²For a chaotic attractor, this can be proven by using the fact that it is bounded and recurrent.

as initial condition. Further, for each of the transient cells the number of mapping steps necessary to end up on the limit cycle is given (transient behaviour information). Hence, under regular SCM more information is obtained about the global transient behaviour. If one is only interested in detecting the attractors and the domains of attraction, the ASCM approach deserves recommendation.

3.2.4 Aeroelastic nonlinear oscillator

The Van der Pol equation treated in the previous subsection is a relatively simple example since only one steady-state solution was dealt with. In this subsection, SCM and ASCM are applied to a 1-DOF autonomous system in which two stable limit cycles coexist. The considered system is a long prism of square cross-section in a normal steady wind (velocity V). The prism, with mass m and length l , is connected to the world by means of a linear damper (damping d) and a linear spring (stiffness k). In Fig. 3.4, a schematic picture of this system is shown.

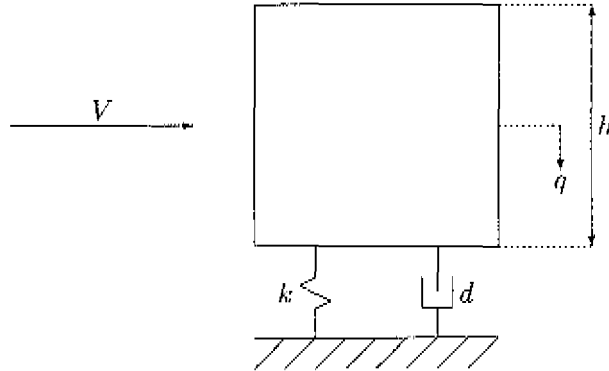


Figure 3.4: Cross-section of square prism under normal steady wind condition. Studied by Parkinson and Smith [26].

In Parkinson and Smith [26], a quasi-steady analysis is made of the transverse galloping of the prism. This results in the following ODE for the nondimensional vibration displacement $y = q/h$ in vertical direction, where q is the real displacement and h the side-length of the square section:

$$y'' + y = nA \left\{ \left(U - \frac{2\beta}{nA} \right) y' - \left(\frac{B}{AU} \right) y^3 + \left(\frac{C}{AU^3} \right) y^5 - \left(\frac{D}{AU^5} \right) y^7 \right\}. \quad (3.3)$$

Here, ()' denotes differentiation with respect to nondimensional time $\tau = \omega t$, where $\omega = \sqrt{k/m}$ is the natural circular frequency. In (3.3), the following nondimensional parameters have additionally been introduced:

$$\begin{aligned}
 \beta &= d/2m\omega & : & \text{nondimensional damping} \\
 n &= \rho h^2 l / 2m & : & \text{mass parameter} \\
 U &= V/\omega h & : & \text{nondimensional air velocity,}
 \end{aligned}
 \tag{3.4}$$

with ρ the air density. Finally, A, B, C, D are positive constants which can be determined experimentally.

In [26], the steady-state behaviour of (3.3) has been investigated by means of analytical techniques. For small values of U , only one steady-state solution exists, namely $(y, y') = (0, 0)$. For $U > U_0 = 2\beta/nA$, this solution becomes unstable and a stable limit cycle (L1) comes into existence. For $U_1 < U < U_2$, a second stable limit cycle (L2) with a larger amplitude comes into existence, coexisting with L1. Both limit cycles are separated by an unstable limit cycle. Here, $U_1 \approx 1.2 U_0$ and $U_2 \approx 1.8 U_0$. Finally, for $U > U_2$ only limit cycle L2 remains.

To obtain a situation of coexistence of two stable limit cycles, $U = 1.5 U_0$ is taken. Further, $\beta = 0.5$ and $n = 4.3 * 10^{-4}$ is taken. These choices imply a large value for U , resulting in a large nondimensional displacement y and velocity y' . To apply SCM for these parameters, a large region of interest Ω is taken: $-402 \leq y, y' \leq 402$. Ω is divided into 201×201 cells of size 4.0×4.0 . Image cells are determined by means of integration over 2.0 seconds for each cell. This results in three periodic groups: a $P - 62$ group representing L2, a $P - 92$ group representing L1, and a $P - 1$ cell representing the unstable equilibrium point (see Fig. 3.5). Small dots (·) are used to mark cells which are mapped to L1, the white area in Fig. 3.5 contains all cells which lead to L2. The necessary CPU-time for this calculation was 62.8 s.

In Fig. 3.6, the results are shown of an ASCM application to the same system, taking $\Sigma : y' = 0$ and $\Omega' : -402 \leq y \leq 402$. For discretization, 201 intervals of size 4.0 are used. In this approach, 4 groups are found: A $P - 2$ group representing L2, two $P - 2$ groups representing L1, and one $P - 1$ cell representing the unstable equilibrium point. The basins of attraction of both limit cycles restricted to Σ are also shown in Fig. 3.6. The necessary CPU-time for this calculation was only 0.4 s.

The unstable limit cycle, separating the basins of attraction of the two stable limit cycles, has not been found in both calculations. Under SCM however, a graphical approximation for the unstable limit cycle is of course given by the basin boundary of both basins of attraction. In the same way,

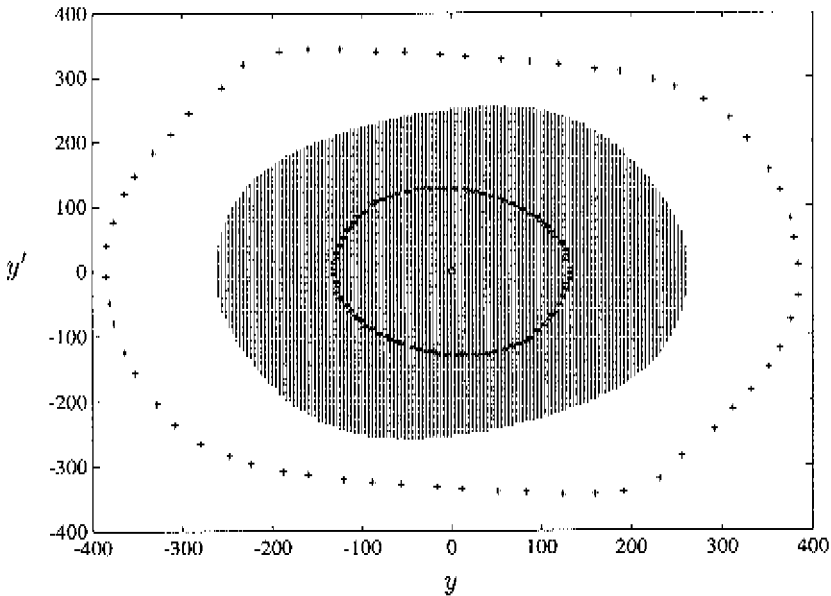


Figure 3.5: SCM results for the aeroelastic oscillator (3.3): Large amplitude limit cycle (+) and basin of attraction (left blank); small amplitude limit cycle (*) and basin of attraction (·); unstable equilibrium point (o).

an approximation of the intersections of the unstable limit cycle with Σ is obtained under ASCM. Determination of the trajectory emanating from these approximations by means of numerical integration yields an approximation for the complete unstable limit cycle. In this way, the basins of attraction in Ω can be obtained. Again, this shows that the results produced by SCM can also be produced by means of ASCM (taking very little CPU-time) and an additional integration over a short time-interval.

3.2.5 Remarks

An alternative SCM approach for autonomous systems has been presented, termed ASCM. This approach produces the Poincaré sections of attractors and basins of attraction in the autonomous state space. Compared to regular SCM, only a fraction of the CPU-time is required under ASCM. An analogous approach can be applied to ICM and GCM.

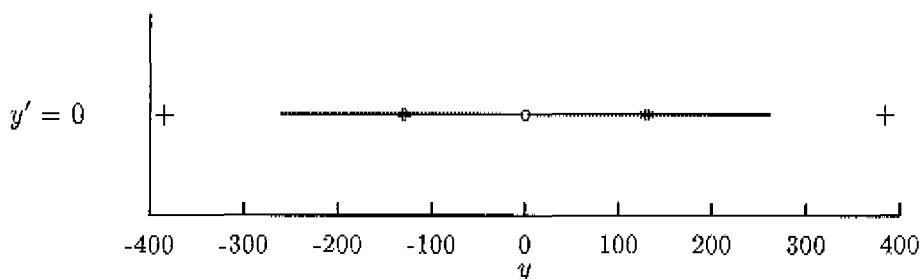


Figure 3.6: ASCM results for the aeroelastic oscillator (3.3): Large amplitude limit cycle (+) and basin of attraction (left blank); small amplitude limit cycle (*) and basin of attraction (·); unstable equilibrium point (o).

The idea behind the ASCM method is briefly mentioned in Hsu [14, page 154]. Since no examples are presented there, it was considered useful to include this approach here. Recently, a similar approach has been introduced by Levitas [22]. In his approach, two or more Poincaré sections are used in the autonomous state space.

Finally, it is remarked here that a new CM method for autonomous systems has been presented recently, termed *adjoining* cell mapping [38, 10]. Under adjoining cell mapping, the integration interval Δt for each cell ξ is chosen such that ξ is adjoining³ to its image cell. In doing so, Δt is kept very small for each cell, in which way the CPU-time is kept very low.

3.3 Modifications for discontinuous systems

3.3.1 Introduction

A special class of dynamic systems which is very often met in mechanical engineering is formed by systems with discontinuities. These are systems which involve clearances, impact problems, and so on. As a result, the mathematical model of such a system contains discontinuous changes in one or more of the state variables.

When applying CM methods to discontinuous dynamic systems, some modifications need to be made. This is shown on the basis of a forced

³In Chapter 4, a definition of adjoining is given.

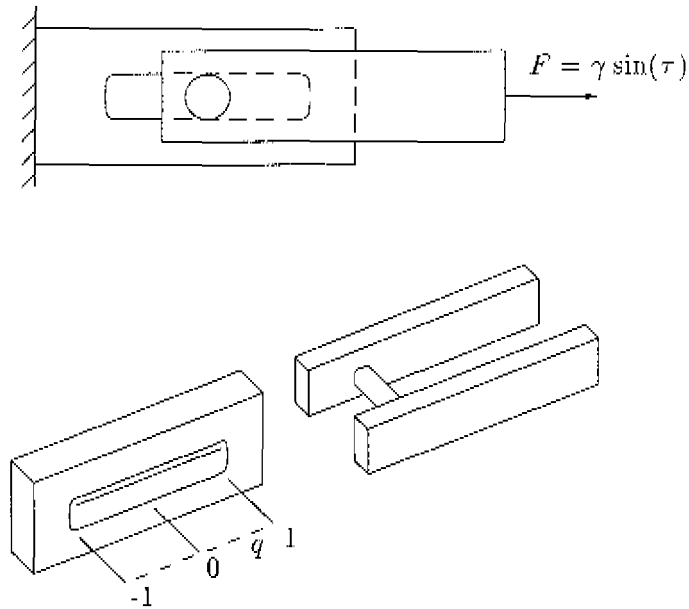


Figure 3.7: Mechanical oscillator consisting of two parts, joined by a smooth pin with play, studied by Li et al. [23].

zero-stiffness impact oscillator, a dynamic system with a discontinuity. This system is discussed in the next subsection and treated by means of SCM and ICM in the following subsections. The results are found to match quite well with the results obtained by numerical integration.

3.3.2 A forced zero-stiffness impact oscillator

The behaviour of a simple mechanical oscillator is considered. The system consists of two parts: one fixed, having a slot, and one constrained to translate along a straight line, joined by a smooth pin with play (Fig. 3.7). The movable part is excited by a periodic force and encounters no resistance except inertia until the pin reaches the end of the slot. The impact of the pin on the fixed member is inelastic and is modelled by a coefficient of restitution r , with $0 < r < 1$. The system is governed by the following nondimensional differential equation and boundary conditions:

$$\begin{aligned} q'' &= \gamma \sin(\tau) & \text{for } |q| < 1, \\ q' &\rightarrow -rq' & \text{for } |q| = 1. \end{aligned} \quad (3.5)$$

Here, q measures the position of the pin and γ is the forcing amplitude.

This system was studied by Li et al. [23], who showed the existence of periodic solutions for certain values of r and γ by means of analytical techniques. For instance, for $r = 0.5$ and $\gamma = 0.20826$ a periodic motion was found with period 2π having two impacts during each period. In Van der Spek et al. [36], the existence of a chaotic attractor for the same parameter values was shown.

3.3.3 Simple cell mapping

To apply the SCM method to the impact oscillator, a region of interest Ω is chosen. Obviously, q satisfies $|q| \leq 1$. To obtain a region Ω which includes both the periodic and the chaotic attractors it is sufficient to choose $|q'| \leq 1$ [36]. Next, Ω is divided into 101×101 rectangular cells of equal size. For each cell, the image cell is determined by means of the center point method.

When integrating (3.5), one has to deal with the discontinuity in the velocity at $|q| = 1$. Integration must be performed until $|q| = 1$; after changing the velocity q' into $-rq'$, integration can be continued until $|q| = 1$ again. To realize this procedure, the Hénon method is used [11]. Here, the Hénon method means rearranging (3.5) in such a way that q becomes the independent variable and τ the dependent one. This is achieved by writing the equation of motion for $|q| < 1$ in (3.5) as a first order system:

$$\begin{aligned} \frac{dx_1}{d\tau} &= x_2, \\ \frac{dx_2}{d\tau} &= \gamma \sin(\tau). \end{aligned} \tag{3.6}$$

with $x_1 = q$, $x_2 = q'$. Dividing the second equation by the first one and inverting the first one yields:

$$\begin{aligned} \frac{d\tau}{dx_1} &= \frac{1}{x_2}, \\ \frac{dx_2}{dx_1} &= \frac{1}{x_2} \gamma \sin(\tau). \end{aligned} \tag{3.7}$$

To describe the procedure followed during numerical integration, the following definitions are introduced:

- τ^j : value of τ after j -th integration step
- \mathbf{x}^j : calculated value of $\mathbf{x} = (x_1, x_2)$ after j -th integration step
- x_i^j : calculated value of x_i ($i = 1, 2$) after j -th integration step
- h^j : applied stepsize in j -th integration step

Numerical integration starts with (3.6). When for some j $|x_1^j| > 1$ holds, a switch is made to (3.7) and one integration step is carried out with initial condition (τ^{j-1}, x_2^{j-1}) and stepsize $x_1 = \text{sgn}(x_1^j) - x_1^{j-1}$. In this way, the values of τ and x_2 at $|x_1| = 1$ are easily obtained. After multiplying x_2 by $-r$, integration is continued with (3.6) until $|x_1| > 1$ again. However, when x_2 is small, (3.7) becomes a set of stiff differential equations, which are hard to integrate. For $x_2 = 0$, the system derivatives are even infinitely large. Hence, the Hénon method is not very practical for small values of x_2 .

When x_2 is too small, a less sophisticated but more robust way is used to integrate over the discontinuity at $|x_1| = 1$. When for some j $|x_1^j| > 1$ holds and x_2^{j-1} is small, a new integration is performed from $x^{j-1} = (x_1^{j-1}, x_2^{j-1})$ with stepsize $h_1^j = \frac{1}{2}h^j = \frac{1}{2}(\tau_j - \tau_{j-1})$ which yields a new x_1^j . Next, a new integration is carried out with stepsize h_2^j , with

$$h_2^j = \begin{cases} h_1^j + h^j/4 & \text{if } |x_1^j| < 1, \\ h_1^j - h^j/4 & \text{if } |x_1^j| > 1. \end{cases} \quad (3.8)$$

This procedure is repeated until $||x_1^j| - 1| < 10^{-3}$. Since every integration starts from the same state, no accumulation of integration errors will appear.

The two procedures treated above are used in the SCM application. Whenever $x_2 < 0.05$, the stepsize-halving method is used, otherwise, the Hénon method is applied. The corresponding results are shown in Fig. 3.8. The periodic solution is represented by 5 clustered cells of period 1 (\circ). The transient cells (\cdot) leading to one of these cells together form the basin of attraction of the periodic solution. The chaotic attractor is represented by a $P - 17$ group ($*$). Its basin of attraction is left blank in Fig. 3.8.

To check the correctness of these results, numerical integration for all cell center points is carried out. Here, integration is continued until convergence is reached (convergence criterion: $\text{EPS} = 10^{-6}$), with a maximum integration time of $40T$ (80π). If no convergence is obtained within this time limit, the trajectory is considered to be chaotic.

Fig. 3.9 shows the results obtained by numerical integration: A periodic solution (\circ) at $(-0.894, -0.828)$, its basin of attraction ($::$), and the chaotic attractor, which is produced by the end points of all chaotic trajectories. The basin of attraction of the chaotic attractor is left blank. It can be seen that the basins of attraction reasonably match with the SCM results, with the exception of the the area $-1 \leq x_1 \leq -0.5$, $0.7 \leq x_2 \leq 1.0$. Unlike the periodic attractor, the chaotic attractor found under SCM (the $P - 17$ group)

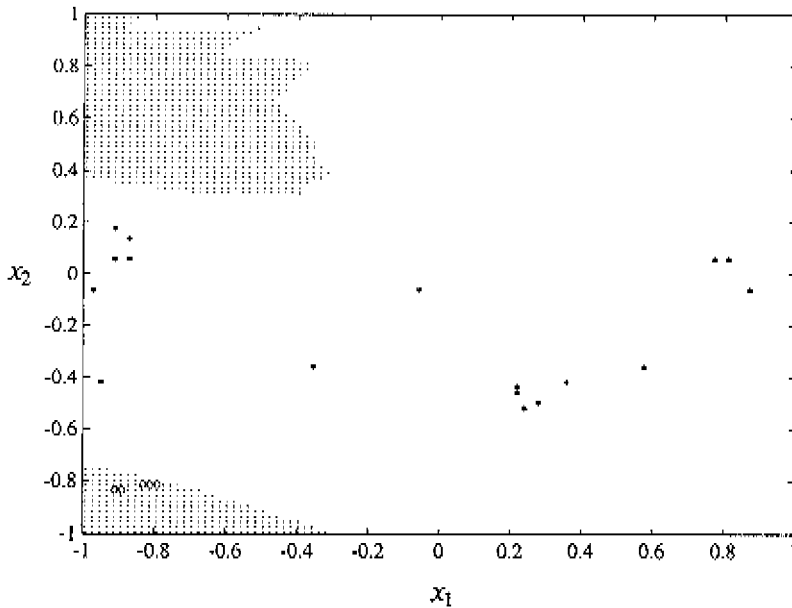


Figure 3.8: SCM results for the impact oscillator (3.5) for $r = 0.5$, $\gamma = 0.20826$: 5 $P - 1$ cells (\circ) and transient cells (\cdot); $P - 17$ group ($*$) and transient cells (left blank).

does not resemble the actual attractor. As is usual under SCM, additional numerical integration is necessary to obtain a correct chaotic attractor.

3.3.4 Interpolated cell mapping

For applying ICM to the impact oscillator, a grid of points distributed over Ω is needed. Since every state in Ω must have four surrounding grid points, the grid points must lie on the boundary of Ω as well. For this reason, the center points of the cells used under SCM cannot be used. Hence, an additional numerical integration over one forcing period has to be performed for a completely new grid, given by (ih_1, jh_2) , $i, j = -50, \dots, 50$, $h_1 = h_2 = 0.02$.

The discontinuity in (3.5) introduces an additional difficulty for ICM. Interpolation only gives a good approximation of the actual state of the system when the image points of the relevant interpolation points are not too far apart. This is not the case when the corresponding trajectories have

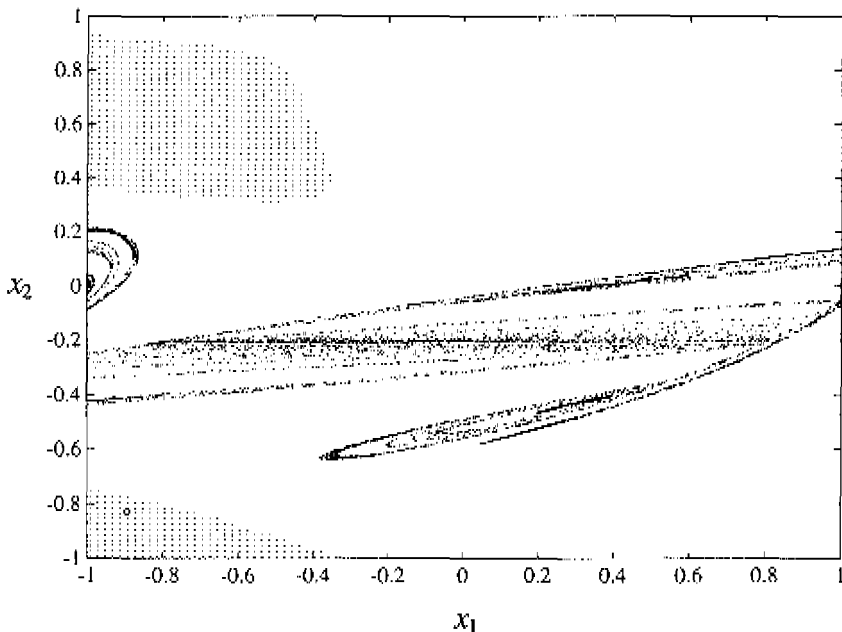


Figure 3.9: Numerical integration results: Periodic attractor (\circ) and basin of attraction ($::$); chaotic attractor (\cdot) and basin of attraction (left blank).

a different number of impacts. Since interpolation will give spurious results in this situation, an ordinary numerical integration should be carried out instead. Of course, all integrations have to be executed with the integration procedure, given in Subsection 3.3.3, to handle the discontinuities.

Fig. 3.10 shows the ICM results for $\text{EPS} = 10^{-3}$ and $\text{IMAX} = 40$. The periodic solution is found at $(-0.895, -0.828)$ (\circ). Further, a saddle solution is found at $(-0.762, -0.807)$ ($+$). Trajectories that do not show convergence within 40 interpolation/integration steps are assumed to end up on the chaotic attractor. The corresponding basin of attraction is given by the initial states of these trajectories (left blank in Fig. 3.10).

Comparing these results with those obtained by numerical integration, it can be concluded that the periodic solution is found almost exactly, as well as its basin of attraction. The chaotic attractor also matches very well with the one obtained by numerical integration. Additionally, the determination of the saddle solution is an important result.

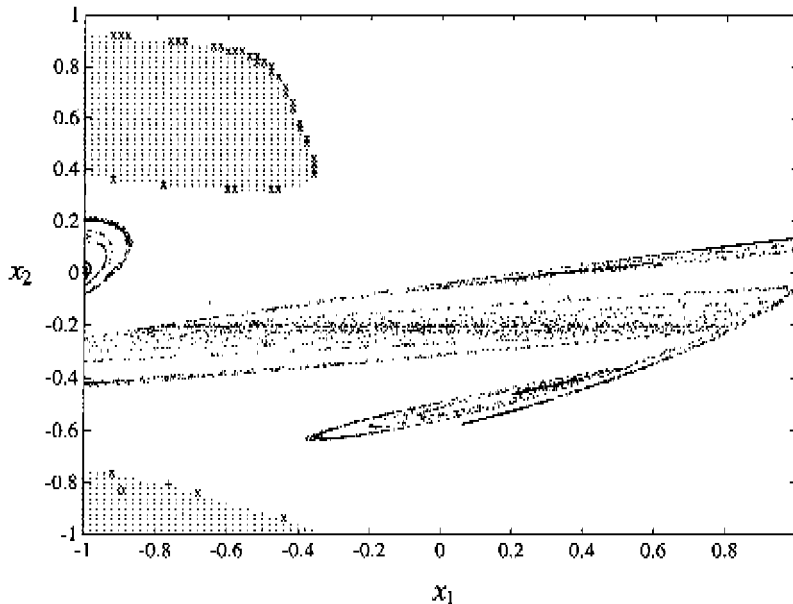


Figure 3.10: ICM results: Stable periodic solution (\circ) and basin of attraction ($::$); saddle solution ($+$) and stable manifold (x); chaotic attractor (\cdot) and basin of attraction (left blank).

3.3.5 Conclusion

It has been shown that CM methods can successfully be applied to discontinuous systems. To this end, the following modifications to the basic procedures need to be performed:

- Modification of the numerical integration procedure to overcome the discontinuity.
- Under ICM and MM: Replacement of interpolation by integration when the interpolation trajectories show an extreme divergence due to the discontinuity.

As a consequence, ICM and MM require a (relatively) high CPU-time when applied to discontinuous systems.

3.4 Modified ICM procedure

3.4.1 Introduction

In this section, a modification of ICM, termed MICM, is described, with which a substantial gain in CPU-time may be achieved. Although the ICM method is quite efficient, it can become very time-consuming. Especially this is the case when one is dealing with discontinuous systems (see previous section). However, a small change in the concept of ICM can reduce the CPU-time drastically, as will be shown. The presented modification can also be applied to MM, in which case the method is termed MMM.

3.4.2 The modification

Under ICM, a trajectory is approximated by means of interpolation. The interpolation is stopped when one of the following criteria is satisfied:

- Convergence to an attractor has been achieved according to a convergence criterion.
- The number of interpolation steps has exceeded a certain maximum.

In both cases, the created trajectory has settled on an attractor (in the latter case: a chaotic attractor). The starting point of the trajectory is added to the corresponding basin of attraction.

The process of interpolation can be stopped at an earlier stage, having not fulfilled any of the two above-mentioned criteria yet. It is sufficient to perform interpolation until a state \mathbf{y} has been reached of which the surrounding grid points $\mathbf{x}^1 \dots \mathbf{x}^{2^N}$ (N : state space dimension) are already known to lead to one and the same attractor A . Since further interpolation will also lead to A in almost any case, it can be stopped at this stage. The initial state of the interpolated trajectory can then immediately be added to the corresponding basin of attraction.

There may be very rare situations in which this premature ending of the interpolation process produces spurious results. It can go wrong e.g. when inside the area of the N -dimensional cube, defined by the 2^N interpolation points, a region of initial states exists leading to a different attractor than the attractor corresponding to the surrounding interpolation points. If this is the case, the interpolation is not justified anyway. To obtain correct results, the interpolation grid should be chosen finer than. The production of spurious

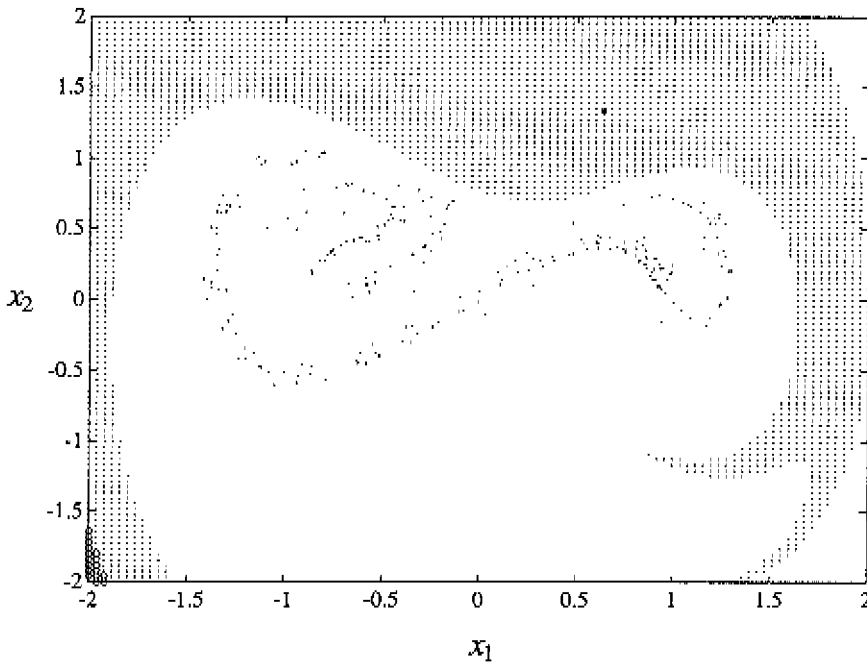


Figure 3.11: MICM results for the modified Duffing equation (2.4) for $d = 0.15$, $\alpha = 0.3$, $\omega = 1.0$: Periodic attractor ($*$) and basin of attraction ($::$); chaotic attractor (\cdot) and basin of attraction (left blank); cells leading to the sink cell (\circ).

results when applying MICM or MMM may in particular occur when dealing with fractal basins of attraction.

3.4.3 Examples

As a first example, the modified Duffing equation (2.4) is considered. Using the same grid and criteria as in Section 2.3, the MICM method is applied. In Fig. 3.11, the results are shown. Compared to Fig. 2.9, almost identical basins of attraction are obtained. The MICM method, however, is 1.5 times faster than ICM, as can be seen in Table 3.1. Further, due to the modification, fewer transient dots are found under MICM.

As a second example, the impact oscillator (3.5) is considered. Fig. 3.12 shows the results found with the MICM method. Here, the same region Ω

is used as in Subsection 3.3.4, as well as the same grid and criteria. Apart from the chaotic attractor, the MICM results perfectly match with the ICM results. However, the MICM method is more than five times as fast (see Table 3.1). As explained in Subsection 3.3.4, interpolation should be replaced by integration whenever the interpolation trajectories have a different number of impacts. Because of this aspect, use of the MICM method causes a very large gain in CPU-time for this example.

From both examples, it can be seen that under MICM the chaotic attractor is formed by much fewer points than under ICM. This can be elucidated by the fact that only terminate points of trajectories that have not converged within IMAX interpolation steps are supposed to be part of a chaotic attractor. Due to the premature ending of the interpolation process under MICM, most trajectories leading to the chaotic attractor are classified as being chaotic at an early stage, in which case they have not settled on the attractor yet. However, the chaotic attractor can be obtained afterwards by means of regular numerical integration. Integration of the equations of motion over 5000 forcing periods gives an accurate picture of the chaotic attractor. The necessary CPU-time for such an integration takes only 7.4 s for the modified Duffing equation and 5.8 s for the impact oscillator, which implies that MICM is still to be preferred to ICM.

Additionally, MMM has been applied to both systems. Since the results obtained are similar to those obtained by MICM, they are not shown here. Compared with MM, identical basins of attraction are found. The chaotic attractors are formed by less points than under MM.

In Table 3.1, the CPU-times are given for all methods and both examples. The modified concept turns out to be faster in all cases. For the modified Duffing equation, the modified methods are 1.5 times as fast as the original methods. For the impact oscillator, the difference in CPU-time is up to a factor 6.

Table 3.1: CPU (s) with and without modification.

Method	Mod. Duf.	Imp. Osc.
ICM	31.9	118.6
MICM	21.8	18.7
MM	38.3	88.3
MMM	25.6	16.7

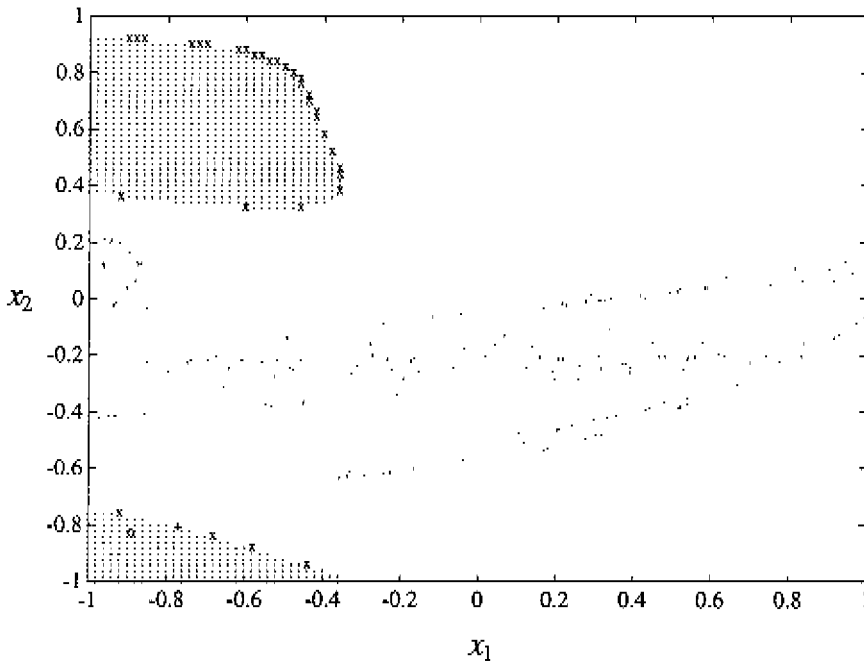


Figure 3.12: MICM results for the impact oscillator (3.5) for $\tau = 0.5$, $\gamma = 0.20826$: Periodic attractor (o) and basin of attraction (::); chaotic attractor (.) and basin of attraction (left blank); saddle solution (+) and stable manifold (x).

3.4.4 Conclusion

Modifications of ICM and MM, termed MICM and MMM, have been introduced. These modifications produce almost identical basins of attraction in less CPU-time. For discontinuous systems, the gain in CPU-time can be a factor five or more. Chaotic attractors are formed by fewer points, which implies that additional numerical integration has to be performed to obtain a complete picture. For systems with fractal basins of attraction, the presented modifications may produce spurious results.

3.5 Mixed cell mapping

3.5.1 Introduction

In Section 2.4, the multiple mapping (MM) method has been introduced as a variation on ICM. Under MM, the regular map over one forcing period is replaced by two maps, each covering half of the integration interval. The idea behind MM is the expectation that a shorter interpolation interval will improve the accuracy of the trajectory determination [32]. However, this does not need to be true. In fact, halving the interpolation interval makes only sense for states that are being interpolated between trajectories that have diverged in some way at $t = T/2$. Therefore, a combination of MM and ICM is introduced, termed *mixed cell mapping* (MCM).

3.5.2 Method explanation

Under MCM, a regular ICM is used unless one of the following situations occurs: (a) The interpolation trajectories have diverged at $t = T/2$ with respect to the interpolation grid; (b) The interpolation trajectories enclose a concave area at $t = T$. In both cases MM is used to obtain the next image point. Divergence of interpolation trajectories is defined to take place when $d > 1$, with

$$d = \frac{1}{2^N - 1} \sum_{j=1}^{2^N - 1} \frac{d_j}{h_j}.$$

Here, h_j and d_j ($j = 1, \dots, 2^N - 1$) represent the distance between \mathbf{x}^{j+1} and \mathbf{x}^1 at $t = 0$ and $t = T/2$ respectively, as is shown in Fig. 3.13 for $N = 2$.

The use of the MCM method in practice will take more CPU-time than both ICM and MM. For each cell center point an integration has to be carried out for $t = 0$ to $t = T$ and one for $t = T/2$ to $t = T$, which implies an enlargement of the CPU-time with a factor 1.5 compared to ICM and MM. However, the results obtained by MCM are by definition at least as accurate as those obtained by ICM and MM, and in many cases more accurate. Other options to improve the accuracy under ICM or MM—such as the reduction of the cell size—may enlarge the CPU-time with a larger factor or may have less influence on the accuracy of the results.

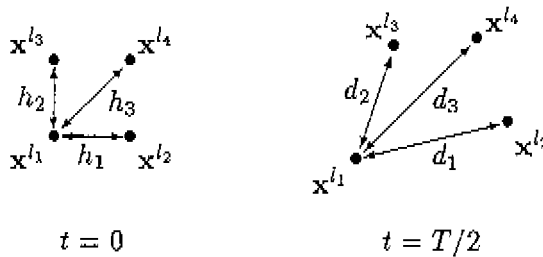


Figure 3.13: Definition of state space divergence.

3.5.3 Example: modified Duffing equation

As an example of application, the modified Duffing equation (2.4) is considered, with $d = 0.1$, $a = 3.2$, $\omega = 0.4776$. These parameters—for which two stable second order subharmonic solutions coexist—were chosen by Tongue [32], to compare ICM and MM. On the basis of fractal dimension calculations, Tongue proved that MM is more accurate than ICM. Here, application of both methods as well as MCM is performed and compared to results obtained by numerical integration. The values of IMAX and EPS, not mentioned by Tongue, are taken to be 100 and 0.001, respectively, while $\Omega = \{(x_1, x_2) \mid |x_1| \leq 2.5 \wedge |x_2| \leq 4.0\}$; the interpolation grid is given by (ih_1, jh_2) , with $h_1 = 0.05$, $h_2 = 0.08$ and $i, j = -50, \dots, 50$.

Fig. 3.14 shows the results obtained by MCM. The two subharmonic solutions have been found as $P - 2$ groups ((\circ) and $(*)$). Each solution has a large basin of attraction. Approximately 600 points $(+)$ are mapped into the sink cell. Because of the fractal nature of the basins of attraction, the modification presented in the previous section is not used here.

Application of ICM produces similar results. To obtain an exact comparison with MCM, numerical integration is carried out for all grid points, using the same criteria for convergence. For every grid point in the basin of attraction of one of the two $P - 2$ solutions found under ICM and MCM, it is checked if numerical integration leads to the same attractor. It is found that ICM produces approximately 300 errors more than MCM. The CPU-time for ICM and MCM is 85.8 s and 135.0 s, respectively.

Under application of MM, more than 2000 grid points are mapped into the sink cell. Apparently, the first of the two interpolation mappings produces a state outside Ω many times. This problem is solved by choosing a different interpolation grid for the second mapping, covering all the end

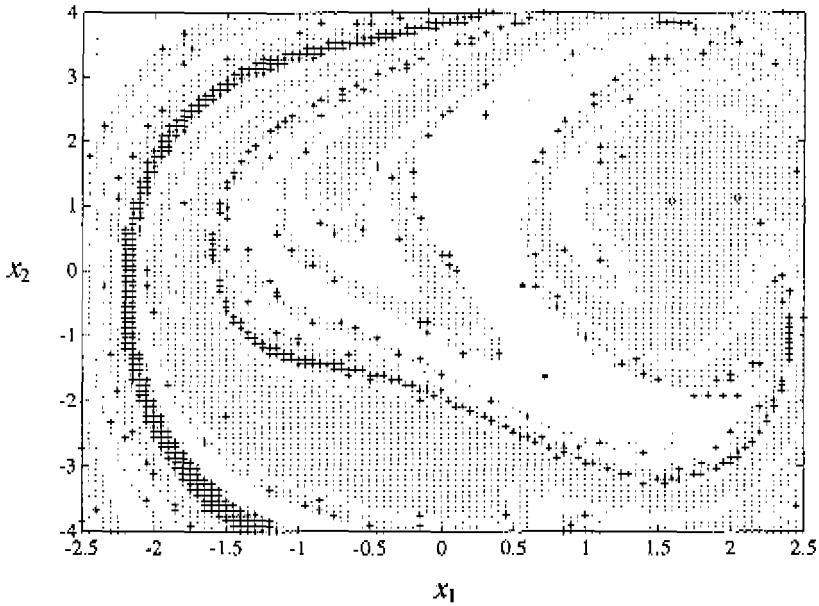


Figure 3.14: MCM results for the modified Duffing equation (2.4) for $d = 0.1$, $a = 3.2$, $\omega = 0.4776$: Periodic attractor (\circ) and basin of attraction (\cdot); periodic attractor ($*$) and basin of attraction (left blank); cells leading to the sink cell ($+$).

points of the first mapping. In doing so, the number of cells leading to the sink cell is reduced to approximately 500. However, MM still produces the same order of errors as ICM (compared with numerical integration) and is therefore less accurate than MCM. The CPU-time for MM is 95.3 s.

3.5.4 Conclusion

A modification has been added to the existing cell mapping techniques, termed *mixed* cell mapping (MCM). MCM is a combination of ICM and MM, producing more accurate results at the cost of more CPU-time. When applying MCM to discontinuous systems, even a gain in CPU-time may be achieved. This was shown in Van der Spek et al. [36], where the MCM method was applied to the impact oscillator (3.5).

3.6 Integration interval extension

In this section, it is shown what can go wrong when investigating nonlinear dynamic systems by means of CM methods. As an example, a beam with nonlinear support is chosen. It is shown that the use of CM in its regular way produces spurious results for this system. The system characteristics urge the user to introduce an extended integration interval.

3.6.1 Beam with nonlinear support

A pinned-pinned steel beam with a central nonlinear support is considered. The beam is harmonically excited by a transversal load and is supported by a linear damper and a one-sided linear spring. In Fig. 3.15, a schematic picture of the beam system is shown. This system was studied by Fey [8], who investigated the long term behaviour by means of CMS (component mode synthesis) methods and finite difference techniques. Here, CM methods are used to investigate the long term behaviour for one set of system parameters.

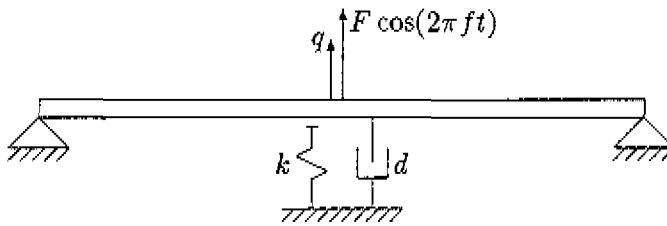


Figure 3.15: Beam system with nonlinear support. Studied by Fey [8].

A 1-DOF model of the beam system is given by the following equation:

$$M\ddot{q} + d\dot{q} + (1 + 6H(-q))kq = F \cos(2\pi ft), \tag{3.9}$$

with $M = 1.0358$ kg, $d = 116.61\xi$ Ns/m, $k = 3282.2$ N/m, $F = 19.693$ N. In (3.9), q represents the displacement of the beam, while the Heavyside function $H(x)$ represents the one-sided character of the linear spring. The ratio of the spring stiffness and the beam stiffness equals six. In [8], the existence of periodic motions is shown for $f \in [0, 40]$ Hz and $\xi = 0.01, 0.05, 0.1$ by means of the above-mentioned methods and path-following techniques. In particular, a $1/2$ subharmonic solution was found for $f = 22$ Hz and $\xi = 0.01$.

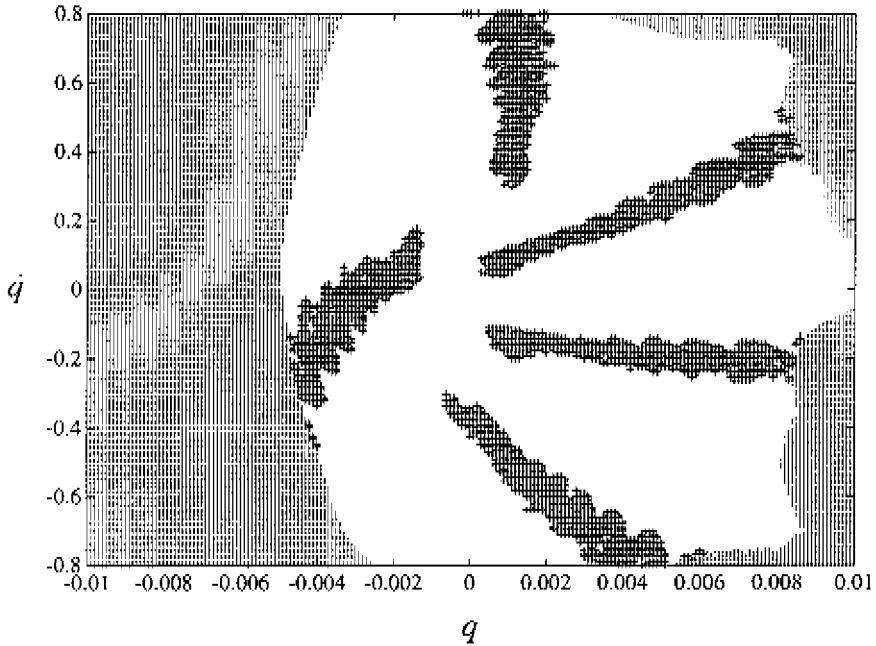


Figure 3.16: SCM results for the beam system (3.9) for $\Delta t = T$: Basin of attraction of the $1/2$ subharmonic solution (left blank); basin of attraction of the $1/5$ subharmonic solution (+); cells leading to the sink cell (-).

3.6.2 Simple cell mapping

The SCM method is applied to the beam system (3.9) for $f = 22$ Hz, $\xi = 0.01$, $\Omega = \{(q, \dot{q}) \mid |q| \leq 0.01 \wedge |\dot{q}| \leq 0.8\}$, and $\Delta t = T$, with $T = 1/f$. For discretization, 201×201 cells are used. The $1/2$ subharmonic solution is represented by a $P - 38$ group and a $P - 8$ group. Further, four $P - 5$ groups are found, representing a $1/5$ subharmonic solution. In Fig. 3.16, the basins of attraction of the periodic groups are shown.

Two aspects of the obtained results are striking: the large number of cells leading to the sink cell and the large number of periodic cells representing low order subharmonic attractors. Both aspects can be explained at the hand of characteristics of the investigated system. The large number of transient cells is caused by the large amplitude excitation, causing the system to undergo large amplitude transient behaviour before settling on one of the attractors

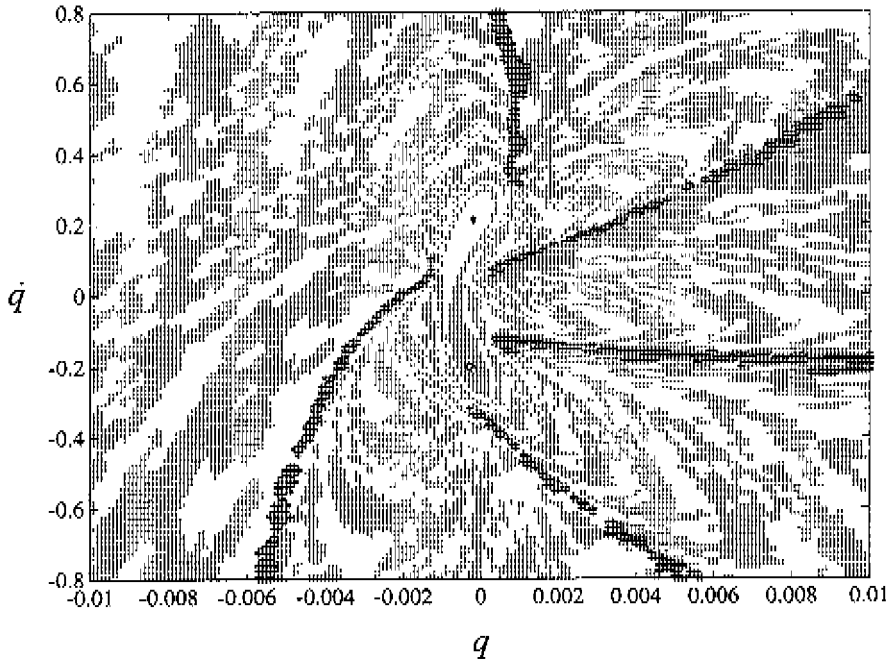


Figure 3.17: SCM results for the beam system (3.9) for $\Delta t = 20T$: 1/2 subharmonic solution (\circ) and basin of attraction (\cdot); coexisting 1/2 subharmonic solution ($*$) and basin of attraction (left blank); basin of attraction of 1/5 subharmonic solution ($+$).

in Ω . Further, the occurrence of many spurious periodic cells is caused by the low system damping. For those cells, an integration-interval of one forcing period is too short to leave the cell when starting in its center point.

Both problems can be tackled by extending the integration interval Δt . In Fig. 3.17, the results are shown of an SCM application for the same Ω and cell discretization, taking $\Delta t = 20T$. As a result, no cells are mapped into the sink cell and the periodic attractors are represented by only a few groups. Taking an even number of system periods has another advantage here. When a 1/2 subharmonic solution exists, actually two 1/2 subharmonic solutions coexist which are equal apart from a phase shift π . Taking $\Delta t = nT$, with n even, the determination of each solution and corresponding basin of attraction is accomplished.

3.6.3 Conclusion

The extension of the integration interval for the determination of image cells (or image points, under ICM) to two or more forcing periods can be applied to accomplish the following:

- Reduction of the number of cells mapped into the sink cell due to transient behaviour.
- Reduction of spurious periodic cells found due to low damping.

This has been shown at the hand of a beam system with nonlinear support, excited by a large amplitude force and experiencing little damping.

It has been shown that cell mapping is a useful addition to periodic solvers. By means of SCM, an additional attractor has been found for the considered beam system for $f = 22$ Hz. In Van der Spek [35], the same beam system was investigated by means of SCM and ICM. This resulted in the detection of additional attractors for $f = 8.34$ Hz and $f = 21.5$ Hz.

Chapter 4

Extensions of Cell Mapping Methods

In this chapter, two important extensions of cell mapping methods are presented. In Section 4.1, parameter variation methods for cell mapping are introduced. After an initial cell mapping application, the proposed methods enable the determination of the basins of attraction for a new system parameter value in relatively little computation time. In Section 4.2, the question how to handle multi-DOF systems by means of cell mapping is dealt with. To reduce the CPU-time and memory demands to reasonable proportions, a general approach is presented for these systems.

4.1 Parameter variation methods for cell mapping

4.1.1 Introduction

The equations of motion of a nonlinear dynamic system usually contain one or more system parameters, which are unknown or can change within a certain bounded interval. An essential step in the research of a nonlinear dynamic system is the study of the influence of the system parameter(s) on the long term behaviour. Methods used for this kind of research are called parameter variation methods or *continuation* methods.

Continuation methods are frequently used in combination with periodic solvers, such as the *shooting* method or the *time discretization* method [3, 8]. Periodic solvers yield a periodic solution (if there exists one) of a set of

ODE's. A continuation method determines the evolution of the periodic solution when a system parameter is changed. For more information about continuation methods, the reader is referred to Seydel [27].

One thing that is still lacking in the established CM methods is a parameter variation method. This method should be capable of determining the evolution of the basin boundaries when a system parameter is varied. Of course, the determination of the basin boundaries for the new parameter value should take less CPU-time than a complete new CM execution. For systems of two or more degrees of freedom, application of cell mapping methods may be very time-consuming. The existence of a continuation method greatly improves the applicability of CM methods to those systems.

In this section, methods are presented which predict the basin boundary evolution of the attractors of a nonlinear dynamic system, which is investigated by means of SCM or ICM. These methods are termed PVSCM and PVICM, respectively. After a regular CM application, yielding two or more attractors and basins of attraction, the specific parameter variation method predicts the basin boundaries and hence the basins of attraction for a varied system parameter value. The necessary CPU-time for one variation step is much smaller than for a new CM execution, as will be shown.

In the next subsections, the PVSCM and PVICM methods are presented. The concept of parameter variation is explained and corresponding algorithms are given. Application of the methods to a modified Duffing equation is discussed. A comparison is made with a regular CM application for the new parameter value. The proposed methods turn out to be very efficient and accurate.

4.1.2 PVSCM Method

Method explanation

A 1-DOF nonlinear dynamic system is considered:

$$\begin{aligned}\dot{x}_1 &= x_2, \\ \dot{x}_2 &= f(x_1, x_2, t, \mu).\end{aligned}\tag{4.1}$$

Here, x_1 and x_2 represent the displacement and velocity of the system, respectively, t stands for time, and μ is a system parameter. It is assumed that f is periodic in t with period T .

The starting-point of the PVSCM method is a regular SCM application to (4.1) for $\mu = \mu_0$. For this purpose, a region of interest Ω in the state

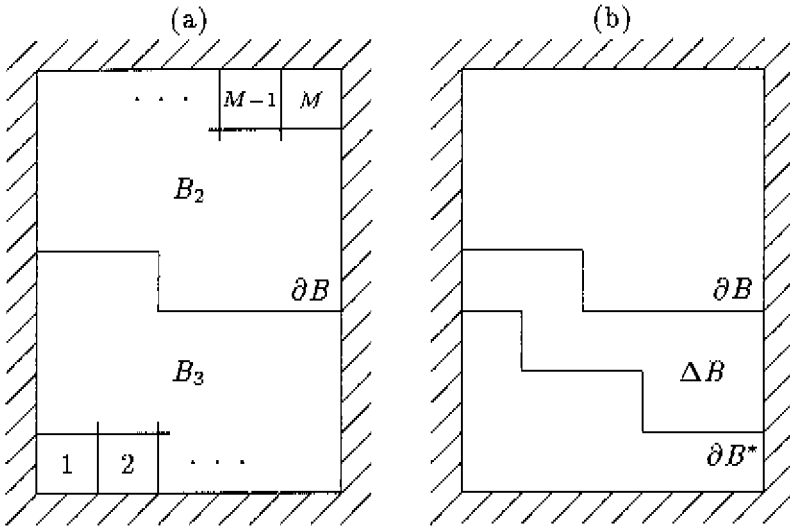


Figure 4.1: (a) Partition of region of interest Ω in basins of attraction separated by basin boundary ∂B . (b) Definition of ΔB .

space is chosen and is discretized in cells, numbered $1, \dots, M$. For each regular cell, the image cell is determined by means of the center point method (see Subsection 2.1.4) with integration interval $\Delta t = T$. After SCM application, each cell $z \in \{1, \dots, M\}$ has obtained a group number $G = G(z)$ which denotes to which group z belongs (as a periodic or as a transient cell).

For illustration purposes, it is assumed that two periodic groups have been found in the SCM application, each representing an attractor. These groups are numbered 2 and 3 (no. 1 is reserved for the sink cell, which is by definition also a periodic group). For the sake of simplicity, it is assumed that each cell in Ω belongs to one of these groups (as a periodic or as a transient cell), which implies that no cells are mapped into the sink cell. Hence, each regular cell z satisfies either $G(z) = 2$ or $G(z) = 3$. The region Ω can be divided in two corresponding basins of attraction B_2, B_3 , separated by the basin boundary ∂B (see Fig. 4.1a).

The aim of the PVSCM method is to determine the position of the basin boundary ∂B^* for $\mu = \mu^* = \mu_0 + \Delta\mu$ in less CPU-time than is necessary for a regular SCM execution. This is achieved by only determining the new image cells (i.e. for $\mu = \mu^*$) for a limited number of cells. When no bifurcations occur, the basin boundary wanders through the state space in a continuous

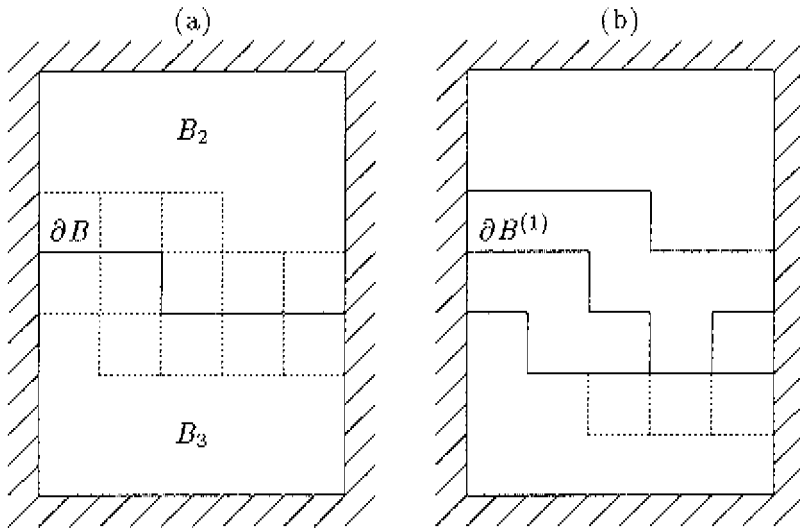


Figure 4.2: (a) Definition of boundary cells. (b) Definition of new boundary cells.

way when a system parameter is continuously varied. For $\mu = \mu^*$, the basin boundary has moved over an area ΔB which is bounded by ∂B and ∂B^* (see Fig 4.1b). By iteratively creating an area B which is as small as possible but which contains ΔB , a set of cells is obtained of which the new group numbers define the new basin boundary. These cells are referred to as B -cells.

Before giving the necessary steps in the PVSCM procedure, the following definitions are introduced:

Definition 1: Two cells z and z' are called *adjoining* if they have at least one cell corner point in common.

Definition 2: A cell z is called a *boundary cell* if there exists a cell z' which is adjoining to z with $G(z) \neq G(z')$.

In Fig. 4.2a, the boundary cells in Ω are shown for $\mu = \mu_0$.

In the PVSCM method, the following steps are taken initially:

1. Determination of the boundary cells for $\mu = \mu_0$. The set of boundary cells is taken as initial set for B .
2. Determination of the image cell $C(z)$ for each cell $z \in B$ for $\mu = \mu^*$.
3. Determination of the group number $G(z)$ for each cell $z \in B$ for $\mu = \mu^*$.

For the determination of group numbers, a cell sequence $z, C(z), C^2(z), \dots$ is created for each $z \in B$ (see Appendix A), making use of the new image cells. When a cell sequence leads to a cell \tilde{z} outside B , all cells in the sequence receive the same group number as \tilde{z} .

The newly determined group numbers produce a new basin boundary $\partial B^{(1)}$, which lies inside B . At places where $\partial B^{(1)}$ touches the boundary of B , B should be expanded. This is done by determining the *new* boundary cells; these are cells which do not belong to B , but satisfy the definition of a boundary cell, due to the new group numbers of the cells in B . The new boundary cells can then be added to B . In Fig. 4.2b, the new boundary cells are indicated. Steps 4 and 5 in the PVSCM algorithm are hence given by:

4. Determination of the new boundary cells.
5. Addition of the new boundary cells to B .

To complete the expansion of B , steps 2-5 are repeated until no new boundary cells are found. In step 2 of course, the image cell needs to be determined only for the *new* B -cells. In step 3 however, it is necessary to determine the new group numbers not only for the new B -cells, but for each B -cell z which eventually maps outside B , hence which satisfies $G(z) \leq 3$ for the considered example. This is done to restore possible errors. After all, when a new boundary cell \tilde{z} receives a group number $G(\tilde{z}; \mu^*) \neq G(\tilde{z}; \mu_0)$, all cells $z \in B$ which are mapped onto \tilde{z} , need to be given the correct group number $G(\tilde{z}; \mu^*)$. This is achieved by re-determining the group number of all B -cells characterized by a group number $G \leq 3$ (cells with $G > 3$ have received their group number on the basis of new data, i.e. for $\mu = \mu^*$, so a re-determination of group numbers is not necessary for these cells). When no new boundary cells are found, the new basin boundary ∂B^* is defined by the group numbers $G(z; \mu^*)$ of all cells $z \in B$.

Here, two remarks need to be made regarding the given procedure. First, it is possible that during the expansion of B a new periodic group is found, e.g. a saddle solution. This does not change anything to the procedure. Groups found inside B receive group number 4, 5, .. and so on.

Second, it should be noted that the PVSCM method determines the new basin boundaries in a minimal CPU-time. The time-consuming part in SCM is the determination of the image cells, in which integration is involved. Here, only for a limited number of cells—the B -cells—the image cell has been determined. The profit with respect to a regular SCM performance is obvious.

PVSCM algorithm

The PVSCM algorithm makes use of the group numbers G determined in a SCM calculation. The group numbers have been stored in the array \mathbf{g} . For each regular cell z , the group number $G(z)$ is given by $\mathbf{g}[z]$. Let N_g be the number of groups (including the sink cell) found under SCM, then $1 \leq \mathbf{g}[z] \leq N_g$ holds for $z = 1, \dots, M$. In the PVSCM algorithm, the following arrays and variables are additionally used:

- $\mathbf{c}[z]$: image cell of z , $z = 1, \dots, M$,
- N_b : number of B -cells,
- K : number of *new* B -cells,
- $\mathbf{b}[i]$: i -th B -cell, $i = 1, \dots, N_b$,
- $\mathbf{ind}[z]$: equals 1 if z is a B -cell, 0 otherwise, $z = 1, \dots, M$.

The first step in the PVSCM method is the determination of the boundary cells. When all cells have been checked, K boundary cells have been found and stored in the array \mathbf{b} . Hence, initially $N_b = K$ and $\mathbf{ind}[\mathbf{b}[i]] = 1$ holds, ($i = 1, \dots, K$).

Steps 2-5, given in the previous subsection, define the general loop of the program. While $K > 0$ holds, the following is repeated:

1. For $i = N_b - K + 1, \dots, N_b$ (i.e., for all new B -cells):
determine the image cell $\mathbf{c}[\mathbf{b}[i]]$ for $\mu = \mu^*$.
2. For $i = 1, \dots, N_b$:
if $\mathbf{g}[\mathbf{b}[i]] \leq N_g$ then $\mathbf{g}[\mathbf{b}[i]] := 0$.
3. For $i = 1, \dots, N_b$:
if $\mathbf{g}[\mathbf{b}[i]] = 0$ then determine the new group number for $\mathbf{b}[i]$.
4. $K := 0$.
5. For $z = 1, \dots, M$:
if z is a boundary cell and $\mathbf{ind}[z] = 0$ then

$$\begin{aligned} K &:= K + 1, \\ \mathbf{b}[N_b + K] &:= z, \\ \mathbf{ind}[z] &:= 1. \end{aligned}$$

6. $N_b := N_b + K$.

In the second step of this loop, all B -cells for which a new group number needs to be determined (new B -cells as well as cells which eventually map outside B , both characterized by a group number $G \leq N_g$) are tagged as *virgin* cells by giving them group number 0 (see also Appendix A). The search for new boundary cells, which is done in the fifth step of the loop, is quite trivial and can be programmed in many ways.

Example of application: modified Duffing equation

As an example of application of the PVSCM method, the modified Duffing equation (2.4) is considered with $d = 0.15$, $a = 0.3$, $\omega = 1.0$. SCM application to this system has been discussed in Section 2.1, with $\Omega: |x_i| \leq 2.02$, $i = 1, 2$, and a cell discretization of 101×101 cells. In Fig. 2.3, the attractors and basins of attraction obtained by SCM are shown.

The PVSCM algorithm is used to determine the basins of attraction for $d = 0.17$. For this purpose, it is necessary to change the group numbers. In the SCM execution for $d = 0.15$, 6 groups were found. However, 3 of them represent the same chaotic attractor. Hence, only 4 different groups need to be distinguished ($N_g = 4$). After the group numbers have been changed and stored, the PVSCM algorithm can be applied.

The results obtained by PVSCM are shown in Fig. 4.3. The basins of attraction of both attractors have been determined for $d = 0.17$. The new position of the saddle solution has also been found. To check these results, the domains of attraction have been determined by means of SCM for $d = 0.17$. The results of both methods perfectly match. In Fig. 4.3, the only cell which belongs to different basins of attraction in both simulations is indicated (\circ). The corresponding CPU-times are 6.4 s (PVSCM) and 21.2 s (SCM).

Remarks

The PVSCM method only produces the basins of attraction for the new parameter value, not the location of the attractors. This information however can easily be obtained by regular numerical integration. Only when a solution lies in the region B (e.g. the saddle solution in the previous example), a corresponding group may be found. Under SCM however, attractors are always represented by periodic groups which approximate the exact location of the attractors. To obtain the exact position and type of the attractors, additional research is necessary. In general, integration over a short interval

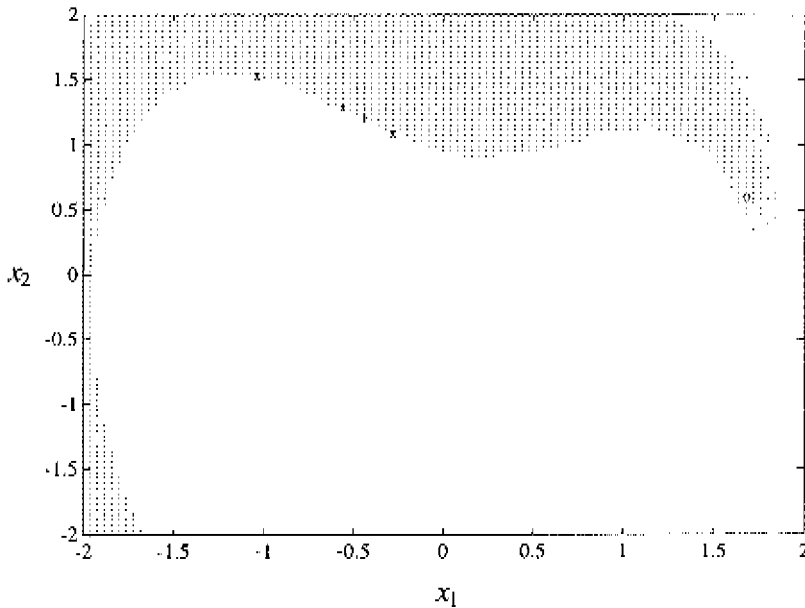


Figure 4.3: SCM and PVSCM results for the modified Duffing equation (2.4) for $d = 0.17$, $a = 0.3$, $\omega = 1.0$: Periodic basin (\cdot); chaotic basin (left blank); saddle solution (+) and stable manifold (x); (\circ) belongs to periodic basin under PVSCM, to chaotic basin under SCM.

starting from one of the cells which represent the attractor is sufficient to get the desired information. In this respect, the absence of periodic groups in the results of a PVSCM execution can not be seen as a shortcoming.

The basins of attraction obtained by PVSCM are approximations for those obtained by SCM. By means of adaptively enlarging the set of B -cells, the approximation error is kept as small as possible. However, things can go wrong when a B -cell z is mapped onto a cell $\tilde{z} \notin B$ with $G(\tilde{z}; \mu^*) \neq G(\tilde{z}; \mu_0)$. Then, z receives a wrong group number $G(\tilde{z}; \mu_0)$. When \tilde{z} is never going to be part of B , cell z —as well as all cells in B which received their group number due to leading to \tilde{z} —will keep this wrong group number. The chance for this to happen is small, assuming that the basin boundaries change smoothly and that generally the state of the investigated system moves away from the basin boundary towards the attractor. When the parameter variation step $\Delta\mu$ is increased, the probability of error-introductions grows.

In the example of the modified Duffing equation, an extended starting set for B was used. Besides the initial boundary cells, all cells bordering on the sink cell were added to B as well. When a parameter is varied, changes in the basin boundary can also occur along the boundary of Ω . To predict this kind of changes, the extension of the starting set for B is necessary. Application of the PVSCM method to (2.4) with $\Delta d = 0.02$ using only the boundary cells as starting set for B did not predict the basin boundary changes in the upper left corner of Ω . Apart from that, the results were identical. The necessary CPU-time for this simulation was 5.5 s.

4.1.3 PVICM method

Method explanation

The parameter variation technique presented in the previous section can be applied to ICM in a similar way. Under ICM, cells actually do not play a role. By regarding the ICM grid points as cell center points, the parameter variation concept for SCM is suited for ICM as well. Suppose ICM has been applied to (4.1) for $\mu = \mu_0$, yielding two attractors, numbered 2 and 3, and corresponding basins of attraction. Then, for each regular cell z a group number $G(z)$ exists, which denotes to which basin z belongs, as well as an image point $\mathbf{x}(z)$, determined by numerical integration over T seconds. To obtain the basin boundary for $\mu = \mu^* = \mu_0 + \Delta\mu$, again a region B is created which covers all the cells between the old and new basin boundary.

The procedure for the creation of B is the same as under PVSCM, apart from a few (trivial) differences. First, for each new B -cell z the image point $\mathbf{x}(z)$ is determined instead of the image cell $C(z)$. Second, interpolation is used to determine a cell's group number. During interpolation, the new image points (determined for $\mu = \mu^*$) should be used when available.

PVICM algorithm

In the PVICM algorithm, two arrays are used from the ICM execution for $\mu = \mu_0$. Besides the array of group numbers g , a two-dimensional array ip is available. Here, $ip[z][i]$ initially contains the i -th coordinate of the image point $\mathbf{x}(z)$ for $\mu = \mu_0$. Whenever for a B -cell z the new image point is determined in the algorithm, ip is updated. The array ip contains all the necessary data for the interpolation of trajectories. Further, the same arrays and variables are used as under PVSCM, except for the array c which is not relevant under ICM.

The first step in the PVICM algorithm is the same as under PVSCM: determination and storage of the initial boundary cells. Next, the following steps are repeated until the number K of boundary cells equals zero:

1. For $i = N_b - K + 1, \dots, N_b$:
determine the image point $\mathbf{x}(\mathbf{b}[i])$ for $\mu = \mu^*$ and store it in ip .
2. For $i = 1, \dots, N_b$:
if $\mathbf{g}[\mathbf{b}[i]] \leq N_g$ then determine the new group number for $\mathbf{b}[i]$.
3. $K := 0$.
4. For $z = 1, \dots, M$:
if z is a boundary cell and $\text{ind}[z] = 0$ then

$$\begin{aligned} K &:= K + 1, \\ \mathbf{b}[N_b + K] &:= z, \\ \text{ind}[z] &:= 1. \end{aligned}$$

5. $N_b := N_b + K$.

The determination of group numbers is realized by means of interpolation, which is continued until convergence is obtained or until a state is reached of which the surrounding grid points belong to cells which have identical group numbers (MICM method, see Section 3.4). When no convergence is obtained within IMAX interpolation steps, the trajectory is considered to be chaotic. The cell containing the initial point is accordingly tagged by receiving group number 0.

Example of application: modified Duffing equation

In Section 2.3, ICM has been applied to the modified Duffing equation (2.4) for $d = 0.15$, $a = 0.3$, $\omega = 1.0$. This resulted in the location of the periodic and the chaotic attractor as well as the domains of attraction (Fig. 2.9). Due to the periodicity criterion and the recurrent character of the chaotic attractor, 8 additional periodic groups were found on the chaotic attractor. The corresponding basins of attraction, which only consisted of very few points, were added to the chaotic attractor's basin of attraction. These results are used as a reference for PVICM.

After re-numbering the group numbers, the PVICM method is applied to (2.4) with $\Delta d = 0.02$. Fig. 4.4 shows the new basins of attraction as well

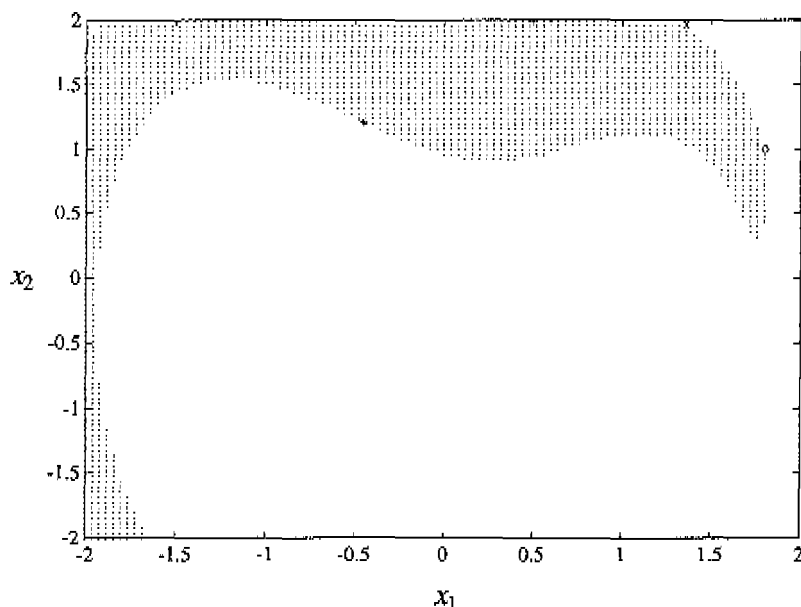


Figure 4.4: ICM and PVICM results for the modified Duffing equation (2.4) for $d = 0.17$, $a = 0.3$, $\omega = 1.0$: Periodic basin (\cdot); chaotic basin (left blank); saddle solution ($+$) and transient cell (x); (\circ) belongs to periodic basin under PVICM, to chaotic basin under ICM.

as the newly found saddle solution. Here, also the cells bordering on the sink cell have been included in the starting set for B . To check the results, ICM has been applied for $d = 0.17$. In Fig. 4.4, discrepancies between PVICM and ICM results are indicated (\circ). Again, a very good resemblance in the basins of attraction is achieved. Also the location of the saddle solution is identical for both methods. The CPU-times for both methods are 7.5 s (PVICM) and 35.0 s (ICM).

Next, the PVICM method is applied with $\Delta d = 0.03$, which implies a damping variation of 20%. All grid points are found to lead to the chaotic attractor for this case. A regular ICM performance for $d = 0.18$ proved the correctness of these results. Hence, the vanishing of the periodic attractor, which happens somewhere between $d = 0.17$ and $d = 0.18$, can be predicted by means of the PVICM method. Here, the necessary CPU-times for the ICM and PVICM executions are 36.1 s and 15.6 s, respectively.

Remarks

The additional information of ICM with respect to SCM is the location of the chaotic attractor. Unlike under SCM, where the chaotic attractor is represented only by a few periodic groups, the end points of chaotic trajectories form a reasonable approximation of the chaotic attractor. This additional information is missing when using the PVICM method. However, the chaotic attractor obtained by regular ICM is still not very accurate when regarding the end points near the periodic attractor. These points belong to trajectories which need more than IMAX steps to converge to the periodic attractor. Further, the chaotic attractor is partly formed by end points of trajectories which have not converged to this attractor yet, resulting in a disorderly picture of the attractor (compared with the picture obtained by regular numerical integration in Fig. 1.3). Hence, for a correct chaotic attractor, a regular numerical integration is necessary anyway. This means that the lacking of a chaotic attractor for $\mu = \mu^*$ again is not a real shortcoming of the PVICM method.

The chaotic attractor's basin of attraction for $\mu = \mu^*$, obtained by regular ICM, not only consists of initial points of chaotic trajectories, but also of grid points leading to periodic groups on the chaotic attractor. To obtain the correct basin of attraction, all basins of these periodic groups need to be included. Under PVICM however, the correct basins of attraction are directly obtained without ad-hoc interference by the user.

4.1.4 Conclusions

A parameter variation (PV) method for cell mapping has been introduced. It has been shown that the method can be applied to both SCM and ICM, in which case it is termed PVSCM and PVICM, respectively. The PV methods determine the evolution of the basin boundaries, initially determined by SCM or ICM, when a system parameter is varied. Corresponding algorithms have been presented.

Application of the PVSCM and PVICM methods to a modified Duffing equation has been performed. The obtained results perfectly match with regular cell mapping executions for the new parameter value. The PV methods however are up to five times as fast.

The presented methods may not work when global bifurcations occur during the parameter variation, due to discontinuous changes in the basin boundaries. However, results obtained by the PV methods can be used to

predict global bifurcations for additional parameter variation. The vanishing of attractors during variation can be handled in general. In that case, the CPU-time profit may be smaller than usual. Application to systems with fractal basins of attraction may even produce no profit at all. In that case, due to the followed concept, the number of cells for which a new image cell needs to be determined will be much larger.

4.2 Cell mapping for multi-DOF systems

4.2.1 Introduction

When applying CM methods in their regular form to systems of many DOF's, problems of computational kind can be expected. For a dynamic system of l DOF's, the corresponding state space has dimension $N = 2l$. According to (2.2), the number M of regular cells for a SCM application grows exponentially with N . Additionally, the necessary CPU-time to determine a cell's image cell grows linearly with N , since N first-order ODE's need to be integrated for this purpose. This means that for $N > 4$ extremely high CPU-times will occur.

Under regular SCM, several arrays of length M are created in the algorithm. For each cell $z \in \{1, \dots, M\}$, the image cell $C(z)$ is stored as well as its group number $G(z)$ and the step number $S(z)$, which is the number of mapping steps required for z to end up on a periodic group ([14], Appendix A). Under GCM, a cell can have several image cells, which means that even more arrays are needed. Under ICM, all (N) coordinates of the image point of each grid point need to be stored. Hence, for too large values of M , the computer memory capacity will be exceeded for any CM method.

The present-day hardware memory capacity and processing speed put a limit on the number of cells and hence on the number of DOF's of the investigated system. Systems modelled by two DOF's probably form the limit for regular CM application. In Hsu [14], a 2-DOF Van der Pol system was investigated by means of SCM using 59^4 cells. For the determination of image cells, an integration interval $\tau = 2.2$ was used. This simulation took 19 hours on a VAX-11/750. The same simulation has been repeated by the author on a SG Challenge, in which case 2.5 hours were needed. However, an additional DOF will increase the CPU-time with another factor 59^2 when the same number of cells is used for discretization in the additional dimensions. Hence, it seems that applying CM methods to systems of three or more DOF's is hardly possible, unless M is kept relatively small by using very large

cells. In doing so however, the errors introduced by the cell discretization will also be very large.

It is concluded that new CM techniques are necessary for the investigation of systems of three or more DOF's. An example of such a new technique is the MDCM (multi-DOF cell mapping) method, which is presented in the next subsection. The MDCM method is deduced from SCM and can be applied to systems of arbitrary number of DOF's. In Subsection 4.2.5, application is performed to a 4-DOF dynamic system.

4.2.2 MDCM concept

Under regular SCM, the attractors and basins of attraction are determined in a region of interest Ω in the N -dimensional state space. However, a two-dimensional subspace Σ needs to be chosen for representation purposes. For large N , many choices for Σ are possible. Hence, the user has to decide which choices are most relevant. This means that many data are not used in practice. Therefore, it seems meaningful to make these choices beforehand and to determine the long term behaviour only for the initial states lying in the subspace of interest. This point of view is the basis for MDCM.

The aim of the MDCM method is the determination of the intersections of the basins of attraction of a N -dimensional dynamic system ($N \geq 3$) with a two-dimensional subspace Σ . For this purpose, the following steps are taken:

- A two-dimensional subspace $\Sigma \subset \mathbb{R}^N$ is chosen.
- In Σ , a region of interest Ω' is chosen.
- A set of cells S is defined, covering Ω' .
- For each cell $z \in S$, the group number $G(z)$ is determined by creating a cell processing sequence $z, C(z), C^2(z), \dots$

The final step is explained in detail in the next subsection. The intersections of the basins of attraction with Σ are given by the cells in S with equal group number. Since only for cells in the processing sequences the image cell is determined instead of for all cells in Ω under regular SCM the CPU-time and memory demand is reduced drastically in this way. Under MDCM, there is no real restriction on the system dimension.

An interesting aspect of MDCM is the possibility of re-using stored group numbers of processed cells. Having applied MDCM for a certain subspace

Σ^1 , use can be made of these group numbers when applying MDCM for another subspace Σ^2 . When a cell sequence starting from a cell $z \in \Sigma^2$ leads to a cell z' which has already been processed in the first application, the sequence can be terminated. All cells in the sequence then obtain the same group number as z' . In this way, the creation of each processing sequence is stopped at an early stage, yielding an extra gain in CPU-time.

4.2.3 MDCM method

Consider a N -dimensional dynamic system governed by

$$\dot{x}_i = F_i(x_1, \dots, x_N, t), \quad i = 1, \dots, N, \tag{4.2}$$

with F_i periodic in t with period T ($i = 1, \dots, N$). In the state space \mathbb{R}^N , a N -dimensional cell structure is created. To this end, N cell sizes h_1, \dots, h_N are chosen. Each cell in this structure is denoted by a cell vector $\mathbf{z} = [z_1 \dots z_N]^T$, with $z_i \in \mathbb{Z}$ ($i = 1, \dots, N$). A cell \mathbf{z} contains all states $\mathbf{x} = [x_1 \dots x_N]^T$ with

$$(z_i - 1/2) h_i \leq x_i \leq (z_i + 1/2) h_i, \quad i = 1, \dots, N. \tag{4.3}$$

As a result, the center point of a cell \mathbf{z} is given by $\mathbf{c} = [c_1 \dots c_N]^T$ with

$$c_i = h_i z_i, \quad i = 1, \dots, N. \tag{4.4}$$

The definition of a two-dimensional subspace Σ is realized by giving $N - 2$ cell indices a constant value, e.g. $z_3 = \dots = z_N = 0$. Σ is then defined by the corresponding center points, hence $\Sigma : x_3 = \dots = x_N = 0$. On Σ , a bounded region Ω' is defined by introducing an upper and lower limit for the remaining two state variables:

$$\Omega' = \{\mathbf{x} \in \mathbb{R}^N \mid x_i^{(l)} \leq x_i \leq x_i^{(u)}, \quad i = 1, 2 \wedge x_i = 0, \quad i = 3, \dots, N\}. \tag{4.5}$$

The set S of cells covering Ω' is then given by

$$S = \{\mathbf{z} \in \mathbb{Z}^N \mid z_i^{(l)} \leq z_i \leq z_i^{(u)}, \quad i = 1, 2 \wedge z_i = 0, \quad i = 3, \dots, N\}, \tag{4.6}$$

where $z_i^{(l)}$ and $z_i^{(u)}$ are related to $x_i^{(l)}$ and $x_i^{(u)}$ according to (4.3). The number of cells in S is given by M , with

$$M = (1 + z_1^{(u)} - z_1^{(l)})(1 + z_2^{(u)} - z_2^{(l)}). \tag{4.7}$$

To determine the long term behaviour for each $\mathbf{z} \in S$, a cell sequence $\mathbf{z}, C(\mathbf{z}), C^2(\mathbf{z}), \dots$ is created, with $C : \mathbb{Z}^N \rightarrow \mathbb{Z}^N$. The determination of

an image cell $C(\mathbf{z})$ for a cell $\mathbf{z} = [z_1 \dots z_N]^T$ is realized by means of the center point method: First, the center point \mathbf{c} is obtained by means of (4.4). Second, numerical integration of (4.2) is performed over an interval $\Delta t = T$ using \mathbf{c} as initial state. This integration yields a state $\mathbf{y} = [y_1 \dots y_N]^T$. Third, the image cell $\mathbf{z}^* = [z_1^* \dots z_N^*]^T$ is determined, which is the cell containing \mathbf{y} . The cell indices of \mathbf{z}^* are given by

$$z_i^* = \text{int}(y_i/h_i + 1/2), \quad (4.8)$$

where $\text{int}(x)$ denotes the largest integer which is less than or equal to x . A cell sequence is terminated when a cell is found which already occurred in the sequence or which has already been tagged in a previous sequence. In the former case, a new periodic group has been found; in the latter one, all cells in the sequence are transient cells, leading to an already discovered group, and are accordingly tagged.

Under MDCM, it is not necessary to define a sink cell. After all, for each state $\mathbf{x} \in \mathbb{R}^N$ a corresponding cell exists according to (4.8). Hence, a cell sequence will not be terminated because of ending up in the sink cell, as under SCM, but can be continued until a periodic group is found. Without the existence of a sink cell however, the number of cells in the state space is infinite. This implies the possibility of a never ending cell sequence. Just as under ICM, this problem is tackled by introducing a maximum number of cells in a sequence. When this maximum is exceeded, all cells in the sequence are assumed to lead to a chaotic attractor.

4.2.4 MDCM algorithm

Compared with SCM, a different way of storing cell data is applied in the MDCM algorithm. Under SCM, the group number, the step number, and the index of the image cell are stored for each regular cell. Under MDCM, this approach is impossible because of the infinite number of regular cells in the state space. For storing purposes, the following arrays and variables are used:

- N_{pc} : number of processed cells, i.e. cells which have obtained a definite group number.
- K : number of cells under processing, i.e. cells in the current processing sequence.

- **pc**: two-dimensional array containing all cells processed or under processing. Here, $\text{pc}[i]$ denotes the i -th cell in **pc** while $\text{pc}[i][j]$ contains the j -th index of $\text{pc}[i]$ ($j = 1, \dots, N, i = 1, \dots, N_{\text{pc}} + K$).
- **g**: one-dimensional array containing the group numbers of all cells in **pc**. Hence, the group number of $\text{pc}[i]$ is given by $\mathbf{g}[i]$ ($i = 1, \dots, N_{\text{pc}} + K$).
- **ind**: one-dimensional array containing the position in **pc** of cells in the current sequence. Hence, the i -th cell in the current sequence is given by $\text{pc}[\text{ind}[i]]$ ($i = 1, \dots, K$).

During the generation of a cell sequence, it has to be checked if the latest determined cell \mathbf{z} has already occurred in the current or in a previous sequence. This information is obtained by scanning the array **pc**. The CPU-time required for this operation is proportional to the number of cells stored in **pc**, which is given by $m := N_{\text{pc}} + K$. Since m grows during the algorithm and at least will be equal to M , it is useful to reduce this CPU-time by sorting the cells in **pc**: If $1 \leq i < j \leq m$ then $\text{pc}[i] < \text{pc}[j]$. Here, the relation $<$ for two vectors \mathbf{x} and \mathbf{y} of length N is defined as

$$\mathbf{x} < \mathbf{y} \iff \exists_{j \in \{1, \dots, N\}} \{x_j < y_j \wedge x_i = y_i \ 1 \leq i < j\}. \quad (4.9)$$

When **pc** is sorted in this way, the search for a certain cell takes a CPU-time which is proportional to $\log(m)$ (see e.g. [34]).

Let N_g denote the number of periodic groups found in the MDCM algorithm. The initialization of the algorithm is then given by

- $N_g := 0$
- $N_{\text{pc}} := 0$.

Let the cells in S be denoted by $\mathbf{z}^1, \dots, \mathbf{z}^M$. To determine the group number of $\mathbf{z} = \mathbf{z}^i$ ($i = 1, \dots, M$) the following is performed: First, it is checked if \mathbf{z} already occurs in **pc**, by means of the assignment

- $B := \text{SCAN}(\mathbf{z}, \text{pc}, I)$,

where **SCAN** is a function returning **TRUE** if \mathbf{z} occurs in **pc**, **FALSE** otherwise. In the former case, I receives the corresponding index, which means that afterwards $\text{pc}[I] = \mathbf{z}$ holds. In the latter case, I receives the index of the smallest cell in **pc** larger than \mathbf{z} . If no such cell exists, $\mathbf{z} > \text{pc}[N_{\text{pc}}]$ holds and I is set equal to $N_{\text{pc}} + 1$.

After calling SCAN, two possibilities exist. When $B = \text{TRUE}$, z has already been processed in a previous sequence. In that case, the current investigation is terminated and the procedure is restarted for the next cell z^{i+1} . When $B = \text{FALSE}$, z has not occurred in any sequence. In that case, a cell sequence is generated, starting from z . To this end, the number K of cells in the current sequence is initially set equal to zero:

- $K := 0$.

Next, the following steps are performed:

1. $K := K + 1$
2. for $(j = I + 1, \dots, N_{pc} + K)$: $pc[j] := pc[j - 1]$
3. $pc[I] := z$
4. for $(j = I + 1, \dots, N_{pc} + K)$: $g[j] := g[j - 1]$
5. $g[I] := -1$
6. for $(j = 1, \dots, K - 1)$: if $(ind[j] \geq I)$ $ind[j] = ind[j] + 1$
7. $ind[K] := I$
8. $z := \text{IMCELL}(z)$
9. $B := \text{SCAN}(z, pc, I)$

In step 1, K is updated. In steps 2 and 3, z is stored in pc at position I and pc is accordingly updated. In steps 4 and 5, g is updated and z is tagged as a cell under processing by receiving a temporary group number -1 . In step 6, the array ind is adjusted according to the changes in pc . In step 7, the index of the latest determined cell z is stored in ind . In step 8, z is set equal to its image cell $C(z)$, which is determined by means of the function IMCELL . Finally, pc is scanned for the occurrence of z in step 9.

Steps 1-9 are repeated until one of the following situations occurs:

(A) $B = \text{TRUE}$: In this case, the latest determined cell z already occurs in pc . Depending on the corresponding group number $g[I]$ of z , the following situations are distinguished:

(A1) $g[I] = -1$: In this case, z already occurred in the current sequence, which means that a new periodic group has been found. As a result, N_g is updated and all cells in the current sequence are tagged:

- $N_g := N_g + 1$
- for $(i = 1, \dots, K)$ $g[\text{ind}[i]] := N_g$.

(A2) $g[I] \geq 0$: In this case, z has already occurred in a previous sequence. The cells in the current sequence then lead to the same attractor as z and hence receive the same group number:

- for $(i = 1, \dots, K)$ $g[\text{ind}[i]] := g[I]$.

(B) $K = \text{MAX}$: In this case, the number of cells in the current sequence equals the maximum number MAX without visiting a cell which is stored in pc . Then, all cells in the sequence are assumed to lead to a chaotic attractor and are accordingly tagged by receiving group number 0. Additionally, the latest determined cell z needs to be stored in pc and hence g and pc need to be updated. Hence,

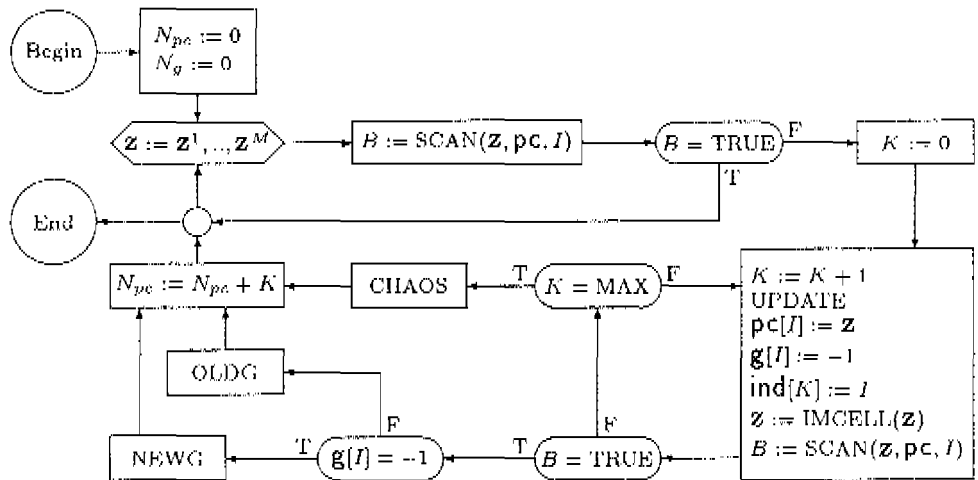
- $K := K + 1$
- for $(i = 1, \dots, K - 1)$ $g[\text{ind}[i]] := 0$.
- for $(j = I + 1, \dots, N_{pc} + K)$ $pc[j] := pc[j - 1]$
- $pc[I] := z$
- for $(j = I + 1, \dots, N_{pc} + K)$ $g[j] := g[j - 1]$
- $g[I] := 0$

In both (A) and (B), all cells in the sequence have been processed. Hence, N_{pc} is updated as follows:

- $N_{pc} := N_{pc} + K$.

This completes the investigation for z^i . The procedure can now be repeated for the next cell in S . In Fig. 4.5, a flowchart is given of the MDCM-algorithm.

Having determined the group number of each cell in S , the research is finished. If desired, a new set of cells S' can be chosen for investigation. In that case, the same procedure is applied, starting with the current values for N_g and N_{pc} and using the data stored in pc and g .



Subroutine UPDATE:

for $(i = I + 1, \dots, N_{pc} + K)$ { $pc[i] := pc[i - 1]$; $g[i] := g[i - 1]$ }
 for $(i = 1, \dots, K - 1)$ {if $(ind[i] \geq I)$ $ind[i] := ind[i + 1]$ }

Subroutine CHAOS:

$K := K + 1$; UPDATE; $pc[I] := z$; $ind[K] := I$;
 for $(i = 1, \dots, K)$ { $g[ind[i]] := 0$ }

Subroutine NEWG:

$N_g := N_g + 1$
 for $(i = 1, \dots, K)$ { $g[ind[i]] := N_g$ }

Subroutine OLDG:

for $(i = 1, \dots, K)$ { $g[ind[i]] := g[I]$ }

Figure 4.5: Flow chart of the MDCM algorithm.

4.2.5 Application: 4-DOF beam with nonlinear support

The beam system with nonlinear support discussed in Section 3.6 is used as application for the MDCM method. A 4-DOF model of this system is given by the following set of equations:

$$M\ddot{\mathbf{q}} + D\dot{\mathbf{q}} + K\mathbf{q} + \mathbf{f}(\mathbf{q}) = \mathbf{F}(t). \quad (4.10)$$

Here, $\mathbf{q} = [q_1 \ q_2 \ q_3 \ q_4]^T$ is an approximation of the real displacement field, containing three free-interface eigenmodes and one residual flexibility mode (see [8, page 84]). Further, M , D , and K are the corresponding mass, damping, and stiffness matrices, respectively, which are given by

$$M = \begin{bmatrix} 1.38 & 0.38 & -0.38 & -0.39 \\ 0.38 & 1.38 & -0.38 & -0.39 \\ -0.38 & -0.38 & 1.38 & 0.39 \\ -0.39 & -0.39 & 0.39 & 0.39 \end{bmatrix} \quad D = \begin{bmatrix} 0 & 0 & 0 & 0 \\ 0 & 0 & 0 & 0 \\ 0 & 0 & 0 & 0 \\ 0 & 0 & 0 & 116.61\xi \end{bmatrix}$$

$$K = \begin{bmatrix} 62.91 & 43.21 & -43.19 & -43.98 \\ 43.21 & 43.30 & -43.25 & -44.04 \\ -43.19 & -43.25 & 45.80 & 44.02 \\ -43.98 & -44.04 & 44.02 & 44.82 \end{bmatrix} \cdot 10^5. \quad (4.11)$$

Here, ξ is a nondimensional damping coefficient. Finally, $\mathbf{f}(\mathbf{q})$ and $\mathbf{F}(t)$ contain the nonlinearity and the external excitation of the system, respectively. For the considered system, they are given by

$$\mathbf{f}(\mathbf{q}) = \begin{bmatrix} 0 \\ 0 \\ 0 \\ 19690\text{H}(-q_4)q_4 \end{bmatrix} \quad \mathbf{F}(t) = \begin{bmatrix} 0 \\ 0 \\ 0 \\ 19.69 \cos(2\pi ft) \end{bmatrix}. \quad (4.12)$$

Here, $\text{H}(x)$ is the Heavyside function, representing the one-sided linear spring and f is the frequency of the external excitation.

For $f = 22$ Hz and $\xi = 0.02$, the MDCM method is applied to (4.10). The state of the system is given by $\mathbf{x} = [x_1 \dots x_8]^T$, with $x_i = q_i$, $x_{i+1} = \dot{q}_i$, $i = 1, 3, 5, 7$. In the 8-dimensional state space, a cell structure is defined by introducing 8 cell sizes h_1, \dots, h_8 , given by $6 \cdot 10^{-7}$, $6 \cdot 10^{-4}$, $4 \cdot 10^{-5}$, $8 \cdot 10^{-3}$, $6 \cdot 10^{-6}$, $3 \cdot 10^{-3}$, $4 \cdot 10^{-5}$, $1 \cdot 10^{-2}$, respectively. The (x_1, x_2) -plane is taken as subspace of interest Σ ; this plane corresponds to all cells \mathbf{z} with $z_i = 0$ for $i = 3, \dots, 8$. In Σ , a bounded region Ω' is defined by putting $-25 \leq z_1, z_2 \leq 25$, which implies $|x_1| \leq 1.5 \cdot 10^{-5} \wedge |x_2| \leq 0.015$. Hence,

Ω contains $M = 51 \times 51$ cells. For the determination of image cells, an integration interval $\Delta t = 20T$ is used (see also Section 3.6). The maximum number MAX of cells in a cell sequence is set equal to 20.

In Fig. 4.6a, the results of this simulation are shown. The blank area corresponds to cells which lead to a $1/2$ subharmonic solution. Cells identified by a (\cdot) lead to a $1/6$ subharmonic solution. The necessary CPU-time for this simulation is approximately one hour. In Fig. 4.7, state space representations are shown for all state variables for both solutions.

In Fig. 4.6b-h, the basins of attraction are shown for different choices for Σ . The modifications with respect to (a) are given by $z_4 = 1, 2, \dots, 7$, respectively, which implies $x_4 = 8n \cdot 10^{-3}$, $n = 1, 2, \dots, 7$. For $x_4 = 0.032$ and $x_4 = 0.056$, only the $1/2$ subharmonic solution is found as possible long term behaviour for the considered initial states. It should be noted that in each new simulation use is made of the results obtained in the previous simulations. In this way, the CPU-time is reduced to approximately half an hour per simulation.

4.2.6 Concluding remarks

A CM method for multi-DOF systems has been introduced, termed MDCM. Under MDCM the long term behaviour is determined for a bounded set of initial states in a two-dimensional subspace of the state space. As a result, MDCM yields two-dimensional representations of the actual basins of attraction. The corresponding attractors are represented by periodic groups and by final cells in sequences of length MAX. By means of numerical integration, the exact position and type of the attractors can be found.

With the analysis of a 4-DOF beam system, it has been shown that the MDCM method is an effective tool for investigating multi-DOF systems. Besides a $1/2$ subharmonic solution, which was also found by Fey [8] by means of a periodic solver for different damping values, MDCM detected the existence of a $1/6$ subharmonic solution. This again shows that CM is a useful addition to periodic solvers.

An alternative way of determining the long term behaviour of a two-dimensional set of initial states Ω' in a N -dimensional state space is numerical integration, to be performed for each initial state, and to be continued until convergence to an attractor is accomplished. Results obtained by this approach match quite well with the MDCM results, as far as the 4-DOF beam system is considered. However, the same order of CPU-time is required for each new choice of Ω' (± 3.5 hours for the considered example).

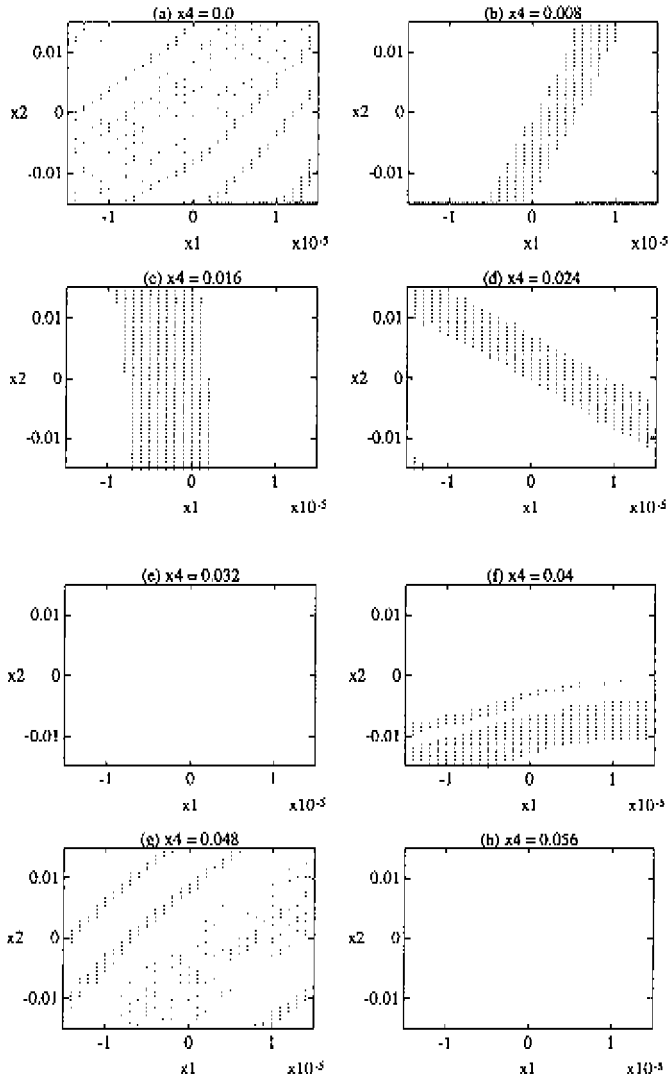


Figure 4.6: MDCM results for the 4-DOF beam system (4.10) for $f = 22$ Hz, $\xi = 0.02$: Cells leading to a $1/2$ subharmonic solution (left blank); cells leading to a $1/6$ subharmonic solution (\cdot). Remaining initial states: $x_3 = x_5 = x_6 = x_7 = x_8 = 0$.

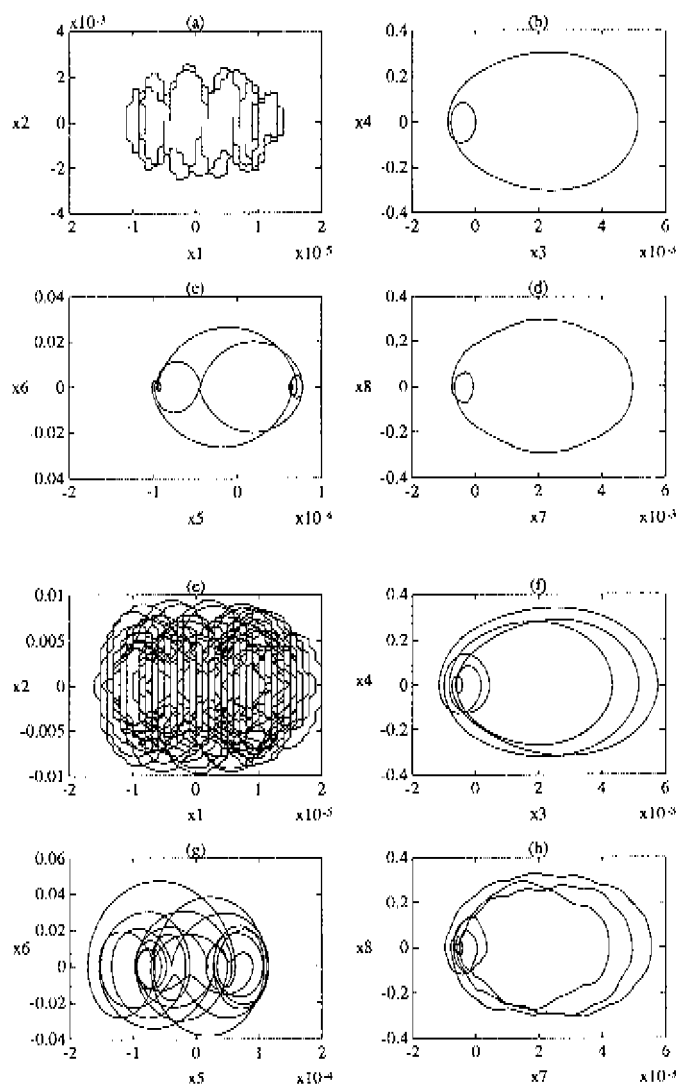


Figure 4.7: Periodic solutions of the 4-DOF beam system (4.10) for $f = 22$ Hz, $\xi = 0.02$: (a)-(d) $1/2$ subharmonic solution. (e)-(h): $1/6$ subharmonic solution.

Chapter 5

Applications

In this chapter, cell mapping methods are applied to some practical nonlinear dynamic systems. First, a rotordynamic rubbing problem is considered, featuring a mass-eccentric elastic rotor which rotates around a rigid shaft. Nonlinear phenomena occur when the rotor touches the shaft (rubbing). Here, the ASCM method is used for investigation. Second, the MDCM method is applied to a 2-DOF model of a portable compact disc player which is hanging on a jogger's shoulder. In this model, the nonlinearities are represented by a one-sided connection between player and pad as well as between shoulder and pad.

5.1 Rotor with rubbing

5.1.1 Introduction

Rotordynamic systems have been studied for many years. This study finds its application in the manufacturing of large turbines as well as small domestic utensils. Knowledge about the phenomena in rotordynamic motion is very important to assure reliability of the machinery as well as to diminish unpleasant side-effects for the user, such as noise and malfunctioning.

In 1919, Jeffcott [17] was the first to present a mathematical description of the whirling response of simple rotor models. In recent investigations, special emphasis has been put on the nonlinear response of rotors [9, 2, 25, 5, 19]. Nonlinear motion can be caused by rubbing between rotor and housing, nonlinear bearings, clearances, or nonlinear supports. The analysis of these problems is mostly carried out by means of periodic solvers, regular numerical integration, and analytical techniques.

In the next subsection, a rotordynamic problem with rubbing is considered featuring an elastic rotor rotating around a fixed shaft. The model is similar to the one studied by Crooijmans [3], in which case rubbing concerned the rotor-housing contact. In [3], the time-discretization method was used to determine periodic solutions of the system. By means of continuation methods, additional bifurcation research was performed. Here, the ASCM method is used to determine all possible responses of the system for a certain set of system parameters.

5.1.2 The rotor model

Geometry of the rotor

A flexible rotor of mass M is considered, which is rotating with constant radial velocity Ω around a fixed rigid shaft. The rotor is mass-eccentric. The inner radius of the rotor is given by R while C denotes the clearance between rotor and shaft. Here, $R \gg C$ holds.

The motion of the rotor is described by two DOF's, x and y , which determine the position of the geometrical center of the rotor, P_g , with respect to the fixed center of the shaft, P_o . The mass unbalance of the rotor is represented by e , which denotes the distance between P_g and the center of mass P_m . In Fig. 5.1, a momentary position of the rotor is shown.

Forces exerted on the rotor

Between rotor and the shaft, no medium is present. This means that the rotor undergoes a free motion as long as contact between rotor and shaft does not occur. In case of contact, i.e. for $\Delta := \sqrt{x^2 + y^2} - C \geq 0$, the shaft exerts a restoring force $\mathbf{F}^s = \mathbf{F}^n + \mathbf{F}^t$ on the rotor, with

$$\mathbf{F}^n = F_n \begin{bmatrix} -\cos \theta \\ -\sin \theta \end{bmatrix}, \quad \mathbf{F}^t = F_t \begin{bmatrix} \sin \theta \\ -\cos \theta \end{bmatrix}. \quad (5.1)$$

The angle θ is defined as the angle between $P_g - P_o$ and the positive x -axis (see Fig. 5.1). The force \mathbf{F}^s applies in the idealized contact point $P_c = -a(\cos \theta, \sin \theta)$, with $a = R - C$ (see Fig. 5.2).

The rotor is made of visco-elastic material, with stiffness k and damping d , while the shaft is rigid. Hence, the normal component F_n of \mathbf{F}^s satisfies

$$F_n = H(\Delta) \max\{0, k\Delta + d\dot{\Delta}\}, \quad (5.2)$$

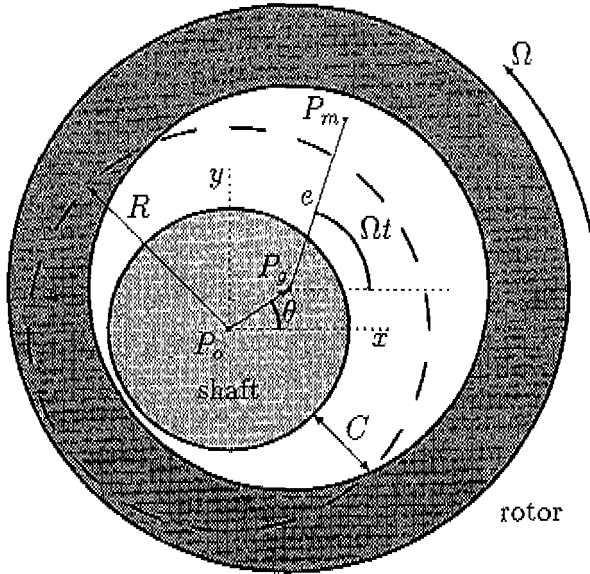


Figure 5.1: Momentary position of the rotor.

where $H(x)$ is the Heavyside function. The tangential component F_t represents the friction force, which is proportional to the normal component F_n (according to Coulomb's law) and opposite to the tangential velocity v_c of the rotor in P_c . Hence

$$F_t = -\text{sgn}(v_c) f F_n, \quad (5.3)$$

with f the friction coefficient of the rotor and v_c given by

$$v_c = \dot{x} \sin \theta - \dot{y} \cos \theta + \Omega R. \quad (5.4)$$

Equations of motion

According to Newton's second law, the equations of motion of the rotor are given by

$$M \begin{bmatrix} \ddot{x} \\ \ddot{y} \end{bmatrix} = M \epsilon \Omega^2 \begin{bmatrix} \cos \Omega t \\ \sin \Omega t \end{bmatrix} + F_n \begin{bmatrix} -\cos \theta \\ -\sin \theta \end{bmatrix} + F_t \begin{bmatrix} \sin \theta \\ -\cos \theta \end{bmatrix}. \quad (5.5)$$

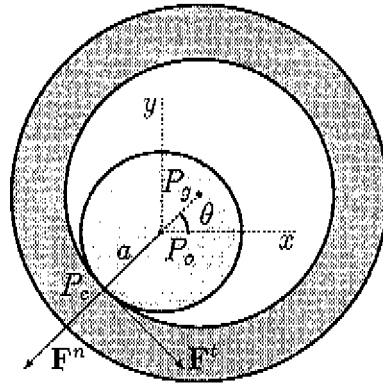


Figure 5.2: Definition of the contact point P_c and the contact forces \mathbf{F}^n and \mathbf{F}^t .

Introducing nondimensional coordinates $\xi = x/C$, $\eta = y/C$ and nondimensional time $\tau = \Omega t$, (5.5) is transformed into

$$\begin{bmatrix} \xi'' \\ \eta'' \end{bmatrix} = \varepsilon \begin{bmatrix} \cos \tau \\ \sin \tau \end{bmatrix} - \psi_n \begin{bmatrix} \cos \theta \\ \sin \theta \end{bmatrix} + \psi_t \begin{bmatrix} \sin \theta \\ -\cos \theta \end{bmatrix}, \quad (5.6)$$

with $(\)' = d(\)/d\tau$. The nondimensional force components ψ_n and ψ_t are given by

$$\begin{aligned} \psi_n &= \mathbf{H}(\delta) \max\{0, \kappa\delta + \beta\delta'\}, \\ \psi_t &= -f \operatorname{sgn}(\nu_c) \psi_n, \end{aligned} \quad (5.7)$$

where $\delta = \sqrt{\xi^2 + \eta^2} - 1$ is the nondimensional indentation of the shaft in the rotor and

$$\nu_c = \xi' \sin \theta - \eta' \cos \theta + \rho \quad (5.8)$$

is the nondimensional tangential velocity of the rotor in the contact point P_c . In (5.6), (5.7), and (5.8), the following non-dimensional parameters have been introduced:

$$\begin{aligned} \varepsilon &= c/C, \\ \kappa &= k/M\Omega^2, \\ \beta &= d/M\Omega, \\ \rho &= R/C. \end{aligned} \quad (5.9)$$

Together with the friction coefficient f , they form the set of relevant system parameters.

Slip or roll

The expression (5.3) for the tangential component F_t of the restoring force \mathbf{F}^s is only valid for $v_c \neq 0$. This applies to a situation in which the rotor is *slipping* along the shaft. When $v_c = 0$, the rotor is *rolling* along the shaft. In that case, F_t is an additional unknown which can be found by means of the equations of motion and the additional algebraic condition $v_c = 0$.

Numerically, the situation of v_c being exactly zero will almost never occur. To make roll behaviour possible in a numerical approach, the concept of *micro-slip* is introduced, which can be interpreted as 'almost roll'. When v_c is small, say $|v_c| < v_{eps}$, F_t is considered to be unknown and is determined by means of substitution of the relation $v_c = 0$ in the equations of motion. This yields (see Appendix C)

$$F_t^{\text{roll}} = M\epsilon\Omega^2(\sin\Omega t \cos\theta - \cos\Omega t \sin\theta) - \frac{M\Omega R}{C(1+\delta)}(\dot{x} \cos\theta + \dot{y} \sin\theta). \quad (5.10)$$

Since the friction force is bounded by the friction force due to slip, the following formula for F_t is obtained in a roll situation:

$$F_t = -\text{sgn}(v_c) \min\{|F_t^{\text{roll}}|, fF_n\}. \quad (5.11)$$

The complete expression for the nondimensional tangential component ψ_t of the restoring force \mathbf{F}^s is now given by

$$\psi_t = -\text{sgn}(v_c) * \begin{cases} f\psi_n & |v_c| \geq v_{eps}, \\ \min\{|\psi_t^{\text{roll}}|, f\psi_n\} & |v_c| < v_{eps}, \end{cases} \quad (5.12)$$

with $v_{eps} \ll 1$, ψ_n given by (5.7), and

$$\psi_t^{\text{roll}} = H(\delta) \left[\varepsilon(\sin\tau \cos\theta - \cos\tau \sin\theta) - \rho \frac{\xi' \cos\theta + \eta' \sin\theta}{1+\delta} \right]. \quad (5.13)$$

5.1.3 Investigation by means of ASCM

To investigate (5.6) by means of CM, the most obvious method is the MDCM method (Section 4.2). After all, the state space of the considered system has dimension $N = 4$, which implies that regular CM will be very time-consuming. By introducing co-rotating coordinates however, (5.6) can be transformed into an autonomous system of the same dimension. By means of the ASCM method (Section 3.2), the dimension of the cell state space

is reduced to three. Hence, ASCM seems to be an appropriate method of investigation for this particular system.

The following co-rotating coordinates are introduced:

$$\begin{aligned} r_1 &= \xi \cos \tau + \eta \sin \tau, \\ r_2 &= -\xi \sin \tau + \eta \cos \tau. \end{aligned} \quad (5.14)$$

Differentiation of (5.14) with respect to τ , substitution of (5.6), and elementary calculation yields the following set of ODE's:

$$\begin{aligned} r_1'' &= r_1 + 2r_2' - \psi_n r_1 - \psi_l r_2 + \varepsilon, \\ r_2'' &= r_2 - 2r_1' - \psi_n r_2 + \psi_l r_1. \end{aligned} \quad (5.15)$$

In the four-dimensional state space spanned by $\{r_1, r_1', r_2, r_2'\}$, a three-dimensional Poincaré section Σ is chosen, given by $r_2' = 0$. Next, a cell mapping $C : \Sigma \rightarrow \Sigma$ is created. To this end, a region of interest Ω' on Σ is defined by $\Omega' : |r_1| \leq 2.5, |r_1'| \leq 100, |r_2| \leq 2.5$ which is divided into $41 \times 41 \times 41$ cells. For each cell, numerical integration is performed until Σ has been intersected for the 20-th time. The cell containing the 20-th intersection point is taken as the image cell.

The ASCM method as described above is applied to (5.15) for $\varepsilon = 3.0, f = 0.01, \rho = 62.5, \kappa = 2850.0, \beta = 8.5$, and $\nu_{eps} = 0.01$. This results in the determination of two coexisting attractors. These attractors represent different types of motion which the rotor may undergo, namely slip and roll. In Fig. 5.3, the basins of attraction of both attractors are shown for four different two-dimensional subsets of Σ , given by (a) $r_1' = 0$, (b) $r_1' = 5$, (c) $r_2 = 0$, (d) $r_2 = 0.125$. By means of the relations

$$\begin{aligned} \xi(0) &= r_1(0), \\ \xi'(0) &= r_1'(0) - r_2(0), \\ \eta(0) &= r_2(0), \\ \eta'(0) &= r_2'(0) + r_1(0), \end{aligned} \quad (5.16)$$

which directly follow from the definitions of r_i ($i = 1, 2$), the basins of attraction are obtained in the original coordinates ξ, η, ξ', η' .

In Fig. 5.3a, the considered set of initial states corresponds to a situation in which the rotor is almost in rest ($\xi, \eta = O(1), \xi', \eta' = O(10^2)$). To obtain roll behaviour, an initial indentation of the shaft in the rotor is necessary. When the rotor is given a larger initial velocity (Fig. 5.3b), roll behaviour can emanate from initial states corresponding to a no-contact situation. When the rotor initially is concentric with the shaft ($\xi = \eta = 0$), large velocities

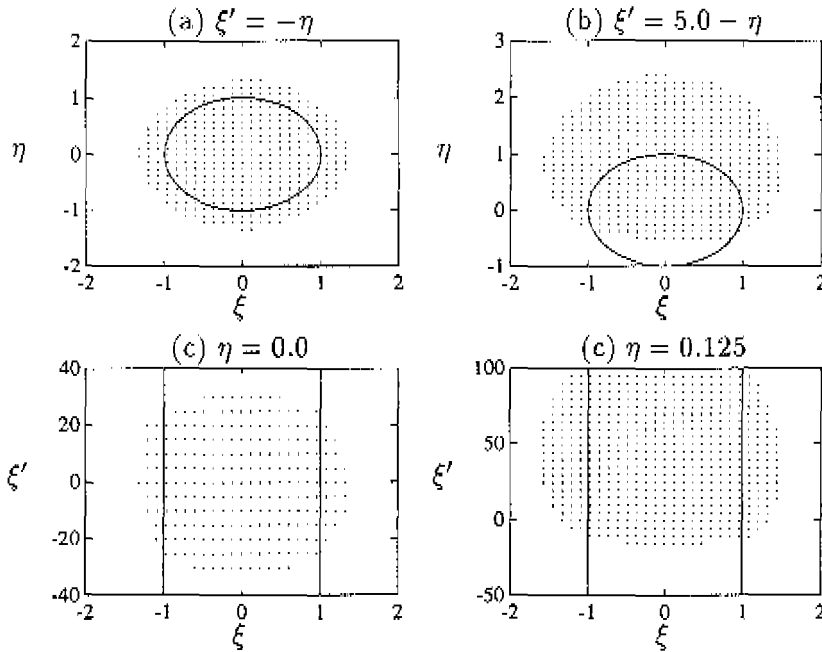


Figure 5.3: Basins of attraction of slip (·) and roll (left blank) for $\eta' = \xi$.

are necessary to obtain roll behaviour; moving away from this concentric position in ξ -direction, smaller velocities are sufficient (Fig. 5.3c). The same effect can be seen for $\eta = 0.125$ (Fig. 5.3d). In Fig. 5.3, the region of no-contact is represented by the inner area of the circle ((a),(b)) and by the area between the two vertical lines ((c),(d)).

In Fig. 5.4, a closer look is taken at the attractor representing slip behaviour. Fig. 5.3 shows that an initial state of $\xi = \xi' = \eta = \eta' = 0$ leads to slip. The trajectory calculated by straightforward numerical integration of (5.6) starting from this initial state is shown in Fig. 5.4a for $\tau = 0 - 200$. Due to its mass-eccentricity, the rotor moves outwards until it hits the shaft. When transient behaviour has vanished, the rotor undergoes a slip motion along the shaft. For $\tau > 150$, the slip motion is interspersed with short periods of free motion. In Fig. 5.4b, a Poincaré section of this trajectory is shown, representing the state at $\tau = 2n\pi$, $n = 2000, 2001, \dots, 5000$. The fractal form of the Poincaré section indicates that the slip-motion actually is a chaotic motion. This is confirmed when focussing on parts of the attractor (Fig. 5.4c,d).

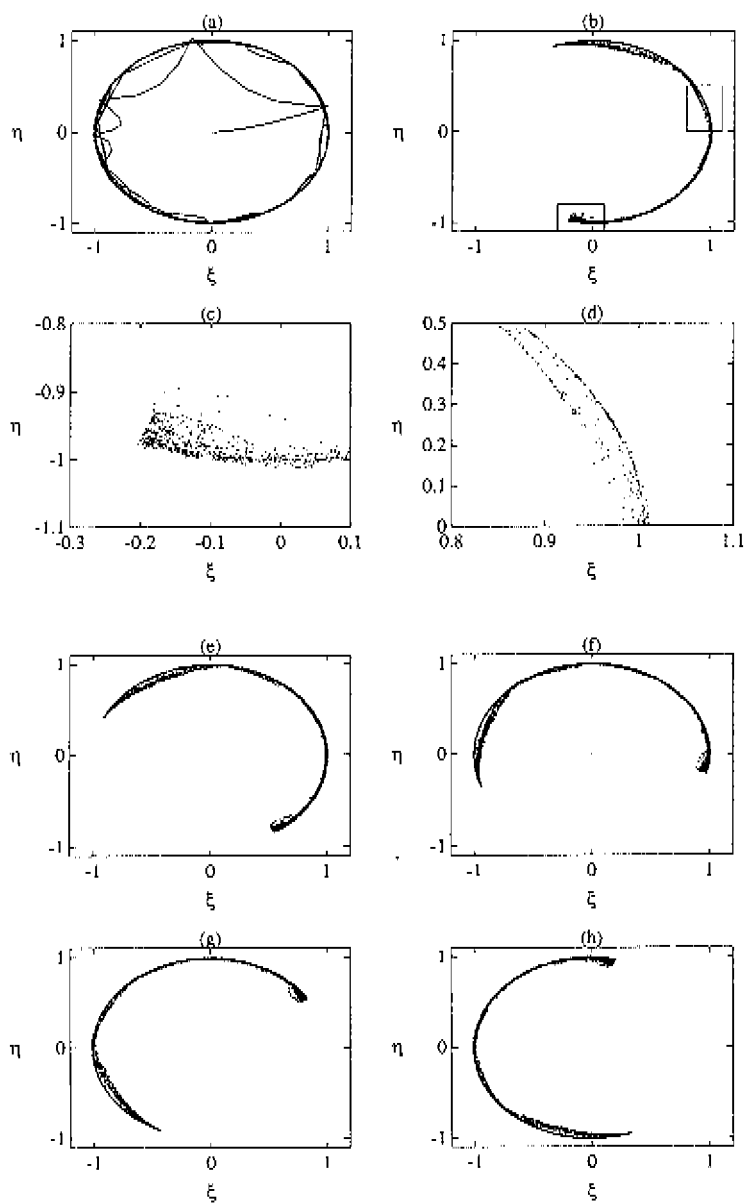


Figure 5.4: State representations of the center of the rotor in case of slip. (a) Trajectory. (b) Poincaré section. (c)-(d) Magnifications of (b). (e)-(h) Poincaré sections for different phase angles.

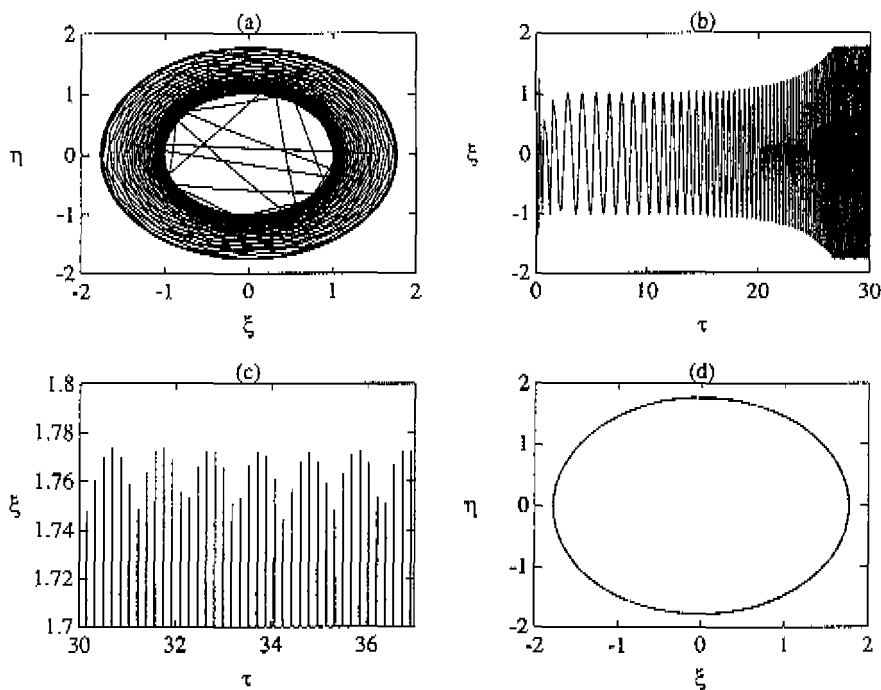


Figure 5.5: State representations of the center of the rotor in case of roll.

(a)-(c) Trajectories. (d) Poincaré section.

Finally, in Fig. 5.4e-h, Poincaré sections of the state of the rotor are shown for $\tau = 2n\pi + \phi_0$, $n = 2000, 2001, \dots, 5000$, with $\phi_0 = \pi/4, \pi/2, 3\pi/4, \pi$.

In Fig. 5.5a,b, a trajectory is shown which is obtained by integration of (5.6) for $\tau = 0 - 30$ with initial state $\xi = \eta' = 1.5$, $\xi' = \eta = 0$. According to Fig. 5.3, this state should lead to roll behaviour. After transient behaviour has vanished, the motion in the $\xi - \eta$ plane is almost circular with radius $r \approx 1.76$, which implies a nondimensional indentation of 0.76. Hence, large contact forces will occur between rotor and shaft in this case. In Fig. 5.5c, a closer look is taken at the response of the rotor in ξ -direction as a function of time. The two different oscillations that can be clearly distinguished indicate that the considered motion is quasi-periodic. This is confirmed by Fig. 5.5d, showing a Poincaré section of the state at $\tau = 2n\pi$, $n = 6, 7, \dots, 1000$. The closed loop in this figure corresponds to a quasi-periodic motion.

5.1.4 Discussion

In a previous study on the considered rotor system, emphasis was put on the influence of the parameters ε and f on the long term behaviour. For investigation, straightforward numerical integration was applied using $\xi = \eta = \xi' = \eta' = 0.0$ as initial state. The aim of that study was to find out which parameter value combinations lead to slip and which to roll behaviour. Due to the large deformations involved, it was especially important to determine which combinations could prevent the occurrence of roll. Because of the confidential character of this study, no further details can be given here.

The use of cell mapping—in particular ASCM—for the investigation of the rotor system has shown important advantages with respect to regular numerical integration. Under ASCM, the complete state space is 'scanned' for recurrent behaviour while under numerical integration only one initial state is considered and hence only one steady-state solution can be found. By means of ASCM, it has been shown that not only the parameter values but also the initial state of the rotor determines whether slip or roll will occur. In particular, no parameter combinations have been found which completely exclude the occurrence of roll. However, for roll behaviour to happen, large initial velocities or large initial rotor-shaft indentations may be necessary, as in the considered example.

The reader should note that for the considered system the situation occurs in which a chaotic motion is preferred to a regular motion. After all, when the rotor is slipping along the shaft, the motion of its geometrical center is chaotic and hence totally unpredictable. On the other hand, the motion is quasi-periodic and hence totally predictable in a situation of roll. However, it is not the predictability that counts for this system. More important is the avoidance of large rotor deformations and corresponding contact forces, which result in malfunctioning and a noisy performance.

5.1.5 Concluding remarks

It has been shown that the ASCM method can be applied to rotordynamic systems with dimension four in state space. By means of co-rotating coordinates, these systems are transformed into autonomous systems of the same dimension. By using a Poincaré section in the autonomous state space, the dimension of the cell state space can be reduced to three, which implies a substantial reduction of the total number of regular cells. This means that the required CPU-time is acceptable for the user. The simulation presented

in the previous subsection took 4.2 hours CPU-time.

For the investigation of (5.6), the MDCM method can be used as well. The advantage of ASCM with respect to MDCM however, is that the complete state space is scanned for recurrent behaviour. Under MDCM, a reduced set of initial states is considered and hence only attractors corresponding to these initial states can be found. The MDCM method can be seen as the only practical tool for systems with dimension $N > 4$, or as an appropriate tool when only particular sets of initial states have the user's interest.

5.2 Portable CD player under jogging condition

5.2.1 Introduction

The handling of external shocks is one of the main problems in the design of consumer electronics. As an example, one can think of a portable compact disc (CD) player. Knowing the type of external disturbance, measures can be taken to guarantee a high-quality performance. This includes e.g. the design of appropriate suspensions of the internal mechanisms and optimization of the control systems and electronics. For investigation on this topic, based on linear theory, the reader is referred to Draijer et al. [4] and Steinbuch et al. [28].

For a portable CD player, a special type of external disturbance is given by the motion which it experiences during jogging. The ability of the player to perform well under this condition is called 'joggability'. The measures necessary to assure joggability depend on the response of the player to this type of loading. Especially, the occurring acceleration of the player is relevant for this evaluation.

In the next subsection, a simple 2-DOF model is given which characterizes the nonlinear vertical behaviour of an idealized portable CD system. The jogging effect is represented by a harmonic excitation. To determine the long term behaviour of the system, use is made of the MDCM method. This is done for one set of system parameter values.

5.2.2 The CD model

The CD player mainly consists of two parts: the player P (mass m_2) and a carrying strap, containing a shoulder pad B (mass m_1). The vertical displacement of B is denoted by q_1 . The two parts of the strap connecting B

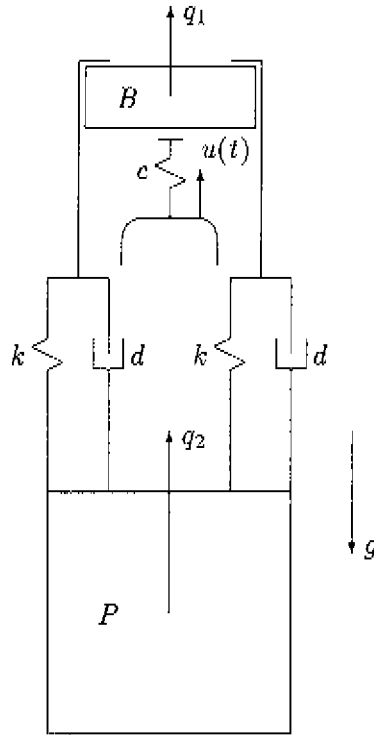


Figure 5.6: 2-DOF model of a portable CD player under jogging condition.

with P are considered massless and are modelled as one-sided linear springs and dampers, each with stiffness k and damping d . The displacement of P is given by q_2 , with $q_2 < q_1$ conforms to the situation in which the strap is being stretched. In Fig. 5.6, the model of the CD player is shown.

During jogging, the motion of the shoulder is assumed to be harmonic. The amplitude and frequency of this harmonic motion are given by a and f , respectively. Hence, the motion of the shoulder is prescribed and given by $u(t) = a \sin(\omega t)$, with $\omega = 2\pi f$. The shoulder itself is modelled as a one-sided linear spring with stiffness c .

The equations of motion of the system are simple and piece-wise linear. Defining $\xi = q_1/a$, $\eta = q_2/a$, $\tau = \omega t$, the nondimensional equations of motion are given by:

$$\begin{bmatrix} \xi'' \\ \eta'' \end{bmatrix} = -\gamma \begin{bmatrix} 1 \\ 1 \end{bmatrix} + \mathbf{F}^b + \mathbf{F}^s. \quad (5.17)$$

Here, $(\)' = d(\)/d\tau$ and $\gamma = g/a\omega^2$, with g the acceleration due to gravity. \mathbf{F}^b represents the strap forces, which are only nonzero when the strap is being stretched ($\xi > \eta$). Hence,

$$\mathbf{F}^b = H(\xi - \eta) \begin{bmatrix} -\max\{0, \kappa_1(\xi - \eta) + \beta_1(\xi' - \eta')\} \\ \max\{0, \kappa_2(\xi - \eta) + \beta_2(\xi' - \eta')\} \end{bmatrix}, \quad (5.18)$$

where $\kappa_i = 2k/m_i\omega^2$, $\beta_i = 2d/m_i\omega$ ($i = 1, 2$), and $H(x)$ is the Heavyside function. \mathbf{F}^s represents the force which the shoulder exerts on B . Hence

$$\mathbf{F}^s = H(\sin \tau - \xi) \begin{bmatrix} \sigma(\sin \tau - \xi) \\ 0 \end{bmatrix}, \quad (5.19)$$

with $\sigma = c/m_1\omega^2$.

5.2.3 MDCM application

The MDCM method (see Section 4.2) is used to investigate the 2-DOF model of the portable CD player, given by (5.17), (5.18), and (5.19). It is assumed that the strap stiffness is equal to the shoulder stiffness: $k = c = 1000$ N/m, while the strap damping is given by $d = 4$ Ns/m. For the jogging amplitude and frequency, $a = 0.05$ m and $f = 2$ Hz is taken, respectively. The masses of B and P are given by $m_1 = 0.05$ kg and $m_2 = 0.35$ kg, respectively.

The aim of applying MDCM is to determine the possible types of response—in particular the occurring acceleration—for the CD player. Looking at the background of the problem, it is obvious to focus on the CD player and the influence of its initial state on its long term behaviour. An appropriate choice for a two-dimensional subspace of relevant initial states is then for example given by $\Sigma : \xi = \xi' = 0$.

The state of the system is given by $\mathbf{x} = [x_1 \dots x_4]^T$ with $x_1 = \xi$, $x_2 = \xi'$, $x_3 = \eta$, $x_4 = \eta'$. In this four-dimensional state space, a cell structure is defined by choosing four cell sizes: $h_1 = h_3 = 0.01$, $h_2 = h_4 = 0.06$. On Σ , a region of interest Ω' is defined by $|x_3| \leq 0.5$, $|x_4| \leq 3$. By means of MDCM, the long term behaviour is determined for initial states in Ω' . For the determination of image cells, a time integration interval of five forcing periods is used ($\Delta\tau = 5/f$).

In Fig. 5.7a, the results of the MDCM application are shown. For the chosen region of interest Ω' , three different types of steady state behaviour have been found. Cells denoted by (\circ) lead to a harmonic solution, shown in Fig. 5.8a. This attractor corresponds to a situation in which there is always

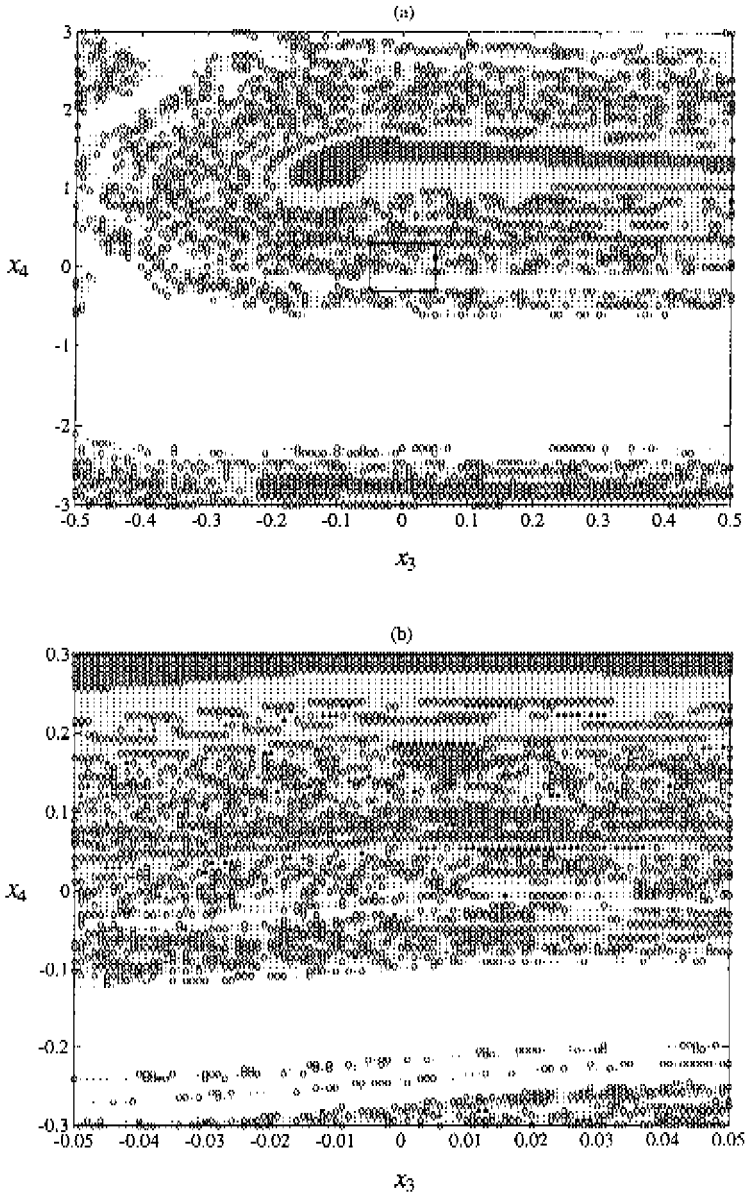


Figure 5.7: Basins of attraction for $x_1 = x_2 = 0$: Harmonic solution (\circ), coexisting harmonic solution (\cdot), quasi-periodic solution (left blank), $1/2$ subharmonic solution ($*$)

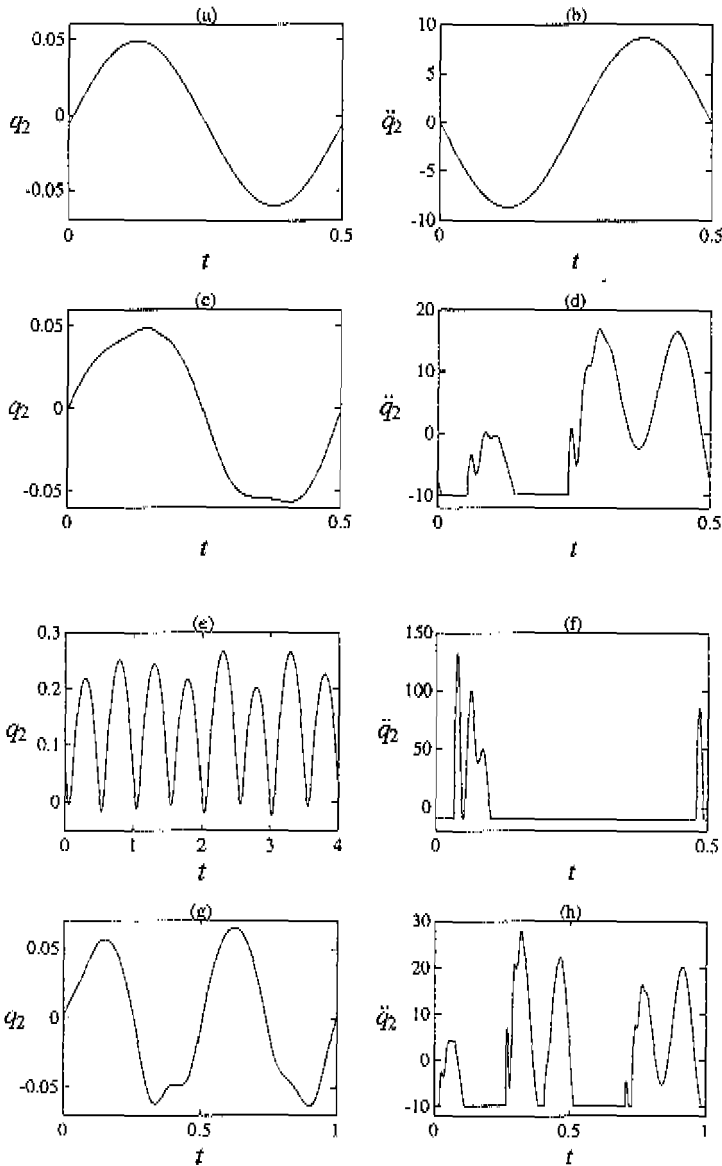


Figure 5.8: Possible responses (m) and accelerations (m/s^2) of the CD player as a function of time (s): (a),(b) Full contact harmonic solution; (c),(d) coexisting harmonic solution; (e),(f) quasi-periodic solution; (g),(h) 1/2 subharmonic solution.

contact between shoulder and pad. Cells denoted by (-) lead to a coexisting harmonic solution (Fig. 5.8c), which shows two intervals of no-contact during each period. Finally, cells which are left blank in Fig. 5.7a lead to a quasi-periodic solution (Fig. 5.8e). The trajectories in Fig. 5.8 are representations of the state of the player in original coordinates as a function of real time.

In Fig. 5.7b, the basins of attraction are shown obtained by an additional MDCM application for a region $\Omega'' \subset \Omega'$. Here, Ω'' is defined by $|x_3| \leq 0.05$, $|x_4| \leq 0.3$. The cell sizes are given by $h_1 = h_3 = 0.001$, $h_2 = h_4 = 0.006$. From this 'magnification window' on Ω' , it can be concluded that the basins of attraction have a fractal structure; changing the initial state only slightly may result in a different steady-state motion. Furthermore, an additional periodic group is found with a small basin of attraction (*). This group represents a 1/2 subharmonic solution (see Fig. 5.8g).

The accelerations of the CD player corresponding to the determined solutions are additionally shown in Fig. 5.8,b,d,f,h. The acceleration in the case of the full-contact solution is perfectly sinusoidal. For the coexisting harmonic solution, the intervals of free motion are represented by intervals of constant acceleration $-g$. It can be seen that the occurring peak acceleration is less than $2g$ for this solution. In the case of quasi-periodic behaviour (Fig. 5.8f) however, accelerations of more than $13g$ are possible. Here, the motion of the player is characterized by large amplitudes (up to five times the shoulder amplitude). Finally, the peak acceleration for the 1/2 subharmonic is approximately $3g$.

The results in Fig. 5.7a,b have been verified by determining the trajectory belonging to four different initial states, each corresponding to a different attractor. In Fig. 5.9, trajectories are shown obtained by integration starting from $\mathbf{x} = [0\ 0\ 0\ x_4]^T$, with $x_4 = 1.4, 1.2, -1.0, 0.18$, respectively. The first three states indeed lead to the attractor as predicted by the MDCM method. For $x_4 = 0.18$, however, the wrong attractor is obtained. Although the transient behaviour of this trajectory is governed by the 1/2 subharmonic, it finally settles on the full-contact harmonic solution. This may be explained by the small basin of attraction of the 1/2 subharmonic solution. Anyway, when the actual basins of attraction have a fractal structure, the representations obtained by means of CM should be interpreted with care. In such a situation, the errors involved with CM have a larger impact than usual.

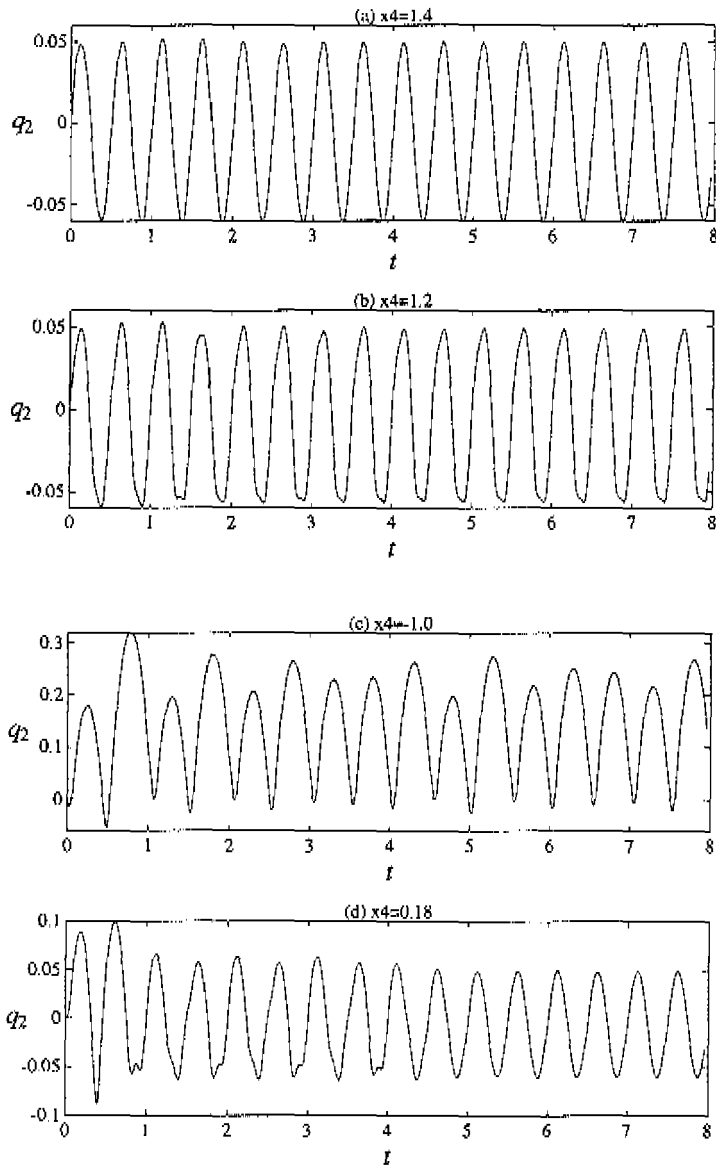


Figure 5.9: Verification of basins of attraction (initial state: $x_i = 0$, $i = 1, 2, 3$):
(a) Full contact harmonic solution; (b) coexisting harmonic solution;
(c) quasi-periodic solution; (d) full contact harmonic solution with $1/2$ subharmonic transient.

5.2.4 Concluding remarks

A 2-DOF model of a portable CD player has been investigated by means of the MDCM method. For an initial region of interest, three different responses were found to be possible: two harmonic solutions and one quasi-periodic solution. By focussing on a small part of the initial region, realized by a MDCM application with very small cells, a $1/2$ subharmonic solution was detected. A second result of this zooming action was the confirmation of the fractal structure of parts of the basins of attraction.

Unlike the (sub)harmonic solutions found, the quasi-periodic solution features large accelerations and a large amplitude motion. Since this solution has a large basin of attraction in the set of relevant initial states, large accelerations are very likely to occur. For the assurance of joggability, it is therefore necessary to cope with these kind of accelerations, or to change one or more system parameters in such a way that only low-acceleration solutions occur.

The presented simulations have shown the existence of four solutions for a set of system parameter values. By means of continuation methods, the evolution of the periodic attractors can be determined when system parameters are varied. The sensitivity of the basin boundaries with respect to the system parameters can be investigated by means of PVSCM. However, the gain in CPU-time with respect to a MDCM application for a new parameter value will probably be small, due to the fractal structure of the basins of attraction.

Chapter 6

Conclusions and Guidelines

In this thesis, recent developments have been presented concerning the application of cell mapping methods as a tool for the global investigation of nonlinear dynamic systems. For the sake of accuracy and efficiency but in particular applicability, a number of modifications and extensions have been presented and evaluated. In this chapter, a recapitulation is given of the main conclusions that can be drawn. Additionally, some general guidelines are given for the use of cell mapping methods and their extensions.

6.1 Conclusions

Modifications

- For autonomous systems, the necessary CPU-time can be reduced tremendously by introducing a Poincaré section and taking this as the cell state space.
- For discontinuous systems, the following modifications are necessary:
 - Adaptation of the integration routine to overcome the discontinuity.
 - When interpolation is involved, replacement of interpolation by integration when the interpolation trajectories show an extreme divergence due to the discontinuity.
- Under ICM, a gain in CPU-time can be achieved when a new criterion is added to the interpolation procedure: When a state is reached of

which the surrounding interpolation points lead to one and the same attractor, further interpolation will generally lead also to this attractor and is therefore not performed.

- ICM and MM can be combined to MCM. MCM produces more accurate results at the cost of more CPU-time.
- The extension of the time integration interval, for the determination of image cells or points, results in
 - the reduction of the number of spurious periodic cells or points,
 - the reduction of the number of cells mapped into the sink cell.

Extensions

- By means of the PVSCM and PVICM methods, the sensitivity of results obtained by SCM and ICM with respect to system parameters can be studied very effectively and straightforward. In this way, global bifurcations can be predicted.
- By means of MDCM, systems of arbitrary state space dimension can be scanned for attractors. Two-dimensional intersections of the corresponding basins of attraction are obtained.

General conclusion

When a global overview of the attractors and corresponding basins of attraction of a complex nonlinear dynamic system is wanted, CM is the most suited method. In several applications discussed in this thesis, CM yielded additional information with respect to previous investigations performed by periodic solvers and direct integration for one initial state. Numerical integration for a huge number of initial states—the only alternative for a global investigation—is much more time-consuming than CM.

6.2 Guidelines

Which method to use for solving the equations of motion?

- When only one specific periodic solution is desired: Periodic solvers.
- When only a few initial states are relevant: Numerical integration.

- When an overview of all attractors (periodic, quasi-periodic, chaotic) and corresponding basins of attraction is desired: Cell mapping.

Which CM method to use?

- For state space dimension $N = 2$:
 - Generally: SCM, (M)ICM, (M)MM, MCM.
 - For autonomous systems: ASCM.
 - To obtain probabilistic properties: GCM.
- For $N = 3, 4$:
 - Generally: SCM, MDCM.
 - For autonomous systems: ASCM.
- For $N > 4$: MDCM.

Combination of CM with other methods

- To determine the type and exact position of an attractor, represented by a periodic group found with CM, the following methods can be applied:
 - Numerical integration.
 - Liapunov exponents or attractor dimension determination.
- To obtain a complete bifurcation diagram for a certain system parameter, the following procedure should be followed:
 - Determination of all attractors by means of CM, for an initial value of the system parameter.
 - Determination of periodic branches as a function of the varied system parameter value, by applying a path-following method to each periodic attractor.

Guide for applying CM

- How to choose Ω and Σ ?
 - On the basis of state restrictions of the system.

- On the basis of relevancy.
- On the basis of foreknowledge, e.g. obtained by means of numerical integration.
- How to choose the time integration interval?
 - For periodically forced non-autonomous systems: Equal to one or more forcing periods.
 - For autonomous systems: Arbitrary (but not too small) under regular CM; prescribed under ASCM.
 - For small damping and large amplitude transient behaviour, an extension of the interval is recommended (see Conclusions).

General guidelines

- Whenever an attractor has been found by means of CM, it deserves recommendation to determine its type and location in the state space, e.g. by means of numerical integration over only a short period. Under CM, an attractor is often represented by several periodic groups. Numerical integration thus yields which groups represent the same attractor. To obtain the correct basin of attraction for an attractor, the basins of attraction of all its corresponding groups need to be collected.
- Generally, the choice for the integration interval under CM is not obvious. In that case, the smallest value (as possible for the applied method) is recommended. When spurious results are obtained, integration can be continued, using the end points of the trajectories as starting points. This process can be proceeded until satisfying results are obtained. In doing so, the integration interval and hence the CPU-time is kept minimal. The necessary CPU-time for the classification of cells and other administrative procedures, which have to be performed after every new integration, can be neglected with respect to the CPU-time for integration.

Appendix A

SCM algorithm

Under SCM, cells are classified by a group number and a step number. For each cell z , the group number $G(z)$ denotes to which periodic group z belongs; the step number $S(z)$ stands for the number of mappings necessary for z to end up on a periodic group. Hence, periodic cells are characterized by a zero step number.

In the SCM algorithm, the arrays $\mathbf{g}[z]$ and $\mathbf{s}[z]$ represent the group and step number of z , while $\mathbf{c}[z]$ contains the index of the image cell of z ($z = 0, 1, \dots, M$). The sink cell (index 0), which is a periodic cell by definition, is regarded as the first periodic group. This results in the following assignments:

$$\begin{aligned}\mathbf{g}[0] &:= 1 \\ \mathbf{s}[0] &:= 0 \\ \mathbf{c}[0] &:= 0 \\ N_g &:= 1\end{aligned}$$

where N_g denotes the number of periodic groups found in the algorithm.

For the determination of the group and step number of the remaining cells, the following procedure is followed: Initially, all regular cells are tagged as *virgin* cells by giving them a zero group number:

$$\text{for } (z = 1, \dots, M) \mathbf{g}[z] := 0$$

Next, a cell sequence $z, C(z), C^2(z), \dots$ is created for each regular cell z . Cells in the sequence are tagged as cells *under processing* by giving them a temporary group number -1 . As long as the latest determined cell in the sequence is a virgin cell, creation of the sequence is continued. Let z be the initial cell

of a sequence and let $\text{IMCELL}(z)$ be the subroutine returning the image cell of z , then the cell sequence creation is given by the following assignments:

```

j := 0
b := z
while (g[b] = 0)
    g[b] := -1
    c[b] := IMCELL(b)
    b := c[b]
    j := j + 1

```

When the sequence has been terminated, two possibilities exist for its final cell $b = C^j(z)$: $\mathbf{g}[b] = -1$ or $\mathbf{g}[b] > 0$. If $\mathbf{g}[b] = -1$ holds then cell b already occurred in the sequence. This means that $b = C^i(z)$ for a certain $i \in \{0, \dots, j-1\}$. Hence, a new periodic group has been found, given by $b, C(b), \dots, C^{j-i-1}(b)$. As a result, N_g can be updated and all cells in the sequence can be given a group and step number as follows:

```

N_g := N_g + 1
for (l = 0, ..., i - 1)
    g[z] := N_g
    s[z] := i - l
    z := c[z]
for (l = i, ..., j - 1)
    g[z] := N_g
    s[z] := 0
    z := c[z]

```

If $\mathbf{g}[b] > 0$ holds then cell b is either the sink cell or a regular cell which has already been tagged in a previous sequence. In both cases, all cells in the current sequence are tagged as transient cells, leading to the same periodic group as b . Hence

```

for (l = 0, ..., j - 1)
    g[z] := g[b]
    s[z] := s[b] + j - l
    z := c[z]

```

When for all regular cells this procedure has been carried out, all group and step numbers are known. As a result, all periodic groups and corresponding basins of attraction are obtained. A more detailed explanation of the SCM algorithm is given in Hsu [14].

Appendix B

Interpolation Indices and Functions

In the ICM algorithm, state space trajectories are approximated by means of interpolation. For all M grid points, covering the region of interest Ω , the image points are calculated by means of numerical integration. The image point of a grid point \mathbf{x}^l is denoted by \mathbf{y}^l ($l = 1, \dots, M$). To obtain the image point \mathbf{y} of an arbitrary state $\mathbf{x} = [x_1 \dots x_N]^T \in \Omega$, multi-linear interpolation is performed between the image points of the 2^N grid points which surround \mathbf{x} :

$$\mathbf{y} = \sum_{i=1}^{2^N} P_i(\mathbf{x}) \mathbf{y}^{i_i}. \quad (\text{B.1})$$

The indices l_1, \dots, l_{2^N} of the grid points surrounding \mathbf{x} are given by:

$$\begin{aligned} l_1 &= 1 + k_1 + \sum_{i=2}^N k_i \prod_{j=1}^{i-1} M_j, \\ l_2 &= l_1 + 1, \\ l_j &= l_{(j-2^{m-1})} + \prod_{i=1}^{m-1} M_i, \quad m = 2, \dots, N, j = 2^{m-1} + 1, \dots, 2^m, \end{aligned}$$

with

$$k_i = \text{int} \left(\frac{x_i - x_i^{(1)}}{h_i} \right), \quad i = 1, \dots, N.$$

The interpolation functions P_1, \dots, P_{2^N} in (B.1) are given by:

$$P_1(\mathbf{x}) = \prod_{i=1}^N L_0(\xi_i),$$
$$P_j(\mathbf{x}) = P_{(j-2^{m-1})} * \frac{L_1(\xi_m)}{L_0(\xi_m)}, \quad m = 1, \dots, N, j = 2^{m-1} + 1, \dots, 2^m,$$

with

$$\xi_i = \frac{x_i - x_i^{i_1}}{h_i}, \quad i = 1, \dots, N,$$

and

$$L_0(x) = 1 - x,$$
$$L_1(x) = x.$$

Appendix C

Derivation of Equation (5.10)

In the case of micro-slip (almost roll), the tangential velocity of the rotor in the contact point is assumed to be zero. According to (5.4), this means

$$\dot{x} \sin \theta - \dot{y} \cos \theta + \Omega R = 0. \quad (\text{C.1})$$

Differentiation with respect to time yields

$$\dot{x} \sin \theta + \dot{x} \dot{\theta} \cos \theta - \dot{y} \cos \theta + \dot{y} \dot{\theta} \sin \theta = 0. \quad (\text{C.2})$$

Next, $\dot{\theta}$ is eliminated from the above equation. Since

$$\theta = \arctan(y/x) + C,$$

with $C = 0, \pi$ or 2π , it follows that

$$\begin{aligned} \dot{\theta} &= \frac{1}{(y/x)^2 + 1} \left(\frac{\dot{y}}{x} - \frac{y\dot{x}}{x^2} \right) \\ &= \frac{x\dot{y} - y\dot{x}}{x^2 + y^2} \\ &= \frac{\dot{y} \cos \theta - \dot{x} \sin \theta}{\sqrt{x^2 + y^2}} \\ &= \frac{\dot{y} \cos \theta - \dot{x} \sin \theta}{C(1 + \delta)}. \end{aligned} \quad (\text{C.3})$$

Substitution of (C.1) in (C.3) yields

$$\dot{\theta} = \frac{\Omega R}{C(1 + \delta)}. \quad (\text{C.4})$$

Elimination of $\dot{\theta}$ from (C.2) using (C.4) yields:

$$\ddot{x} \sin \theta + \dot{x} \frac{\Omega R}{C(1+\delta)} \cos \theta - \ddot{y} \cos \theta + \dot{y} \frac{\Omega R}{C(1+\delta)} \sin \theta = 0. \quad (\text{C.5})$$

Consider the equations of motion (5.5):

$$M\ddot{x} = Me\Omega^2 \cos \Omega t - F_n \cos \theta + F_t \sin \theta, \quad (\text{C.6})$$

$$M\ddot{y} = Me\Omega^2 \sin \Omega t - F_n \sin \theta - F_t \cos \theta. \quad (\text{C.7})$$

Substitution of (C.7) in (C.5) yields:

$$\begin{aligned} \ddot{x} \sin \theta + \dot{x} \frac{\Omega R}{C(1+\delta)} \cos \theta + \dot{y} \frac{\Omega R}{C(1+\delta)} \sin \theta = \\ \frac{1}{M} (-F_n \sin \theta - F_t \cos \theta + Me\Omega^2 \sin \Omega t) \cos \theta. \end{aligned} \quad (\text{C.8})$$

Elimination of \ddot{x} using (C.6) yields:

$$\begin{aligned} \frac{1}{M} (-F_n \cos \theta + F_t \sin \theta + Me\Omega^2 \cos \Omega t) \sin \theta \\ = \frac{1}{M} (-F_n \sin \theta - F_t \cos \theta + Me\Omega^2 \sin \Omega t) \cos \theta \\ - \frac{\Omega R}{C(1+\delta)} (\dot{x} \cos \theta + \dot{y} \sin \theta). \end{aligned} \quad (\text{C.9})$$

Hence, F_t satisfies the following relation:

$$\begin{aligned} F_t = Me\Omega^2 (\sin \Omega t \cos \theta - \cos \Omega t \sin \theta) \\ - \frac{M\Omega R}{C(1+\delta)} (\dot{x} \cos \theta + \dot{y} \sin \theta). \end{aligned} \quad (\text{C.10})$$

References

- [1] D. Bestle and E. Kreuzer. A modification and extension of an algorithm for generalized cell mapping. *Computer Methods in Applied Mechanics and Engineering*, 59:1–9, 1986.
- [2] Y.S. Choi and S.T. Noah. Nonlinear steady-state response of a rotor-support system. *Journal of Vibration, Acoustics, Stress, and Reliability in Design*, 109:255–261, 1987.
- [3] M.T.M. Crooijmans. *On the Computation of Stationary Deterministic Behaviour of Non-linear Dynamic Systems with Applications to Rotor-bearing Structures*. PhD thesis, Eindhoven University of Technology, The Netherlands, 1987.
- [4] W. Draijer, M. Steinbuch, and O.H. Bosgra. Adaptive control of the radial servo system of a compact disc player. *IFAC Automatica*, 28:455–462, 1992.
- [5] F.F. Ehrich. Some observations of chaotic vibration phenomena in high-speed rotordynamics. *Transactions of the ASME*, 113:50–57, 1991.
- [6] R. England. *Automatic Methods for Solving Systems of Ordinary Differential Equations*. PhD thesis, University of Liverpool, 1967.
- [7] R. England. Error estimates for Runge-Kutta type solutions to systems of ordinary differential equations. *Computation J.*, 12:166–169, 1969.
- [8] R.H.B. Fey. *Steady-State Behaviour of Reduced Dynamic Systems with Local Nonlinearities*. PhD thesis, Eindhoven University of Technology, The Netherlands, 1992.
- [9] E.J. Gunter and R.H. Humphris. Influence of unbalance on the nonlinear dynamical response and stability of flexible rotor-bearing systems. In

- M.L. Adams, editor, *Rotor Dynamical Instability*, pages 37–58. Kluwer Academic Publishers, 1983.
- [10] R.S. Guttalu and P.J. Zufiria. The adjoining cell mapping and its recursive unraveling, part ii: Application to selected problems. *Nonlinear Dynamics*, 4:309–336, 1993.
- [11] M. Hénon. On the numerical computation of Poincaré maps. *Physica D*, 5:412–414, 1982.
- [12] C.S. Hsu. A theory of cell-to-cell mapping dynamical systems. *Journal of Applied Mechanics*, 47:931–939, 1980.
- [13] C.S. Hsu. A generalized theory of cell-to-cell mapping for nonlinear dynamical systems. *Journal of Applied Mechanics*, 48:834–842, 1981.
- [14] C.S. Hsu. *Cell to Cell Mapping; A Method of Global Analysis for Nonlinear Systems*. Springer-Verlag, 1987.
- [15] C.S. Hsu, R.S. Guttalu, and W.H. Zhu. A method of analyzing generalized cell mappings. *Journal of Applied Mechanics*, 49:885–894, 1982.
- [16] D.L. Isaacson and R.W. Madsen. *Markov Chains: Theory and Applications*. John Wiley & Sons, 1976.
- [17] N.N. Jeffcott. The lateral vibration of loaded shafts in the neighbourhood of a whirling speed—the effect of want of balance. *Philosophical Magazine*, 37:304–314, 1919.
- [18] M.C. Kim and C.S. Hsu. Computation of the largest Liapunov exponent by the generalized cell mapping. *Journal of Statistical Physics*, 45:49–61, 1986.
- [19] Y.B. Kim and S.T. Noah. Response and bifurcation analysis of a mdof rotor system with a strong nonlinearity. *Nonlinear Dynamics*, 2:215–234, 1991.
- [20] E.J. Kreuzer. Analysis of chaotic systems using the cell mapping approach. *Ingenieur-Archiv*, 55:285–294, 1985.
- [21] J.D. Lambert. *Computational Methods in Ordinary Differential Equations*. John Wiley & Sons, 1973.

- [22] J. Levitas. *Poincaré-Like Simple Cell Mapping for Nonlinear Dynamical Systems*. PhD thesis, Israel Institute of Technology, Haifa, Israel, 1992.
- [23] G.X. Li, R.H. Rand, and F.C. Moon. Bifurcation and chaos in a forced zero-stiffness impact oscillator. *International Journal of Non-linear Mechanics*, 25:417-432, 1990.
- [24] J.P. Meijaard. *Algorithms for a Numerical Investigation of the Behaviour of Nonlinear Discrete Models*. PhD thesis, Delft University of Technology, The Netherlands, 1991.
- [25] R.D. Neilson and A.D.S. Barr. Dynamics of a rigid rotor mounted on discontinuously non-linear elastic supports. *Proc. Instn. Mech. Engrs.*, 202:369-376, 1988.
- [26] G.V. Parkinson and J.D. Smith. The square prism as an aeroelastic nonlinear oscillator. *Quart. Journ. Mech. and Applied Math.*, 17:225-239, 1964.
- [27] R. Seydel. Tutorial on continuation. *International Journal of Bifurcation and Chaos*, 1:3-11, 1991.
- [28] M. Steinbuch, G. Schootstra, and O.H. Bosgra. Robust control of a compact disc player. In *Proc. 1992 IEEE Conference on Decision and Control*, pages 2596-2600, 1992.
- [29] J.M.T. Thompson and H.B. Stewart. *Nonlinear Dynamics and Chaos*. John Wiley & Sons, 1987.
- [30] B.H. Tongue. On obtaining global nonlinear system characteristics through interpolated cell mapping. *Physica D*, 28:401-408, 1987.
- [31] B.H. Tongue. Interpolated cell mapping of dynamical systems. *Journal of Applied Mechanics*, 55:461-466, 1988.
- [32] B.H. Tongue. A multiple-map strategy for interpolated mapping. *International Journal of Non-linear Mechanics*, 25:177-186, 1990.
- [33] B.H. Tongue and K. Gu. A higher order method of interpolated cell mapping. *Journal of Sound and Vibration*, 25:169-179, 1988.
- [34] J.J. van Amstel and J.A.A.M. Poitiers. *Continued Programming; the Design of Data Structures and Algorithms (in Dutch)*. Academic Service, 1985.

- [35] J.A.W. van der Spek. Application of cell mapping methods to a nonlinear dynamic system. In J.F. Dijkstra and F.T.M. Nieuwstadt, editors, *Topics in Applied Mechanics*, pages 285-292. Kluwer Academic Publishers, 1993.
- [36] J.A.W. van der Spek, C.A.L. de Hoon, A. de Kraker, and D.H. van Campen. Application of cell mapping methods to a discontinuous dynamic system. *Nonlinear Dynamics*, in press.
- [37] P.G.Th. van der Varst. *On normal mode vibrations of nonlinear conservative systems*. PhD thesis, Eindhoven University of Technology, The Netherlands, 1982.
- [38] P.J. Zufiria and R.S. Guttalu. The adjoining cell mapping and its recursive unraveling, part i: Description of adaptive and recursive algorithms. *Nonlinear Dynamics*, 4:207-226, 1993.

Samenvatting

In dit proefschrift worden modificaties en uitbreidingen gepresenteerd voor *cell mapping* (CM) methoden. CM methoden worden gebruikt om het lange termijn gedrag van niet-lineaire dynamische systemen globaal te onderzoeken. Met behulp van CM kunnen zowel periodieke als chaotische oplossingen van de bewegingsvergelijkingen bepaald worden. Tevens maakt toepassing van CM de bepaling van de attractiegebieden van de stabiele oplossingen mogelijk.

Eerst wordt een overzicht gegeven van de belangrijkste CM methoden. De *simple cell mapping* (SCM) methode is gebaseerd op een discretisatie van de toestandsruimte in cellen, gevolg door de bepaling—via numerieke integratie—van de bijbehorende beeldcellen. Het lange termijn gedrag van een systeem wordt hier gerepresenteerd door groepen periodieke cellen. De *generalized cell mapping* (GCM) methode is een generalisatie van SCM. Vanwege de probabilistische benadering is GCM met name geschikt voor de beschrijving van chaotisch gedrag. Bij de *interpolated cell mapping* (ICM) methode worden met behulp van interpolatie benaderingen bepaald van de trajectories van het systeem in de toestandsruimte. *Multiple mapping* (MM) tenslotte is een gemodificeerde versie van ICM welke betere resultaten oplevert in geval van grote toestandsruimte-vertormingen.

Vervolgens worden enige modificaties gepresenteerd, welke dienen om de nauwkeurigheid en efficiëntie van de bestaande CM methoden te vergroten. Voor autonome systemen wordt een dimensie-reductie methode besproken. Vervolgens worden modificaties gegeven welke noodzakelijk zijn om CM methoden toe te passen op discontinue systemen. Voor ICM wordt een aanpassing geïntroduceerd waarmee het interpolatieproces wordt versneld. Verder wordt een combinatie besproken van ICM en MM, *mized cell mapping* (MCM) genaamd. Tenslotte worden de voordelen getoond van het gebruik van een verlengd integratie-interval voor SCM.

Naast deze modificaties worden twee wezenlijke uitbreidingen op de bestaande CM methoden geïntroduceerd. De eerste behelst een parameter-

variatie techniek waarmee de gevoeligheid van CM-resultaten met betrekking tot systeemparameters kan worden geanalyseerd. Met behulp van deze techniek kan in relatief weinig rekentijd de evolutie van de attractiegebieden bepaald worden wanneer een systeemparameter wordt gevarieerd. Op deze manier kunnen globale bifurcaties gemakkelijk voorspeld worden. Het geïntroduceerde idee is uitgewerkt voor zowel SCM als ICM.

De tweede uitbreiding bestaat uit een nieuwe CM methode, *multi-DOF* cell mapping (MDCM) genaamd, welke toepasbaar is op systemen met veel vrijheidsgraden. Omdat het aantal cellen—en dientengevolge ook de rekentijd en geheugenruimte—exponentieel toeneemt met de dimensie van de toestandruimte, is toepassing van de conventionele CM methoden op dergelijke systemen erg onpraktisch. Bij de MDCM methode loopt de rekentijd slechts evenredig op met de systeemdimensie terwijl de vereiste geheugenruimte qua orde-grootte constant blijft.

Ter illustratie wordt CM toegepast op twee praktische niet-lineaire dynamische systemen. Eerst wordt het globale gedrag onderzocht van een rotor-lager systeem. Hier ligt de nadruk op de attractiegebieden van een quasi-periodieke en een coëxisterende chaotische oplossing, welke overeenkomen met respectievelijk een rol- en een slip-beweging van de rotor. Vervolgens wordt het 'joggend vermogen' van een draagbare CD-speler bestudeerd. Met behulp van MDCM wordt voor een verzameling relevante begintoestanden de respons van de CD-speler bepaald op een periodieke excitatie.

Geconcludeerd wordt dat de gepresenteerde modificaties en uitbreidingen waardevol zijn. Verder wordt de toegevoegde waarde benadrukt van CM methoden ten opzichte van de meer ingeburgerde onderzoeksmethoden, zoals reguliere numerieke integratie en periodieke oplossingsmethoden. Tenslotte worden algemene richtlijnen gegeven voor het onderzoeken van niet-lineaire dynamische systemen alsmede voor het gebruik van CM methoden.

Acknowledgements

The author wishes to thank everyone who has contributed in any way to the realization of this thesis. He owes special thanks to the students who have participated in the project:

- Corné de Hoon
- Didier Lemmens
- Edwin Thijssen,

for their research in the field of cell mapping,

- Josu Xavier Piña Bilbao
- Tom de Jonge,

for their investigation of rotordynamic structures, and

- Marko de Jager

for his contribution to the creation of order in chaos. Finally, the author wishes to acknowledge his appreciation to his colleague

- Pieter Vosbeek

for the TEX- and UNIX-support throughout the years.

Curriculum Vitae

- 7-5-1966: Born in Asten, The Netherlands.
- 1978–1984: St. Willibrord Gymnasium Deurne (grammar school).
- 1984–1989: Eindhoven University of Technology: Studies at the Faculty of Mathematics and Computing Science.
- 1990–1994: Eindhoven University of Technology: Research assistant at the Faculty of Mechanical Engineering, Section of Computational and Experimental Mechanics.

Stellingen

behorende bij het proefschrift

Cell Mapping Methods: Modifications and Extensions

1. Bij de analytische bepaling van de beweging van een rollende schijf over een plat vlak merkt Ginsberg op dat substitutie van de constraints in de bewegingsvergelijkingen leidt tot gecompliceerdere vergelijkingen. Het tegendeel is echter waar.
 - J.H. Ginsberg. *Advanced Engineering Dynamics*. Harper & Row, 1988. p. 297.
2. De bovenmatige aandacht die de chaos-theorie heden ten dage krijgt is met name te danken aan de schoonheid van fractals, die in deze theorie overigens een—wettenschappelijk gezien—ondergeschikte rol spelen.
3. Voor het onderzoeken van niet-lineaire dynamische systemen vormen cell-mapping-methoden een wezenlijke aanvulling op andere methoden waarmee periodieke oplossingen bepaald kunnen worden.
 - dit proefschrift
4. Cell-mapping-methoden zijn toepasbaar op discontinue dynamische systemen, mits de nodige modificaties worden aangebracht.
 - dit proefschrift
5. De MDCM-methode (multi-degree-of-freedom cell-mapping) kan worden toegepast op niet-lineaire dynamische systemen met een willekeurig aantal vrijheidsgraden.
 - dit proefschrift
6. Voor de interpretatie van resultaten verkregen met de cell-mapping-methode is additioneel onderzoek zonder meer nodig.
 - dit proefschrift
7. Voor de bepaling van het snelheidsveld op het oppervlak van een rotatie-symmetrisch viscous incompressibel vloeistoflichaam, welk onder invloed van de oppervlaktespanning vervormt, is de invoering van de fundamentele singuliere oplossing van de ge-lineariseerde Navier-Stokes vergelijkingen te prefereren boven een aanpak die stoelt op de stroomfunctie en de vorticheit.
 - J.A.W. van der Spek. *Inverse Formulations for a Viscous Stating Problem*. Master's thesis. Eindhoven University of Technology, The Netherlands, 1989.

8. De afstelling van verkeerslichten voor voetgangers is in het algemeen niet optimaal, in die zin dat de wachttijden onnodig lang zijn.
9. Uit oogpunt van productiviteit zou het sporten onder werktijd gestimuleerd moeten worden.
10. Dwergpapegaaien kunnen luidruchtig, agressief en destructief zijn.

Eindhoven, 16 februari 1994

Jeroen van der Spek